TECHNIQUES FOR FRACTIONATION, ISOLATION AND CHARACTERIZATION OF SUBVISIBLE AND SUBMICRON PARTICLES IN BIOPHARMACEUTICAL PREPARATIONS

Inauguraldissertation
zur
Erlangung der Würde eines Doktors der Philosophie
vorgelegt der
Philosophisch-Naturwissenschaftlichen Fakultät
der Universität Basel

von

Emilien Georges Pascal FOLZER
aus Mulhouse, Frankreich

Basel, 2016

Genehmigt von der Philosophisch-Naturwissenschaftlichen Fakultät

auf Antrag von

Prof. Dr. Jörg Huwyler (Faculty representative), Dr. Atanas Koulov und Prof. Dr. Wolfgang Friess

Basel, 13. Oktober 2015

Dean of Faculty: Prof. Dr. Jörg Schibler

LABOR OMNIA VINCIT IMPROBUS.

Harte Arbeit siegt über alles.

Virgile, *Géorgiques*.

FÜR MEINE ELTERN

ACKNOWLEDGEMENTS

My first "huge thank you" is for Prof. Jörg Huwyler, my PhD supervisor from the university Basel. I would like to express my deepest gratitude to Jörg for the possibility to carry out my PhD in his research group and for his encouraging support that always motivated me. Thanks a lot for keeping up the good spirit in the group; I always felt as a part of the team although my regular work place was at Hoffmann-La Roche. Many thanks to Christina Erb, Maya Schnell and Carola Seuret who organized the different team events and administrative paper work.

I want to deeply thank Roland Schmidt and Atanas Koulov (Hoffmann-La Roche, Basel), my successive line managers during the PhD, for their continuous enthusiasm and interest in my work, for the scientific input and advice over the last years. I would also like to thank Prof. Dr. Wolfgang Friess from Ludwig-Maximilians-University Munich for taking time and kindly being co-referee of this thesis.

The opportunity to carry out my PhD in Late-Stage Pharmaceutical & Processing Development (Hoffmann-La Roche, Basel) came from PD Dr. Hanns-Christian Mahler. I am most deeply indebted to him for his outstanding and reliable support in every phase of the project. I enjoyed talking and exchanging scientific information concerning my project with him. It was my pleasure working with him and I am very grateful for all his valuable and honest advice (scientifically but also personally). Many thanks for the "always-good-comments" and corrections of the different chapters included into this thesis.

Many thanks are expressed to all the colleagues belonging to Hanns-Christians organization. First, I want to deeply thank the different lab mates that I had during my time in lab 244 building 72: Caroline Hilbert, Andrea Allmendinger, Anacelia Rios, Dominik Ditter and Tarik Khan for the fantastic time, for the fruitful discussions, for the shared lunch-times, for the jokes and for the pleasant atmosphere. I would also like to say thank you to Tarik for the help and time on determining IgG titer for the *in vivo* experiments that were carried out for this thesis. Then, I would like to thank the different lab members (PTDE-P) that made my time inside Roche very enjoyable; special thanks to Stefanie, Severine, Monika, Jason, Mirushe,

Fabian, Tatjana, Roger, Rania, Vanessa W., Raphaela, Jenny, Jennifer, Anita, Kevin, Gerd, Claude, Vincent, Petteri, Tobias W., Sulabh, Andrea K., Carole and all the others. Adeline, Vanessa H., Constanze, Martin, Thomas and Eva-Maria are acknowledged because they helped me to order chemicals, HPLC-columns or other materials. I want to thank the lab-heads that gave me precious advice and took time for me beside their regular project work. Especially, I would like to thank: Claudia Müller, Karin Schoenhammer, Ulla Grauschopf, Sylvia Kiese, Astrid Pappenberger, Carmen Lema-Martinez, Robert Müller, Stefan Fisher, Kishore Ravuri, Heiko Nalenz, Pierre Goldbach, Michael Adler and Felix Heise.

To my colleagues from Penzberg, where I could spend 2 months to learn mass spectrometric methods and analyze my samples, I want to say a huge thank you, especially to Jana Gassner, Lea Bonnington, Dietmar Reusch, Michaela Hook, Marco Thomann, Ingo Lindner, Nadine Floeser, Elisabeth Schirmer, Anna-Katharina Heidenreich, Ulrich Gilles, Nadja Alt, Monika Gerl, Tobias Kailich, Markus Haberger, Martina Suessmair, Susanne Eltner, Britta Peter, Maria Maier, Manuel Schott, Christian Goesswald, Sebastian Malik and Andreas Adler. The team of Patrick Bulau - Katrin Bomans, Katharina Diepold, Sadia Golschan, Ayse Koyuncu, Sabine Fuchs and Michelle Yegres - is kindly acknowledged for the scientific explanations, the precious help and for the wonderful time in lab 110 building 433. Juergen Fichtl and Bernd Maier are deeply acknowledged for their help using the Orbitrap systems and computer software in order to find out cross-linked species in stressed samples.

Beat Ernst, Guy Zielinski, Susanne Elmer and Daniel Fishlock are acknowledged for their help during synthesis and analysis of reference material of chemically cross-linked amino acids. Eric Kusznir and Arne Rufer are acknowledged for their AUC expertise.

I would like to thank our collaboration partners: Juliana Bessa, Antonio Iglesias, Herman Beck, Thomas Bückel, Anja Langenkamp, John Wang, Jun Liu, Tom Patapoff, Valerie Quarmby, Volker Schnaible and Björn Boll for the shared immunogenicity work. From the Joint Particle Lab, I thank Valerie Kempf, Rita Gruebel, Fabian Stump, Johanna Karbe, Lena Josse and Thierry Da Cunha for the nice working atmosphere. From the analytical department, I would also like to express my gratitude to Christof Finkler for welcoming me into his department to continue my PhD studies. I really appreciated working, learning and

talking with qualified and experienced scientists like Stefan Marty and Cécile Avenal. Special thanks to Alexia Schumacher for her good mood, the breaks and funny chat sessions on the messenger.

From the university research group, I would like to thank all the members especially Urs Dutaler, Isabel Meister, Daniel Preisig, Maxim Puchkov, Rainer Alles, Tanja Stirniman, Veronika Eberle, Sandro Sieber, Leonie Hattler, Helen Kettiger, Philip Grossen, Marine Camblin, Fabiola Porta, Gabriella Québatte and Le-Ha Dieu. All colleagues from Jörg's group are kindly acknowledged for their welcoming and integrative attitude and for sharing good time during the supervision of the pharmaceutical technology practical courses.

I would like to say a big thank you for the fantastic time that I spent with all the different people that I could met during Blind-date-lunches; Adeline, Paola, Shijun, Margot, Richard, Christine and Caroline. Specials thanks to Kristina, that always made me laugh and forget work during our lunch times.

I want to thank my friends from sport (handball, running, swimming): Axel, David, Mika, Titi, Christophe, Malik, Tom, Stéphane, Jean-Claude and all the others. Around 1400 trips by train to go and come back from the lab gave me the chance to meet amazing people; all of them contributed to my happiness and good mood during the PhD. Thanks to Liliane, Corine, Yves, Geogette, Jérome, Josée, Marc, Catherine, Kiersten, Jean-Claude, Thierry, Gilles, Claude, Philippe and Malhom for the pleasant discussions and exchanges in the train or on the SNCF-platform (waiting trains that were late!). I also would like to thank my closest friends Louise, Céline, Yannick, Florian, Paméla, Mathieu, Maroussia, Stéphane and Julia: thank you for our precious friendship.

Many thanks go to my new colleagues from the Parenteral Production (Hoffmann-La Roche, Basel) who made me feel welcome as a part of the team since my first day, beginning of May 2015. Therefore I would like to thank Jörn, Regula, James, Elin, Christian, Jonas, Zoran, Alexia, Michael, Ute, Silke, Roman, Lisa, Theresa, Didier, Sieglinde, Sabina, Livia, Theresa, Claudia, Lara, Yvonne, Annika, Marcel, Walter, Antonietta, Tobias, Olivera, Jean-Pierre, Mike, Achim, Jörg, Alice, Flavia, Didier, Andreas, Juri, Christophe, Adrian, Joanna, Gueler,

Cristina, Samantha, Elisabeth and all the others for the pleasant working atmosphere and all the good moments that we shared until now.

Finally, and most important I want to thank my wonderful family and especially my parents (Pascal and Madeleine) and my grandmother for their love, their encouragement, and support throughout my entire study-time.

SUMMARY

Therapeutic proteins have assumed a key role in the treatment of various diseases such as cancer, inflammation, viral infections, metabolic disorders and diseases of the central nervous system.[1] However, physical and chemical instability present a challenge in the development of protein therapeutics. Physical (e.g. unfolding, denaturation, precipitation, aggregation and surface adsorption) and chemical (e.g., Asn deamidation, racemization, scrambling, reduction or oxidation of disulfides, hydrolysis, or amino acid oxidation) degradation can possibly occur during purification, formulation and process development, apart from degradation during storage, transport or possibly, compounding and patient administration.[1,2] Physical degradation includes protein aggregation and proteinaceous (subvisible and visible) particle formation. Both have been reported as a potential critical quality attribute, as being considered potentially relevant to induce immunogenicity.[3] However, to date, the available data in literature for investigations of aggregates, subvisible and visible particles immunogenicity using *in vitro* and *in vivo* experiments is often conflicting and fragmented. Some examples of recent studies are briefly described below.

- Filipe *et al.* have observed that not all IgG aggregates seem to pose the same immunogenic risk after they administered them to transgenic and non-transgenic mice.[4] They found out that oxidation of aggregates had more impact on immunogenicity than any other aggregate features investigated in their work (size, amount, structural conformation, hydrophobicity, morphology and type of intermolecular linkage).
- Fradkin *et al.* could observe that UV treated samples of murine growth hormone have shown an immunogenic response in Balb/c or Nude Balb/c mice.[5] However, they could not find out if the heightened immune response was initiated by chemical damage, the presence of microparticulate aggregates, or a combination of both features.
- Although all of the types of murine mAb aggregates tested by Freitag *et al.* provoked the generation of ADAs, not all of them were equally immunogenic in C57BL/6 J and BALB/c mice.[6] In their manuscript, the most immunogenic aggregates after subcutaneous injection were of relatively large and insoluble nature, with perturbed non-native structures. Therefore they suggested that the characteristics (e.g., size, solubility, extent of chemical modification, conformation) of the aggregates may influence their pharmacokinetics and immunogenicity but in this study they also

concluded that the size of aggregates is not exclusively responsible for ADA formation.

- In a different study, size enriched fraction in the 5-10 μm range of mAb particles obtained by sedimentation and FACS following 20h stir stress, were observed by Telikepalli *et al.* to be able to induce relatively high cytokine response in PBMC donors compared with other size ranges.[7] Those particles presented amorphous morphology, contained protein with partially altered secondary structure, elevated surface hydrophobicity, and trace levels of elemental fluorine.

As described before, a number of studies have been reported in the literature but it is still difficult to draw sound conclusions from the reported results. A more systematic research of different sizes and types of subvisible particles is thus needed in order to understand if a correlation of particles to immunogenicity exists and how specific particle species would relate to immunogenic effects. A major caveat of the published studies to date is the use of complex mixtures of therapeutic protein monomer, various aggregates and particle populations spanning a large range of sizes and possibly including a variety of chemical variations. However, potential effects generated by individual species (*i.e.* different size or modification) are difficult to delineate in such complex mixtures, as individual species are not easy to obtain. Therefore, fractionation methods to obtain subvisible particle fractions having discrete sizes may provide significant advantage in further researching distinct species of proteinaceous subvisible particles in relevant *in vivo* or *in vitro* test systems, possibly being able to identify specific subvisible species primarily relevant for a potential biological consequence, if occurring.

Extended sample characterizations are essential to support and better understand the results obtained from immunogenicity investigations. Although various techniques for the analysis of subvisible particle in parenteral drugs are available on the market (please see Figure 1) with methods having been developed successfully over the years, the quantification of particles in the submicrometer particle size range still remains a significant challenge.

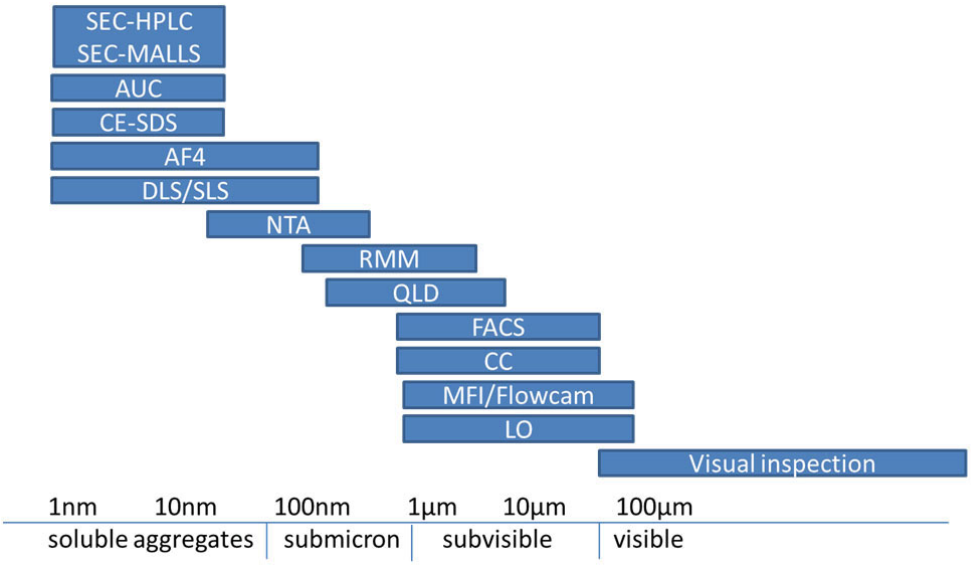

Figure 1: Operation ranges of the more common methods for the analysis of aggregates and subvisible/visible particles (adapted from Zölls and Nahri). SEC-HPLC/MALLS, size-exclusion chromatography/multi-angle light scattering[8-10]; AUC, analytical ultracentrifugation[11]; CE-SDS, sodium dodecyl sulfate capillary electrophoresis [12]; AF4, asymmetrical flow field flow fractionation[13]; DLS/SLS, dynamic light scattering and static light scattering[14], NTA, nanoparticle tracking analysis[15]; RMM, resonant mass measurement[16]; QLD, quantitative laser diffraction[17]; FACS, fluorescence activated cell-sorting[18,19]; CC, coulter counter[20]; MFI/Flowcam, microflow digital imaging[21-23]; LO, light obscuration[24-26]; Visual inspection.

Strengths and weaknesses of the different analytical techniques were evaluated over the last years.[1,27] The different analytical techniques have different principles and therefore different sources of error affecting directly the accuracy and precision of the performed measurements. For example, in the field of protein particle analysis, researchers have been using estimated density values for sizing using Resonant Mass Measurement principle (RMM also known as Archimedes) and for calculating protein particle mass. Such assumptions certainly introduce an error into the results. Chapter 1 describes the determination of the density of proteinaceous particles, without extrapolation, using RMM. The use of various media with different densities allowed to determine the density of artificially generated protein particles in a size range ≤ 5 µm by using a suspended microchannel resonator. Commercially available standard beads (latex, polymethacrylate and melamine) of a defined size and density were used to establish a method to determine the density of the studied protein particles (mAb1, mAb2 and BSA). This step was required, in order to establish and optimize the method parameters.

Most of published studies have evaluated immunogenic potential only by using heterogeneous-sized aggregated and particulated samples.[4,28-31] A major disadvantage of those published studies is the use of complex mixtures of protein monomer, aggregates and subvisible particles of various sizes. In chapter 2, different techniques were evaluated in order to generate preparative well-defined size fractions and isolates of subvisible proteinaceous particles. A comparative evaluation study between a differential centrifugation method and a fractionation using flow cytometry (preparative fluorescence activated cell sorting – FACS) was carried out using a model IgG1. The strengths and weaknesses of each fractionation method are discussed. Fractionation of particles is important, as there is a remaining gap where the actual particle size associated with immune activation has not been thoroughly addressed yet.

Due to the fact that oxidation might be a relevant modification for proteins and protein particles in order to induce immunogenic signals, protocols were generated that selectively induce oxidation products that are prominent and known oxidation side products. Based on published studies, methionine and tryptophan are the most common modifications found in samples generated under forced oxidation reactions (e.g., H_2O_2, t-BHP, AAPH, Fenton reaction, or UV exposure).[32,33] However, the effects and the contribution of individual protein modifications are difficult to delineate as different amino acids are often oxidized simultaneously during those reactions. Chapter 3 describes a method that was developed in order to selectively oxidize methionine and tryptophan. The use of oxidants such as H_2O_2 or AAPH, combined with the use of antioxidants (L-methionine or L-tryptophan) and well-defined reaction conditions (such as incubation temperature and reaction time) allowed us to almost selectively oxidize either methionine or tryptophan in our model mAb, in order to further study the impact of these modifications on immunogenicity. This approach was developed in order to avoid long and complex fractionation processes of oxidized residues.

In chapter 4 the biological effects of proteinaceous subvisible particles using a transgenic mouse model were evaluated. Subvisible particles were generated using artificial heat stress. Unfractionated material of subvisible particles and isolated fractions thereof, differing in size, were prepared using the developed differential centrifugation method and the preparative FACS fractionation method. Non-oxidized subvisible particle samples as well as samples

presenting various levels of oxidized Trp-and Met-residues ((a) high Trp and Met oxidation combined, (b) high Met oxidation only,(c) high Trp oxidation only and (d) a mixture of several oxidized species obtained after UV exposure) were tested *in vivo* in wild-type and transgenic mice after subcutaneous injection. The samples were characterized in detail, using particles measuring instruments (light obscuration, micro flow imaging and resonant mass measurements) and LC/MS peptide mapping. 28 days post immunization blood sera of both wild type and transgenic mice were tested for the presence of anti-drug antibodies (ADAs) by ELISA. The protein structure integrity was assessed using Fourier-transform infrared microscopy (FTIR).

Within the present work, techniques were developed that helped to assess potential immunogenicity of size fractions of subvisible particles and (selectively) oxidized particles in a transgenic mouse model. It was shown that subvisible particles per se, independent of their size, were unable to trigger an immunogenic response. However, subvisible particles having high extent of chemical modifications (oxidation) were able to break tolerance in the transgenic mice.

In summary, this thesis has shown that artificially generated particles (unfractionated material or well-defined fractions) using an IgG1 mAb were not immunogenic in our transgenic mouse model, unless extensively oxidized. However, the specific oxidation products required to trigger the response in transgenic mice could not be identified yet. More work in the field will be needed to understand which specific size and modifications are needed to break tolerance and induce an immune response in transgenic mouse models.

TABLE OF CONTENTS

TABLE OF ABBREVIATIONS

AAPH: 2,2-azobis(2-amidinopropane) dihydrochloride
ADA: anti-drug antibody
AF4: asymmetric-flow field flow fractionation
Asn: asparagine
AUC: analytical ultracentrifugation
CC: coulter counter
CCF: Central composite face-entered
CD: circular dichroism
CE: capillary electrophoresis
D_2O: deuterium oxide, heavy water
DLS: dynamic light scattering
DoE: design of experiments
ELISA: enzyme-linked immunosorbent assay
ESI: electrospray ionization
Fab region: fragment antigen-binding
FACS: fluorescence activated cell sorting
Fc: fragment crystallizable
FC: flow cam
FcRn: neonatal Fc receptor
FDA: food and drug administration
FI: Flow imaging microscopy
FSC: Forward scattering
FTIR: Fourier-transform infrared microscopy
H_2O_2: hydrogen peroxide
Hc: antibody heavy chain
HPLC: high-performance liquid chromatography
IgG_1: immunoglobulin G1
Lc: antibody light chain
LC-MS: liquid chromatography–mass spectrometry
LO: light obscuration
mAb: monoclonal antibody
Met: methionine
MFI: micro flow imaging
MHC: major histocompatibility complex
NTA: nano tracking analysis
QLD: quantitative laser diffraction
RMM: resonant mass measurement
RP-HPLC: reverse phase chromatography
RSM: response surface methodology
SDS: Sodium dodecyl sulfate
SDS-Page: sodium dodecyl sulfate polyacrylamide gel electrophoresis
SE-HPLC: size exclusion chromatography
t-BHP: tert-butyl hydroperoxide
TCR: T cell receptor

Trp: tryptophan
μm: micrometer
UV: ultraviolet light
USP: United States pharmacopeia

Protein pharmaceuticals are increasingly used to treat life threatening and chronic diseases, such as several forms of cancer and inflammation, viral infections, metabolic disorders and central nervous system diseases.[34,35] Millions of lives have been improved or saved, since the beginning of commercialization of monoclonal antibodies and recombinant therapeutic proteins in the 1980s. [1] In the last four years (2010-2014), monoclonal antibodies represented more than a quarter of the new biopharmaceutical products approved by the FDA.[36] In 2011, more than 300 mAb-based therapeutics were in clinical trials.[37] Their market value has been steadily rising, reaching total cumulative sales value of more than $63 billion for 2013.[36] This achievement is the result of many years of research and development addressing myriad discovery and quality challenges.[38] Adverse immune responses severely hamper the successful application of therapeutic proteins.

1.1 Immunogenicity of biotherapeutic products and its assessment using *in vitro/in vivo* models

1.1.1 Adaptive immune response

Since their launch in the mid-1980s, therapeutic monoclonal antibodies (mAb) have evolved from mice, to chimeric and humanized derivatives, to fully human molecules. It was assumed that human therapeutic antibodies, or engineering of antibodies to a human form, would bypass the immunogenicity problem because of the self-tolerance of human for the constant regions of their own antibodies. However, mouse, chimeric, humanized as well as human monoclonal antibodies have shown to elicit a high rate of immunogenicity depending on the dosing regimen and patient population.[3] Some human antibodies developed using phage display may have significant anti-drug antibody (ADA) responses.

Novel structural formats like fusion proteins, multispecific antibodies, single chain fragments, single domain antibodies, and specifically engineered antibodies with mutations (in the constant or variable regions), may elicit immune responses.[3]

Foreign antigens trigger a classical immune reaction that is dependent upon T-cell activation. The likelihood of an immunological reaction is higher because of the higher probability of a

foreign epitope being recognized by a T cell. To trigger an immune response a therapeutic protein interacts with several types of immune cells such as professional antigen-presenting cells (APCs), B-cells and T cells.[39] APCs (e.g., dendritic cells (DCs), macrophages and B cells) have the capacity to take up, process and display linear peptide epitopes from an encountered antigen. Moreover, APCs present the ability to signal and direct T cells to respond in an appropriate manner. DCs are well established to be the most important cell type for guiding immune responses. After the uptake of the antigen, DCs migrate from the peripheral tissues (e.g. subcutaneous space) to the spleen and lymph nodes. After the digestion of antigens by phagocytosis has occurred, the resulting peptides are presented on their surface to other cells of the immune system by major histocompatibility complexes class II (MHC-II). This newly assembled peptide-MHC complex is then transported to the surface of the cell for recognition by T cell receptors (TCRs) from CD4+ T cells. Beside this first signal mediated by the TCR/peptide–MHC interaction, two other signals - co-stimulation and recognition of soluble cytokines - have to be presented as well for activation of a naïve CD4+ T cell (also called T cell maturation). The same peptide-MHC complex is then recognized by the activated CD4+ T cell on a naïve B cell.[39] This activation of B cells starts generating antibody-secreting (short- and long-lived) plasma B cells. Some of the activated B cells also become memory cells, which maintain the pool of long-lived plasma cells and react rapidly to rechallenge by producing short-lived plasma cells. This T cell-dependent immune response is thus usually long lasting and of high titer, particularly for foreign or exogenous proteins.

The human immune system is usually tolerant to proteins of human origin. The T cell population has been selected to not respond to peptides for self-proteins. In the absence of a neoantigen, an immune response against a human protein, though not impossible, is highly unlikely unless the protein is presented to the immune system in a fashion that can reverse tolerance by the earlier mentioned T-cell–dependent pathway.[3]

The elicitation of antibodies towards antigens can also be independent of T cells. Polyvalent antigens such as viral capsids and lipopolysaccharides from bacteria are able to crosslink B cell receptors (BCRs) due to repetitive epitopes on their surface that are arranged in specific steric

distance.[40,41] This mechanism seems to be applicable to protein aggregates that have multivalent surface structure comparable to bacteria or viruses.

1.1.2 Antibody induction - relevance of anti-drug antibodies(ADAs)

The development of unexpected immunogenicity against biotherapeutics poses significant clinical, scientific, and manufacturing challenges. This reaction leads to production of anti-drug-antibodies (ADAs) that can be either neutralizing or non-neutralizing. Non-neutralizing ADAs bind to the therapeutic protein and may alter its pharmacokinetic properties by building immune complexes with the drug. These complexes can enhance clearance of the therapeutic drug from the blood circulation and therefore reduce bioavailability. Neutralizing ADAs can directly interfere with the drug biological activity by binding to epitopes that lie within the active site or by steric hindrances of sites in close proximity to it.[42]

The production of anti-drug-antibodies (ADAs) inactivates the therapeutic effects of the treatment and, in rare cases, induces adverse effects. Unexpected immune responses to therapeutic protein products may result in adverse events not only by inhibiting the efficacy of the therapeutic protein product, but also by cross-reacting to an endogenous protein counterpart, leading to loss of its physiological function.[43-47] Clinically relevant ADA can impact efficacy and/or safety of a biological therapeutic. Despite the development of fully humanized mAbs, there can be a high frequency of anti-drug antibodies in patients.[48,49] The induction of anti-drug antibodies in animals and patients is therefore a key endpoint concerning the immunogenicity of biotherapeutics. In worst-case scenarios, formation of anti-drug antibodies may pose serious safety concerns, and can even be life-threatening.[50] However, the causes of ADAs induction may be patient-, disease- or product-related.[3] The prediction of the immunogenic potential of novel protein therapeutics is therefore a challenge in biotherapy.

1.1.3 Potential risk factors inducing immunogenicity – Immunogenicity drivers

The immunogenic potential of a therapeutic drug is influenced by a variety of factors such as the administration mode, the treated disease, the drug dose, the concomitant medication, patient genetic factors and other undefined variables.[42]

Beside these clinical factors, the intrinsic characteristics of the biological therapeutic play an important role in influencing the development of ADAs. Process related impurities such as host cell protein, DNA, protein A, bovine serum and culture media residues may also lead to a higher risk of immunogenicity.[3] Product related variants including variations in the amino acid sequence (e.g. disulfide bond integrity or mismatch, deamidation, oxidation, high molecular weight aggregates) or different posttranslational modifications such as glycosylation along with neoepitopes generated during protein engineering may induce ADAs formation.[3] The formation of anti-drug antibodies after injection of aggregated proteinaceous material was observed recently in *in vivo* studies.[6,51,52] A breakdown in tolerance following the formation of aggregates with repetitive epitopes was suggested to be an important mechanism by which ADAs are induced.[51] Immunogenicity enhancement by protein aggregates resulting of additional T cell-independent activation of B-cells through cross-linking mechanisms by repetitive and ordered structures in protein aggregates under native forms is another plausible theory.[38,53-55] An additional mechanism for enhanced immunogenicity is related to structural changes induced by chemical linkages, or other chemical modifications leading to protein aggregates.[38,51]

1.1.4 Tools to assess immunogenicity

A range of techniques exist to study the immunogenicity of protein therapeutics which are useful for investigating the presence of antigen-specific antibody; these include immunoassays that can identify antibodies capable of binding to antigen and bioassays that can distinguish between neutralizing and non-neutralizing antibodies. *In silico* prediction tools are available for predicting the T-cell or B-cell epitopes based on protein sequences or structures.[56,57] Experimental approaches, such as *in vitro* major histocompatibility complex (MHC)-peptide binding assays, T-cell proliferation assays are being explored to assess the immunogenicity risk.[58-61]

Animal models are a potentially useful approach to measure antibody responses to biotherapeutics and their degradants.[62] Several transgenic animal models have been generated for this purpose. Transgenic mice are often the preferred *in vivo* model to predict immunogenicity as they are immune tolerant to the administered human protein and can be

used to study the immunogenicity of biotherapeutic aggregates and multiple degradants.[4-6,28,52,63-66]

Although different very useful models are being and were developed, the precise and exact immunological mechanisms for unexpected immunogenicity remain relatively poorly defined until now. Moreover, data from both animal studies and *in vitro* assessments are generally not predictive of the clinical occurrence or outcome. Indeed, immunogenicity studies in animal models do not necessarily predict immunogenicity in humans. I*n vitro* T-cell activation assays and studies in genetically engineered animal models are promising but it has to be mentioned that no model fully recapitulates the human immune response. Therefore, long-term monitoring of immunogenicity in patients during clinical trials and post-marketing is essential.

1.2 Protein stability

Physical and chemical degradation reactions may occur when products are produced, stored, transported or even, during compounding or administration to patients.[34] Susceptible modifications of the structure of a monoclonal antibody might change its activity. Overcoming their limited stability is therefore a major challenge for formulation development scientists.[38,67,68] Among the various degradation mechanisms a protein can undergo, protein aggregation and formation of visible and subvisible protein particles have received significant attention recently.[69-71]

1.2.1 Protein aggregation

Protein aggregation is one physical degradation pathway that occurs in nearly all therapeutic proteins during long-term storage and/or upon stress (denaturants, high/low temperature, agitation, free-thaw, high/low pH).[1,2,67,72-75] Protein aggregation refers to a broad range of diversified self-associated states of monomer units. Soluble or insoluble aggregates include assemblies of protein monomers ranging from dimers to those large enough to be classified as subvisible particles to larger, visible particles (description of particles in next paragraph). Aggregates that are small enough to remain in solution are classified as soluble aggregates in literature.[1] Aggregates that are large enough to be centrifuged down or filtered out of solution

are called insoluble aggregates.[1] Aggregates may be covalent or non-covalently bound. The weak non-covalent interactions often lead to the formation of reversible protein aggregates, which might be in equilibrium with the monomer in the formulation. In contrary, irreversible aggregates are not in equilibrium with the monomer, and they cannot be dissolved by simple dilution using placebo buffer. Recently, a very useful and descriptive classification of aggregates was published by Narhi *et al.*[76]

Since the first investigation of protein aggregation behavior in the 1960s, different models have been introduced to explain their formation.[71,77,78,79] A variety of aggregation pathways are possible depending on the nature of the protein and its close environment.

The aggregate end state might be a combination of native monomer, structurally degraded monomer, partially or even fully unfolded monomer.

1.2.1.1 Impact of protein aggregation

Protein aggregates may show a loss in bioactivity compared to the native protein.[80] In addition, some types of aggregates are discussed to potentially generate an immune response.[1,2,38,55,67,81-85] Aggregation has therefore recently received increased interest from industry, academia and regulators.[1] To date, the data found in literature is contradictory. On one side, all of the types of murine mAb aggregates tested by Freitag *et al.* provoked the generation of ADAs, but not all of them have shown the same immunogenic potential in C57BL/6 J and BALB/c mice. Whereas, Bessa et *al.* have shown that only highly modified soluble aggregates of human IgG1 (induced by harsh UV-treatment) were able to break tolerance in transgenic mice in comparison to non-covalently modified aggregates that did not break tolerance.[86]

1.2.1.2 Analytical tools to characterize soluble/insoluble aggregates and particles (proteinaceous or foreign)

No single analytical technique is sufficient for assessing and monitoring protein aggregates over the full size range due to the measuring size limitation of each instrument.[1,2,76] A summary of the different tools that are available on the market with their strengths and weaknesses is presented in Table 1.

Common and well-established analytical methods like SE-HPLC, AF4, AUC, DLS and electrophoresis (capillary or gel) are used for the analysis and/or quantification of protein aggregates.[15,75,87] These analytical tools are very powerful and versatile widely implemented in industry for characterization purposes.[2]

For counting and size analysis of particles in the nm and low μm-size range, emerging and very promising techniques like nano-tracking analysis (NTA), resonant mass measurement (RMM) and Coulter Counter (electrical zone sensing method) have been used over the last years.[15,16,20,87-90] For analysis of particles larger than 1 μm, flow imaging technologies (MFI or FlowCam) and light obscuration techniques are widely implemented but only light obscuration method is cited in the USP until now.[22,24-26,91,92] More recently, flow cytometry was implemented for the first time to characterize and quantify protein subvisible particles without fluorescent labeling.[93] Different excellent reviews or scientific articles were published to describe in detail those instruments, principles, strength and weaknesses.[1,24,27,75]

Beside particles formed only with protein matter, foreign particles might potentially be present in biopharmaceutical products.[1,75] Particles providing from the packaging material (e.g. silicon oil, rubber, and glass) or introduced during production, filling and packaging processes (e.g. stainless steel, tungsten or cellulose) might be found in commercial products and need to be identified.[76] Silicon oil particles – one of the most common contaminant found in pharmaceutical products filled in syringes – can be detected using RMM technology due to the difference in density between silicon oil and formulation buffer. Indeed silicon oil particles have a lower density than the water based buffer and will therefore be counted as positively buoyant particles when detected in buffer (whereas proteinaceous particle will be classified as negatively buoyant particles due to their higher density).[16,88] Using MFI technology, a differentiation between silicon oil droplets and protein particles is also possible for particles larger than 1 μm using a multiparametric image filter as shown recently in literature.[88,94] Further identification of particles in pharmaceutical products by chemical and/or physical approaches may be needed for trouble shooting root-cause analysis. For this purpose Raman microscopy, Fourier-transform infrared microscopy and/or scanning electron microscopy

(coupled with energy-dispersive X-ray spectroscopy) are used.[1,95,96] However, this last method only provides data on the elemental composition of a sample.

Table 1: Analytical tools used to characterize aggregates and subvisible/visible particles.

Size range	Analytical technique	Advantages	Drawbacks
0.001-0.1µm	Size Exclusion Chromatography (SEC)	Fast High throughput	Limited size range Impact of mobile phase Interaction with matrix
	Field Flow Fractionation (FFF)	High throughput	Interaction with membrane
	SDS-Page Gels	Possible to run under reduced conditions Visualization of protein bands	Limited to low amount of protein Long preparation time
	Capillary electrophoresis (CE-SDS)	High resolution Reproducibility Rapid data analysis Possible to run under reduced conditions	Extensive sample preparation
	Analytical Ultra Centrifugation (AUC)	No matrix interaction	Low throughput
	Dynamic light scattering (DLS)	Fast High throughput	Low resolution
0.03-1µm	Nano Tracking Analysis (NTA)	Tracking of individual particles	High extrapolation factor Not suitable for assessing mixtures of particles with broad distribution of sizes
0.2-5µm	Resonant Mass measurement (Archimedes)	Single particle measurement Differentiation between proteinaceous particles and silicon oil Low volume needed	Low sensitivity to particles with density close to media
0.2-10µm	Quantitative Laser Diffraction (QLD)	Concentration distributions of protein particles in the whole 0.2–10µm diameter range High particle concentration can be measured (10^5-10^9)	Impact of refractive index and solvent

Size range	Analytical technique	Advantages	Drawbacks
0.6-25µm	Label-Free Flow Cytometry Analysis	Possible to quantify and characterize particles based on their physical properties such as density or morphology	Sensitive to refractive index
0.6-25µm	Coulter counter (CC)	Wide dynamic range Individual particles are counted	High conductivity is required Requires several measurement with different aperture tube to cover the whole size range
1-200µm	Flow imaging techniques	Provide information on size, counts and morphology Pictures for individual particles Differentiation between protein particles, silicon oil, and air bubbles	Difficult to detect translucent particles Impact of sample refractive index Fast sedimentation of large particles
1.3-100µm	Light obscuration (LO, HIAC)	Counting of individual particles High reproducibility Robust	Under-sizing effect for proteinaceous particles Not reliable for sample with high viscosity Dilution is needed for high particle counts Does not work well with turbid samples
>100µm	Visual inspection (Seidenader, Optima Lamp, EP box)	Individual vial inspection	Highly trained operators are needed Operator eye fatigue Effect of product on visual inspection outcome

1.2.2 Protein oxidation

Oxidation is a common degradation pathway that affects therapeutic proteins during production, purification, formulation, transportation, storage and product handling. Cysteine, histidine, methionine, phenylalanine, tryptophan and tyrosine residues in a protein can act as oxidation sites in proteins due to the high reactivity of sulfur atoms and aromatic rings towards various reactive oxygen species. Oxidation induced during processing and storage might be the result of contaminating oxidants (contained in excipients or derived from

surfactant), but it might also be due to the presence of transition metal ions or due to the exposure of the product to UV-light.[97,98]

1.2.2.1 Impact and consequences of protein oxidation

Oxidation may extensively modify the primary structure of proteins, by which changes in secondary, tertiary and quaternary structure may arise.[98] The oxidized products that are generated under forced oxidation studies or after long term storage may have different consequences. High oxidation levels might change the biological properties of the therapeutic drug and potentially enhance the immune response of generated sample.[76,77,90]

1.2.2.1.1 Methionine

Altered biological activity and decreased serum half-life following methionine oxidation was reported for insulin, hormones, granulocyte colony-stimulating factor, interferon and other type of proteins. Oxidation of methionine located on the Fc fragment of the monoclonal antibody decreased binding to FcRn receptor (neonatal Fc receptor), binding affinity to protein A/G and also serum half-life.[99-101] Beside these effects, changes in secondary and tertiary structure leading to aggregation were observed for IgG1 and IgG2 presenting methionine oxidation on the Fc fragment.[101,102]

1.2.2.1.2 Tryptophan

Tryptophan oxidation is only reported in few studies where it induced mainly loss of target binding and altered biological activity.[98,103]

1.2.2.1.3 Other amino acids

Cysteine oxidation led to generation of new intramolecular and intermolecular covalent bonds, as observed for interferon, insulin, calcitonin and oxytocin where formation of dimers, trisulfide and tetrasulfide derivatives was reported.[98]

Trace metals, acting as catalyzers, are responsible for histidine oxidation leading to altered activity or major changes on pharmacokinetic profile for the studied protein as reported for hormone and insulin.[98,104]

Tyrosine as well as phenylalanine oxidation leads to tyrosine oxidation products that are very prone to addition reaction, inducing aggregate formation through dityrosine covalent linkage as found in studies for oxytocin, insulin and interferon.[98,105-107]

1.2.2.2 Analytical tools for detection/quantification of oxidation in proteins

Several methods to detect and/or quantify oxidation in mAbs are described.

1.2.2.2.1 Methionine oxidation

Methionine oxidation levels in mAbs can be assessed using affinity chromatography methods like analytical Protein-A or Protein-G chromatography.[108,109] Eventually, oxidation of methionine and tryptophan of an IgG1 can be detected and quantified by hydrophobic interaction chromatography (HIC).[110] Furthermore, RP-HPLC can be employed to detect methionine and tryptophan oxidation in proteins.[32,33,111] Mass spectrometry, e.g. peptide mapping LC/MS(-MS), is the standard method to identify and quantify amino acid modification (such as methionine) at the peptide levels after enzymatic digestions.

1.2.2.2.2 Tryptophan oxidation

RP-HPLC was mainly implemented to detect tryptophan oxidation in proteins as well as peptide mapping LC/MS(-MS).[32,33,111]

1.2.2.2.3 Oxidation of other amino acids and identification of covalent bounds

Recently, histidine oxidation in an IgG1 was detected and quantified for the first time in the Fc part of an IgG1 mAb by mass spectrometry.[112]

Tyrosine and phenylalanine oxidation products can be investigated and quantified using fluorescence methods or electrospray ionization-mass spectrometry (ESI-MS).

Dimerization resulting of cysteine oxidation were identified using SEC-HPLC, ESI-MS and tryptic digest followed by mass spectrometry in the case of salmon calcitonin.[113] LC-MS-MS measurements performed following various enzymatic digests, were lastly perfectly used to investigate and find out the nature of intermolecular/intramolecular cross-linkers induced by

metal catalyzed or UV-light oxidation.[105,114] A combination of techniques such as ^{18}O-labeling and mass spectrometry yielded the discovery and characterization of a photo-oxidative histidine-histidine cross-link in IgG1 antibody.[115]

Nevertheless, characterization of protein cross-links remains challenging due to their structural complexity despite the rapid advancements in mass spectrometry and data analysis algorithms.[116]

References

(1) Mahler, H. C.; Jiskoot, W. Analysis of aggregates and particles in protein pharmaceuticals; Wiley ed. Hoboken NJ, 2011

(2) Mahler, H. C.; Friess, W.; Grauschopf, U.; Kiese, S. J Pharm Sci **2009**, 98, 2909.

(3) Singh, S. K. J Pharm Sci **2011**, 100, 354.

(4) Filipe, V.; Jiskoot, W.; Basmeleh, A. H.; Halim, A.; Schellekens, H.; Brinks, V. MAbs **2012**, 4, 740.

(5) Fradkin, A. H.; Mozziconacci, O.; Schoneich, C.; Carpenter, J. F.; Randolph, T. W. Eur J Pharm Biopharm **2014**, 87, 395.

(6) Freitag, A. J.; Shomali, M.; Michalakis, S.; Biel, M.; Siedler, M.; Kaymakcalan, Z.; Carpenter, J. F.; Randolph, T. W.; Winter, G.; Engert, J. Pharm Res **2014**.

(7) Telikepalli, S.; Shinogle, H. E.; Thapa, P. S.; Kim, J. H.; Deshpande, M.; Jawa, V.; Middaugh, C. R.; Narhi, L. O.; Joubert, M. K.; Volkin, D. B. J Pharm Sci **2015**.

(8) Gabrielson, J. P.; Brader, M. L.; Pekar, A. H.; Mathis, K. B.; Winter, G.; Carpenter, J. F.; Randolph, T. W. J Pharm Sci **2007**, 96, 268.

(9) Carpenter, J. F.; Randolph, T. W.; Jiskoot, W.; Crommelin, D. J.; Middaugh, C. R.; Winter, G. J Pharm Sci **2010**, 99, 2200.

(10) Li, Y.; Weiss, W. F. t.; Roberts, C. J. J Pharm Sci **2009**, 98, 3997.

(11) Lebowitz, J.; Lewis, M. S.; Schuck, P. Protein Sci **2002**, 11, 2067.

(12) Rustandi, R. R.; Washabaugh, M. W.; Wang, Y. Electrophoresis **2008**, 29, 3612.

(13) Cao, S.; Pollastrini, J.; Jiang, Y. Curr Pharm Biotechnol **2009**, 10, 382.

(14) Ahrer, K.; Buchacher, A.; Iberer, G.; Josic, D.; Jungbauer, A. J Chromatogr A **2003**, 1009, 89.

(15) Filipe, V.; Hawe, A.; Jiskoot, W. Pharm Res **2010**, 27, 796.

(16) Patel, A. R.; Lau, D.; Liu, J. Anal Chem **2012**, 84, 6833.

(17) Totoki, S.; Yamamoto, G.; Tsumoto, K.; Uchiyama, S.; Fukui, K. J Pharm Sci **2015**, 104, 618.

(18) Ludwig, D. B.; Trotter, J. T.; Gabrielson, J. P.; Carpenter, J. F.; Randolph, T. W. Anal Biochem **2011**, 410, 191.

(19) Mach, H.; Bhambhani, A.; Meyer, B. K.; Burek, S.; Davis, H.; Blue, J. T.; Evans, R. K. J Pharm Sci **2011**, 100, 1671.

(20) Rhyner, M. N. Aaps J **2011**, 13, 54.

(21) Demeule, B.; Messick, S.; Shire, S. J.; Liu, J. Aaps J **2010**, 12, 708.

(22) Zolls, S.; Weinbuch, D.; Wiggenhorn, M.; Winter, G.; Friess, W.; Jiskoot, W.; Hawe, A. Aaps J **2013**, 15, 1200.

(23) Sharma, D. K.; Oma, P.; Pollo, M. J.; Sukumar, M. J Pharm Sci **2010**, 99, 2628.

(24) Werk, T.; Volkin, D. B.; Mahler, H. C. Eur J Pharm Sci **2014**, 53, 95.

(25) Weinbuch, D.; Jiskoot, W.; Hawe, A. Aaps J **2014**, 16, 1128.

(26) Hawe, A.; Schaubhut, F.; Geidobler, R.; Wiggenhorn, M.; Friess, W.; Rast, M.; de Muynck, C.; Winter, G. Eur J Pharm Biopharm **2013**, 85, 1084.

(27) Narhi, L. O.; Jiang, Y.; Cao, S.; Benedek, K.; Shnek, D. Curr Pharm Biotechnol **2009**, 10, 373.

(28) Bi, V.; Jawa, V.; Joubert, M. K.; Kaliyaperumal, A.; Eakin, C.; Richmond, K.; Pan, O.; Sun, J.; Hokom, M.; Goletz, T. J.; Wypych, J.; Zhou, L.; Kerwin, B. A.; Narhi, L. O.; Arora, T. J Pharm Sci **2013**, 102, 3545.

(29) Hermeling, S.; Aranha, L.; Damen, J. M.; Slijper, M.; Schellekens, H.; Crommelin, D. J.; Jiskoot, W. Pharm Res **2005**, 22, 1997.

(30) Human, P.; Ilsley, H.; Roberson, C.; Grovender, E.; Van Antwerp, B.; Fogt, E.; Zilla, P. J Pharm Sci **2015**, 104, 722.
(31) Joubert, M. K.; Hokom, M.; Eakin, C.; Zhou, L.; Deshpande, M.; Baker, M. P.; Goletz, T. J.; Kerwin, B. A.; Chirmule, N.; Narhi, L. O.; Jawa, V. J Biol Chem **2012**, 287, 25266.
(32) Ji, J. A.; Zhang, B.; Cheng, W.; Wang, Y. J. J Pharm Sci **2009**, 98, 4485.
(33) Yang, J.; Wang, S.; Liu, J.; Raghani, A. J Chromatogr A **2007**, 1156, 174.
(34) Roberts, C. J. Trends Biotechnol **2014**, 32, 372.
(35) Berger, M.; Shankar, V.; Vafai, A. Am J Med Sci **2002**, 324, 14.
(36) Walsh, G. Nat Biotechnol **2014**, 32, 992.
(37) Larrick, J. W. Immunotherapy **2012**, 4, 257.
(38) Wang, W.; Singh, S. K.; Li, N.; Toler, M. R.; King, K. R.; Nema, S. Int J Pharm **2012**, 431, 1.
(39) Khan, T. A.; Reddy, S. T. Acta Biomater **2014**, 10, 1720.
(40) De Groot, A. S.; Scott, D. W. Trends Immunol **2007**, 28, 482.
(41) Rosenberg, A. S. Aaps J **2006**, 8, E501.
(42) Warnke, C. H., C. Lundkvist, M.; Fogdell-Hahn, A. Drugs and Therapy Studies **2012**, 2, 56.
(43) Adm, F. D.; CDER; CBER Biotechnol Law Rep **2014**, 32, 172.
(44) West, R. L.; Zelinkova, Z.; Wolbink, G. J.; Kuipers, E. J.; Stokkers, P. C.; van der Woude, C. J. Aliment Pharmacol Ther **2008**, 28, 1122.
(45) Baert, F.; Noman, M.; Vermeire, S.; Van Assche, G.; G, D. H.; Carbonez, A.; Rutgeerts, P. N Engl J Med **2003**, 348, 601.
(46) Pascual-Salcedo, D.; Plasencia, C.; Ramiro, S.; Nuno, L.; Bonilla, G.; Nagore, D.; Ruiz Del Agua, A.; Martinez, A.; Aarden, L.; Martin-Mola, E.; Balsa, A. Rheumatology (Oxford) **2011**, 50, 1445.
(47) Su, C. G.; Lichtenstein, G. R. Gastroenterology **2003**, 125, 1544.
(48) Getts, D. R.; Getts, M. T.; McCarthy, D. P.; Chastain, E. M.; Miller, S. D. MAbs **2010**, 2, 682.
(49) Anderson, P. J. Semin Arthritis Rheum **2005**, 34, 19.
(50) Svenningsson, A.; Dring, A. M.; Fogdell-Hahn, A.; Jones, I.; Engdahl, E.; Lundkvist, M.; Brannstrom, T.; Gilthorpe, J. D. Neurology **2013**, 80, 965.
(51) Ratanji, K. D.; Derrick, J. P.; Dearman, R. J.; Kimber, I. J Immunotoxicol **2014**, 11, 99.
(52) Shomali, M.; Freitag, A.; Engert, J.; Siedler, M.; Kaymakcalan, Z.; Winter, G.; Carpenter, J. F.; Randolph, T. W. J Pharm Sci **2014**, 103, 78.
(53) Baker, M.; Carr, F. Curr Drug Saf **2010**, 5, 308.
(54) Defrance, T.; Taillardet, M.; Genestier, L. Curr Opin Immunol **2011**, 23, 330.
(55) Sauerborn, M.; Brinks, V.; Jiskoot, W.; Schellekens, H. Trends Pharmacol Sci **2010**, 31, 53.
(56) Koren, E.; De Groot, A. S.; Jawa, V.; Beck, K. D.; Boone, T.; Rivera, D.; Li, L.; Mytych, D.; Koscec, M.; Weeraratne, D.; Swanson, S.; Martin, W. Clin Immunol **2007**, 124, 26.
(57) Barbosa, M. D.; Celis, E. Drug Discov Today **2007**, 12, 674.
(58) Wullner, D.; Zhou, L.; Bramhall, E.; Kuck, A.; Goletz, T. J.; Swanson, S.; Chirmule, N.; Jawa, V. Clin Immunol **2010**, 137, 5.
(59) Kruisbeek, A. M.; Shevach, E.; Thornton, A. M. Curr Protoc Immunol **2004**, Chapter 3, Unit 3 12.
(60) Burshtyn, D. N.; Barber, B. H. J Immunol **1993**, 151, 3082.
(61) Justesen, S.; Harndahl, M.; Lamberth, K.; Nielsen, L. L.; Buus, S. Immunome Res **2009**, 5, 2.
(62) Brinks, V.; Jiskoot, W.; Schellekens, H. Pharm Res **2011**, 28, 2379.

(63) Fradkin, A. H.; Carpenter, J. F.; Randolph, T. W. J Pharm Sci **2011**, 100, 4953.
(64) Fradkin, A. H.; Carpenter, J. F.; Randolph, T. W. J Pharm Sci **2009**, 98, 3247.
(65) Ottesen, J. L.; Nilsson, P.; Jami, J.; Weilguny, D.; Duhrkop, M.; Bucchini, D.; Havelund, S.; Fogh, J. M. Diabetologia **1994**, 37, 1178.
(66) Braun, A.; Kwee, L.; Labow, M. A.; Alsenz, J. Pharm Res **1997**, 14, 1472.
(67) Kiese, S.; Papppenberger, A.; Friess, W.; Mahler, H. C. J Pharm Sci **2008**, 97, 4347.
(68) Wang, W. Int J Pharm **1999**, 185, 129.
(69) Reubsaet, J. L.; Beijnen, J. H.; Bult, A.; van Maanen, R. J.; Marchal, J. A.; Underberg, W. J. J Pharm Biomed Anal **1998**, 17, 979.
(70) Carpenter, J.; Cherney, B.; Lubinecki, A.; Ma, S.; Marszal, E.; Mire-Sluis, A.; Nikolai, T.; Novak, J.; Ragheb, J.; Simak, J. Biologicals **2010**, 38, 602.
(71) Chi, E. Y.; Krishnan, S.; Randolph, T. W.; Carpenter, J. F. Pharm Res **2003**, 20, 1325.
(72) Wang, W. Int J Pharm **2005**, 289, 1.
(73) Maas, C.; Hermeling, S.; Bouma, B.; Jiskoot, W.; Gebbink, M. F. J Biol Chem **2007**, 282, 2229.
(74) Krishnan, S.; Raibekas, A. A. Biophys J **2009**, 96, 199.
(75) Zolls, S.; Tantipolphan, R.; Wiggenhorn, M.; Winter, G.; Jiskoot, W.; Friess, W.; Hawe, A. J Pharm Sci **2012**, 101, 914.
(76) Narhi, L. O.; Schmit, J.; Bechtold-Peters, K.; Sharma, D. J Pharm Sci **2012**, 101, 493.
(77) Kendrick, B. S.; Cleland, J. L.; Lam, X.; Nguyen, T.; Randolph, T. W.; Manning, M. C.; Carpenter, J. F. J Pharm Sci **1998**, 87, 1069.
(78) Marcon, G.; Plakoutsi, G.; Chiti, F. Methods Enzymol **2006**, 413, 75.
(79) Mahler, H. C.; Muller, R.; Friess, W.; Delille, A.; Matheus, S. Eur J Pharm Biopharm **2005**, 59, 407.
(80) Paul, R.; Graff-Meyer, A.; Stahlberg, H.; Lauer, M. E.; Rufer, A. C.; Beck, H.; Briguet, A.; Schnaible, V.; Buckel, T.; Boeckle, S. Pharm Res **2012**, 29, 2047.
(81) Bee, J. S.; Goletz, T. J.; Ragheb, J. A. J Pharm Sci **2012**, 101, 3580.
(82) van Beers, M. M.; Bardor, M. Biotechnol J **2012**, 7, 1473.
(83) Jiskoot, W.; Randolph, T. W.; Volkin, D. B.; Middaugh, C. R.; Schoneich, C.; Winter, G.; Friess, W.; Crommelin, D. J.; Carpenter, J. F. J Pharm Sci **2012**, 101, 946.
(84) Hermeling, S.; Crommelin, D. J.; Schellekens, H.; Jiskoot, W. Pharm Res **2004**, 21, 897.
(85) van Beers, M. M.; Sauerborn, M.; Gilli, F.; Brinks, V.; Schellekens, H.; Jiskoot, W. Pharm Res **2011**, 28, 2393.
(86) Bessa, J.; Boeckle, S.; Beck, H.; Buckel, T.; Schlicht, S.; Ebeling, M.; Kiialainen, A.; Koulov, A.; Boll, B.; Weiser, T.; Singer, T.; Rolink, A. G.; Iglesias, A. Pharm Res **2015**, 32, 2344.
(87) Panchal, J.; Kotarek, J.; Marszal, E.; Topp, E. M. Aaps J **2014**, 16, 440.
(88) Weinbuch, D.; Zolls, S.; Wiggenhorn, M.; Friess, W.; Winter, G.; Jiskoot, W.; Hawe, A. J Pharm Sci **2013**, 102, 2152.
(89) Nejadnik, M. R.; Jiskoot, W. J Pharm Sci **2014**.
(90) Barnard, J. G.; Rhyner, M. N.; Carpenter, J. F. J Pharm Sci **2012**, 101, 140.
(91) Pedersen, J. S.; Persson, M. J Pharm Sci **2014**, 103, 107.
(92) Zolls, S.; Gregoritza, M.; Tantipolphan, R.; Wiggenhorn, M.; Winter, G.; Friess, W.; Hawe, A. J Pharm Sci **2013**, 102, 1434.
(93) Nishi, H.; Mathas, R.; Furst, R.; Winter, G. J Pharm Sci **2014**, 103, 90.
(94) Strehl, R.; Rombach-Riegraf, V.; Diez, M.; Egodage, K.; Bluemel, M.; Jeschke, M.; Koulov, A. V. Pharm Res **2012**, 29, 594.

(95) Lankers, M.; Munhall, J.; Valet, O. Microscopy and Microanalysis **2008**, 14, 1612.
(96) Cao, X.; Wen, Z. Q.; Vance, A.; Torraca, G. Appl Spectrosc **2009**, 63, 830.
(97) Li, S.; Schoneich, C.; Borchardt, R. T. Biotechnol Bioeng **1995**, 48, 490.
(98) Torosantucci, R.; Schoneich, C.; Jiskoot, W. Pharm Res **2014**, 31, 541.
(99) Wang, W.; Vlasak, J.; Li, Y.; Pristatsky, P.; Fang, Y.; Pittman, T.; Roman, J.; Wang, Y.; Prueksaritanont, T.; Ionescu, R. Mol Immunol **2011**, 48, 860.
(100) Pan, H.; Chen, K.; Chu, L.; Kinderman, F.; Apostol, I.; Huang, G. Protein Sci **2009**, 18, 424.
(101) Liu, D.; Ren, D.; Huang, H.; Dankberg, J.; Rosenfeld, R.; Cocco, M. J.; Li, L.; Brems, D. N.; Remmele, R. L., Jr. Biochemistry **2008**, 47, 5088.
(102) Zhang, A.; Hu, P.; MacGregor, P.; Xue, Y.; Fan, H.; Suchecki, P.; Olszewski, L.; Liu, A. Anal Chem **2014**, 86, 3468.
(103) Hensel, M.; Steurer, R.; Fichtl, J.; Elger, C.; Wedekind, F.; Petzold, A.; Schlothauer, T.; Molhoj, M.; Reusch, D.; Bulau, P. Plos One **2011**, 6.
(104) Hovorka, S. W.; Hong, J.; Cleland, J. L.; Schoneich, C. J Pharm Sci **2001**, 90, 58.
(105) Torosantucci, R.; Sharov, V. S.; van Beers, M.; Brinks, V.; Schoneich, C.; Jiskoot, W. Mol Pharmaceut **2013**, 10, 2311.
(106) Hawe, A.; Poole, R.; Romeijn, S.; Kasper, P.; van der Heijden, R.; Jiskoot, W. Pharm Res **2009**, 26, 1679.
(107) Correia, M.; Neves-Petersen, M. T.; Jeppesen, P. B.; Gregersen, S.; Petersen, S. B. Plos One **2012**, 7, e50733.
(108) Gaza-Bulseco, G.; Faldu, S.; Hurkmans, K.; Chumsae, C.; Liu, H. J Chromatogr B Analyt Technol Biomed Life Sci **2008**, 870, 55.
(109) Loew, C.; Knoblich, C.; Fichtl, J.; Alt, N.; Diepold, K.; Bulau, P.; Goldbach, P.; Adler, M.; Mahler, H. C.; Grauschopf, U. J Pharm Sci **2012**, 101, 4248.
(110) Boyd, D.; Kaschak, T.; Yan, B. J Chromatogr B Analyt Technol Biomed Life Sci **2011**, 879, 955.
(111) Grewal, P.; Mallaney, M.; Lau, K.; Sreedhara, A. Mol Pharmaceut **2014**, 11, 1259.
(112) Amano, M.; Kobayashi, N.; Yabuta, M.; Uchiyama, S.; Fukui, K. Anal Chem **2014**, 86, 7536.
(113) Windisch, V.; DeLuccia, F.; Duhau, L.; Herman, F.; Mencel, J. J.; Tang, S. Y.; Vuilhorgne, M. J Pharm Sci **1997**, 86, 359.
(114) Mozziconacci, O.; Kerwin, B. A.; Schoneich, C. Chem Res Toxicol **2010**, 23, 1310.
(115) Liu, M.; Zhang, Z.; Cheetham, J.; Ren, D.; Zhou, Z. S. Anal Chem **2014**, 86, 4940.
(116) Liu, M.; Zhang, Z.; Zang, T.; Spahr, C.; Cheetham, J.; Ren, D.; Zhou, Z. S. Anal Chem **2013**, 85, 5900.

Scope

There is an increased interest from industry, academia and regulators for protein aggregates, subvisible and visible particles due to possible biological consequences, such as immunogenicity, altered bioactivity and modified pharmacokinetic profiles. Aggregates, subvisible and visible particles are important product instabilities, which might be present in every formulation of biotherapeutic products like monoclonal antibody solutions. Especially, the presence of subvisible particles in biotherapeutic products is currently a hot topic and it constantly gains more importance.

The ultimate goal of this thesis is to develop tools and techniques in order to be able to characterize well-defined size fractions of proteinaceous subvisible particles with various desired oxidation profiles using *in vivo* transgenic mouse model. Up to now only a few articles were published and the available data from *in vitro* and *in vivo* experiments on aggregates and subvisible particles is often conflicting and fragmented, which impedes the development of sound conclusions. Moreover, complex mixtures of monomers, aggregates, particles and other degradants were used to draw conclusions.

Only estimated values of protein particle density were used up to now in published studies although it is required to know the density of the measured particles in order to accurately calculate their dimensions and mass. The first aim of this thesis was therefore to develop a method to measure experimentally the protein particle density without extrapolation (Chapter 1). The density for commercially available standard beads (polystyrene, polymethacrylate and melamine) and a large bench of stressed proteinaceous samples was determined with the use of the resonant mass measurement instrument (RMM, Archimedes) and its ability to measure the buoyant mass of individual particles. Various fluids with increasing densities were implemented in order to determine the neutral buoyant mass where the particle density equals the fluid density.

Chapter 2 reports the development of a process to isolate well-defined subvisible fractions using differential centrifugation for a model IgG1 antibody. The process to separate four fractions in the submicron and micrometer size range was developed and successfully

optimized through the use of a design of experiments. The centrifugation technique was compared to an already published fractionation method using a preparative fluorescence-activated cell sorter. Efficiency, advantages and drawbacks for both methods were compared and discussed (Chapter 2).

Oxidation profile of aggregates and subvisible particles seem to be an important attribute regarding induced biological consequences. That is why the next goal was to develop a method for selective oxidation of methionine and tryptophan residues in a model mAb in order to be able to delineate the effects and the contribution of individual protein modifications in the primary structure. This included a large set of experiments where different reaction conditions such as temperature of incubation, reaction time, type and concentration of oxidant (t-BHP, H_2O_2, AAPH) were evaluated in presence (or not) of a large excess of anti-oxidant (free amino acids) in order to protect the corresponding amino acid in a model antibody of the IgG1 subtype (Chapter 3).

To complete the work, unfractionated materials and well-defined size fractions (with well-established oxidation profile) were prepared using the established tools (Chapter 1-3). Those samples were deeply characterized and injected subcutaneously into wild type and transgenic mice for immunization. Anti-drug antibody levels were measured following ELISA in order to assess the immunogenic potential of those preparations (Chapter 4).

CHAPTER 1

DETERMINATION OF THE DENSITY OF PROTEIN PARTICLES USING A SUSPENDED MICROCHANNEL RESONATOR

Journal of Pharmaceutical Sciences

Research Article

Keywords:
protein aggregation
particle size
density determination
suspended microchannel resonator
resonance mass measurement
Archimedes

Authors:
Emilien FOLZER
Tarik KHAN
Roland SCHMIDT
Christof FINKLER
Jörg HUWYLER
Hanns-Christian MAHLER
Atanas KOULOV

Abstract

One of the analytical tools for characterization of subvisible particles which gained popularity over the last years due to its unique capabilities is the Resonance Mass Measurement technique. However, a challenge that this technique presents is the need to know the exact density of the measured particles in order to obtain accurate size calculations. The density of proteinaceous subvisible particles has not been measured experimentally yet and to date researchers have been using estimated density values. In this paper, we report for a first time experimental measurements of the density of protein particles (0.2-5 μm in size) using particles created by stressing three different proteins using four different types of stress conditions. Interestingly, the particle density values which were measured varied between 1.28 and 1.33 g/cm^3 and were lower than previous estimates. Furthermore, it was found that whereas the density of proteinaceous particles was affected to a very low degree by the stress conditions used to generate them, there is relatively larger difference between particles originating from different classes of proteins (e.g. mAb vs. BSA).

Introduction

The analyses of subvisible and submicron particles in therapeutic protein formulations have gained significant attention during the recent years.[1] In addition to light obscuration (which is the method of choice for quality control of biopharmaceuticals), recently, several additional techniques became available for characterization of subvisible particles in therapeutic protein solutions. These include flow imaging microscopy, electrical sensing zone measurements, nano-tracking analysis, label-free flow cytometry and Resonant Mass Measurement.[2-8] Because most of these additional characterization methods have emerged relatively recently, naturally, a number of open questions regarding their performance, utility, strengths and deficiencies still remain.

One of these recently emerged (and very promising) techniques is the resonant mass measurement (abbreviated RMM in literature; also known as "suspended microchannel resonator system" or "Archimedes").[9,10] In the suspended microchannel resonator system, a particle with a diameter between 200 nm and 5 μm (vendor's information) flowing through the fluidic channel alters the resonating frequency of the suspended cantilever. This momentary shift is associated with the change in mass caused by the passage of a particle of differing density than the surrounding media through the cantilever.[11] If the particle density is lower than the sample fluid density a positive frequency shift is induced (positive buoyant particle; e.g. silicon oil droplet in water or placebo buffer) whereas a higher particle density than the sample fluid induces a negative frequency shift (negative buoyant particle; e.g. protein particle in water or placebo buffer). The frequency shift multiplied by the sensitivity of the sensor results in the buoyant mass of the given particle.

This technique has quickly gained popularity for characterization of subvisible particles in biopharmaceuticals owing to its unique abilities to: a) discriminate between different particle types based on their density and b) measure particles in the sub-micrometer size-range.[3,4,7,9,10,12-16] One example of the potential application of these novel capabilities of the method is the differentiation between silicon oil droplets and protein particles specifically in the submicron and low micrometer size range.[9,12] RMM was also used for the determination of single particle mass in biology.[11,17] Burg *et al.* demonstrated that suspended microchannel

resonators can weigh single nanoparticles, single bacterial cells and sub-monolayers of adsorbed proteins in water with sub-femtogram resolution. More recently, the adsorbed protein mass of BSA on polystyrene beads was determined using RMM.[18]

One inherent challenge associated with RMM measurements is the requirement to know the density of the measured particles in order to calculate their dimensions (e.g. equivalent circular diameter) accurately. This aspect of the analysis is particularly important to avoid error in sizing particle populations. Unfortunately, to date the values of the density of proteinaceous particles have not been determined experimentally. This is the reason that all prior published studies reporting characterization of proteinaceous submicron/subvisible particles using RMM utilize estimates of the density of these particles from calculations based on crystallographic studies, also assuming that the density of protein particles does not change significantly with their size or type.[16] The density values used in the literature range between 1.32 g/cm^3 (as suggested by the RMM manufacturer) and 1.35 g/cm^3.[16,18]

The goal of the current study was to determine the density of proteinaceous subvisible particles in the size range between 0.2 – 5.0 μm, generated using different stress conditions and also using different proteins. For that purpose, the capabilities of the suspended microchannel resonator using a modified method for particle density determination used previously for other substances were utilized.[9] As opposed to the previously reported method of linear extrapolation to zero buoyant mass, where the density of the solution matches the density of the particle (neutral density)[9], we used cesium chloride solutions in order to cover a larger density range and be able to determine the particle density experimentally without extrapolation.

To verify the accuracy of the new approach, commercially available and commonly used standard beads were studied using RMM: polystyrene (d=1.05 g/cm^3), polymethacrylate (d=1.19 g/cm^3) and melamine (d=1.51 g/cm^3).

Materials and Methods

Cesium Chloride (purity≥98%), sodium citrate dihydrate (purity ≥99%), sodium phosphate monobasic monohydrate (purity ≥99%), disodium phosphate dibasic anhydrous (purity ≥99%) were obtained from Sigma–Aldrich (St. Louis, Missouri, USA). Trehalose dihydrate (purity ≥98%) was obtained from Ferro Pfanstiehl (Waukegan, Illinois, USA). Sodium chloride (purity ≥99.5%), ethanol absolute for analysis from Merck (Darmstadt, Germany) and deuterium oxide (D_2O, purity=99.96%) from Euriso-top (Saint-Aubin, France) were used. Polysorbate 20 and 80 were obtained from Croda (Edison, New Jersey, USA). Duke polystyrene microsphere size standards (800 nm, 1 μm, 2 μm) were purchased from Thermo Scientific (Waltham, Massachusetts, USA). 1 μm polymethacrylate beads and 2 μm melamine resin microspheres were purchased from Sigma Aldrich (St. Louis, Missouri, USA). Water purified with Milli-Q Advantage A10 from Millipore, with a resistance larger than 18.2 mΩ.cm at 25°C was used in all experiments. Albumin from bovine serum (purity≥96%) from Sigma–Aldrich (St. Louis, Missouri, USA) was used. A 40 mg/ml solution was prepared in PBS. Two monoclonal antibodies (mAb1) and (mAb2) of the IgG1 subtype were provided at 25 mg/ml in 51 mM sodium phosphate, 6 % trehalose, and 0.04 % polysorbate 20 (pH 6.2) and 10 mg/ml in sodium citrate dehydrate, 0.9 % sodium chloride, 0.07% polysorbate 80 (pH is 6.5) by F.Hoffmann-La Roche Ltd. (Basel, Switzerland). mAb1 and mAb2 were initially - filtered through a 0.22 μm Millipore Express plus filter prior use. Millipore 0.22 μm Express plus filters were used for the filtration of all buffer solutions and media used in the RMM measurements before use to avoid contamination with dust or foreign particles.

The densities of each solution were measured using a densitometer (Anton Paar DMA38, Ashland, Virginia, USA) calibrated with water before measurement. PCC-54 Detergent from Pierce (Rockford, Illinois, USA) and Tergazyme® from Alconox (New-York, USA) were used for cleaning of particle measurement instruments when mentioned.

DLS measurements

Different solutions of cesium chloride (0, 20%, 30%, 40%, 50%, 55%) containing increasing concentration of protein (between 0 and 10 mg/ml) were prepared and measured for mAb1 and mAb2 by DLS using a DLS plate reader (Wyatt Technologies Corporation). Sample temperature during measurements was set to 20°C. Measurements were made using a Corning® 96 well black plate with clear flat bottom polystyrene and 150 µl sample in each well. 10 acquisitions per sample were performed and regularization fit was applied to each sample. For determination of hydrodynamic radius the method described by Parmar et al was used.[19]

Stress conditions for BSA, mAb1 and mAb2 heat

1 ml of protein solution was artificially stressed for 3 min at 80°C/1400 rpm using a Thermomixer (Eppendorf). The temperature was chosen to be above the melting temperature of the protein to ensure formation of large amounts of proteinaceous particles. In order to homogenize the artificially generated protein particles, a silicon-oil-free 5 ml luer lock syringe (Henke Sass Wolf, Tuttlingen, Germany) was used, mounted with a 27 G needle and 20 draw-release cycles were applied manually. After centrifugation at 2000 rpm for 1 min to discard the largest particles, the supernatant fractions were collected, aliquoted and stored at -80°C until needed. Stability of protein particles during -80°C storage and after thaw was demonstrated using light obscuration and microflow imaging measurements (data not shown).

Stress conditions for mAb1 and mAb2 solvent-induced precipitation

1 ml of mAb solution was poured into 1 ml of pure ethanol to induce precipitation of the protein. To homogenize and reduce the size of the formed protein particles, 5 draw-release cycles were applied manually using a 5 ml syringe (silicon-oil-free) mounted with a 27 G needle.

Stress conditions for mAb1 shaking stress

Shaking stress was applied at a constant 200 rounds per minute (rpm) by placing 2 ml of mAb1 solution into 6 ml-vials that were placed horizontally at room temperature for 9 months, protected from direct light, onto a horizontal moving shaking plate (HS 260 Control Model IKA GmbH and Co., Stauffen, Germany). After centrifugation at 2000 rpm during 1 minute to discard the largest particles, the supernatant fractions were collected, aliquoted and stored at -80°C until needed.

Stress conditions for BSA, mAb1 and mAb2 stirring

Washed 6 mm × 15 mm Teflon® coated stirrer bars (Semadeni AG, Ostermundigen, Switzerland) were placed directly into the 6 ml-vials where 2 ml protein solution was filled. The stirring stress was generated at a constant 500 rpm by placing the vials vertically, protected from direct light, onto a multi-position magnetic stirrer (RO 15 Model IKA GmbH and Co.) at room temperature for 30 h.

Microflow imaging measurements

The morphological parameters of different samples were analyzed for by micro flow imaging (MFI) using the MFI DPA4200 series instrument (Protein Simple, San Jose, California, USA) equipped with a 470 nm LED light source. Particles with equivalent circular diameter (ECD) larger than 1 μm were analyzed. Size (5 μm ThermoScientific Duke Standard) and count standards (5 μm COUNT-CAL Count Precision Standards, ThermoScientific; USA) were used to check the sizing and counting accuracy of the instrument. At the end of the day, the system was flushed at maximal speed for 5 minutes and then soaked for 30 minutes with 1 % (w/v) Tergazyme®, followed by rinsing with water for 30 min. Flushing with water was repeated after each sample for 30 minutes. For these flushing steps, the flow rate was set to instrument maximum speed. Optimization of illumination was performed prior to analysis, using solutions matching the sample to be analyzed. For measuring, 1 ml of sample was placed in a 1 ml dual-filter tip on the inlet port. The first 0.2 ml was discarded, before a volume of 0.6 ml was analyzed. Each sample was measured in triplicate.

Suspended microchannel resonator measurements (RMM)

The RMM measurements were performed on the Archimedes system (RMM0017, generation 2) from Malvern instruments LTD (Malvern, United Kingdom). Micro sensor chips with internal microchannel dimensions of 8 μm × 8 μm were used for all the experiments. The instrument baseline was between 0.010 and 0.015 Hz. The calibration of each sensor was done after replacement using a diluted 1 μm Duke polystyrene size standards (final concentration=10^6 part/ml in water). The sample was loaded for 40 sec prior to calibration. The calibration was finalized after 300 particles were detected as suggested by the manufacturer.

Different volume of each stock solution (standards beads or protein particles) were spiked before RMM measurement in the different solutions (water, PBS, D_2O, CsCl 20%, CsCl 30%, CsCl 40%, CsCl 50%, CsCl 55% w/w) according to initial particle concentration in order to reach concentrations larger than $5x10^6$, but not higher than $3x10^7$ particle/ml. Each sample was analyzed in triplicate. Prior spiking of artificially produced proteinaceous particles into the corresponding media it was ensured that there is no formation of new particles using RMM or MFI control measurements.

The threshold limit (LOD) was manually set to 0.04 Hz for each analysis (based on previous experiments, data not shown). A stop trigger of 2000 particles or 1 h measurement time was used in order to analyze a representative particle population of each sample. During measurement of microspheres and protein samples the “autoreplenish” function was automatically activated every 120 sec for duration of 2 sec. During the autoreplenish, fresh sample was loaded to the microchannel in order to avoid possible settling down of particles. Moreover, the sample volume analyzed when implementing the autoreplenish function is larger, improving the reproducibility of each measurement series performed on RMM (data not shown here).

Between runs, sensors were rinsed with formulation buffer and water for 10 min as recommended by the manufacturer. The water rinsing step was repeated until a clean frequency trace was achieved. At the end of each measurement day, the sensor and the micro tubing were rinsed with 1% PCC-54 detergent, by applying high pressure on the sample and

reference vials to clean the bypass channels. ParticleLab software (version 1.8.510) provided by Affinity Biosensor was used to process all measurement results.

Determining particle density

Particle density determinations were performed by evaluating the change in the mean buoyant mass of the measured particles relative to changes in solution density. The buoyant mass for the different particles was measured in solutions with increasing densities. The obtained mean value (n=3) for the buoyant mass (reported by the software in fg) for all particles detected during analysis over the full size range was plotted against the corresponding solution densities for particles standards. In the case of monotonic distributions of particles showing significant populations immediately below the accessible size range of the sensor, a restricted size range was used to calculate the mean buoyant mass, and the fitting was performed in an iterative manner to avoid artifacts due to differences in minimum detectable particle sizes that are a result of differences in solution density. The intercept of the linear regression with the Y-axis (where the buoyant mass is equal to zero) gave the density of the measured particles.[9] At this point, the density of the particle has the same density as the fluid and no frequency shift can be detected – *i.e.* neutral density.[9]

Results and discussion

The particle measurement capabilities of the RMM system are a valuable complement to particle counting and sizing methods currently used in numerous industrial and research applications. One advantage of RMM is the ability to directly measure the mass of individual particles. The densities of polystyrene, melamine and silicon oil particles were determined previously by Patel *et al.* by linear extrapolation to zero buoyant mass using sucrose solutions with increasing densities, but the density for protein particles has never been experimentally determined before. The goal of this study was to determine the density of proteinaceous subvisible particles, using the suspended microchannel resonator without extrapolation. For this purpose, series of cesium chloride solutions were used in order to reach high densities and avoid extrapolation. The particle densities were determined by applying linear regression to the measured mean buoyant masses of particles in eight different solutions (n=3 in each case) with varying densities from 1.00 to 1.65 g/cm^3 (water, PBS, D_2O, CsCl solutions – for more details see Materials and Methods). Measurements were carried out using commercially available beads (polystyrene ρ= 1.05 g/cm^3, polymethacrylate ρ= 1.19 g/cm^3 and melamine ρ= 1.50 g/cm^3) as well as artificially generated protein particles.

Density determination for particle standards

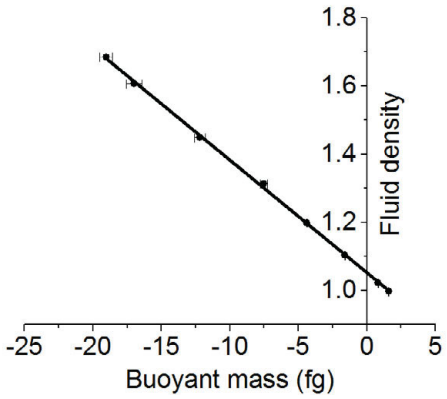

Figure 1: Particle density of polystyrene microspheres 800 nm. Measurement of the microsphere buoyant mass in 8 different surrounding media (water, PBS, D_2O, CsCl 20%, CsCl 30%, CsCl 40%, CsCl 50% and CsCl 55%) with increasing densities allow to find the polystyrene particle density.

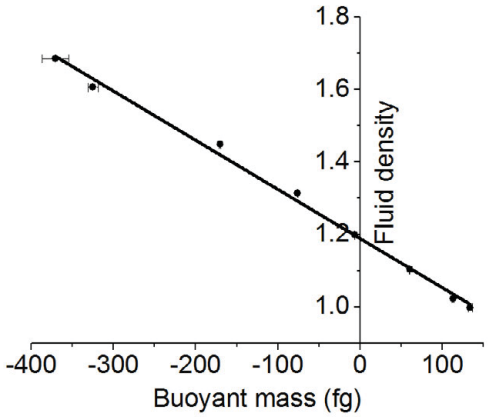

Figure 2: Particle density of polymethacrylate microspheres (1 µm). Measurement of the microsphere buoyant mass in 8 different surrounding media (water, PBS, D_2O, CsCl 20%, CsCl 30%, CsCl 40%, CsCl 50% and CsCl 55%) with increasing densities allow to find the polymethacrylate particle density.

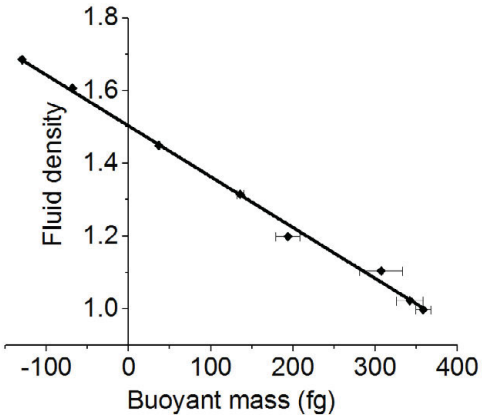

Figure 3: Particle density of melamine microspheres (2 µm). Measurement of the microsphere buoyant mass in 8 different surrounding media (water, PBS, D_2O, CsCl 20%, CsCl 30%, CsCl 40%, CsCl 50% and CsCl 55%) with increasing densities allow to find the melamine particle density.

In order to assess the accuracy of the method, the densities of standard beads were measured. Three different types of beads with densities covering the range of interest were chosen: polystyrene (ρ= 1.05 g/cm^3), polymethacrylate (ρ= 1.19 g/cm^3) and melamine (ρ= 1.50 g/cm^3). The beads were spiked into different media with increasing densities from 1.00 to 1.65 g/cm^3 (water, PBS, D_2O, CsCl 20%, CsCl 30%, CsCl 40%, CsCl 50%, CsCl 55% w/w), and the buoyant masses for each population were measured in triplicate. As explained by Patel *et al.*, the density of the measured particles should correspond to the intercept of the regression line and the Y axis (the point where the particles become "invisible" for the suspended

microchannel resonator).[9] The measured values for particle buoyant masses of polystyrene, polymethacrylate and melamine beads standards in different media including the respective standard deviation (error bars) are depicted in Figures 1 and supplementary Figure 1, Figure 2 and Figure 3, respectively. The intercepts of the regression lines with the solution density axis (Y axis) at zero buoyant mass, the slopes and regression coefficients for the standard beads are presented in Table 1. Using this method the experimentally determined density values for the polystyrene particles and melamine particles were within 0.4 and 0.5% of the expected value of 1.05 g/cm^3 and 1.51 g/cm^3 respectively (no difference in density was observed between 3 different sizes of polystyrene particles – 0.8 μm, 1 μm and 2 μm), whereas the linear fit for polymethacrylate resulted in neutral density of 1.19 g/cm^3 which corresponded exactly to the expected value. The obtained results for the commercially available standard beads correlated very well with published data and supplier information. Unlike the previously reported method for determination of particle densities using sucrose solutions, the method applied in this study does not use extrapolation to determine the density of particles. Thus, the density of relatively dense particles (e.g. melamine: ρ= 1.50 g/cm^3) determined using the new and improved method reported here is very close to the expected value (0.5% deviation), whereas 3.7% deviation was observed in the measurements using extrapolation.[9] The significant increase of the accuracy can be attributed to the closer match of the media density and the density of the measured melamine beads (*i.e.* between 40% and 50% CsCl). It is interesting to notice that for the same reasons, a higher standard deviation for the buoyant mass measurements (n=3) was observed for high densities in the case of polystyrene, and for lower densities in the case of melamine.

Table 1: Summary of linear fit results obtained from the experimental points represented in Figure 1-6 and supplementary Figure 1-3. The results are presented for standard beads (polystyrene, polymethacrylate and melamine); artificially generated particles obtained using BSA, mAb1 and mAb2. The intercept (*i.e.* particle density; neutral density), the slope of the regression line and the coefficient of determination R-Square are listed for the analyzed mAb1 protein particles.

Sample name	Intercept		Slope	Adj. R-Square
	Value	Standard Error	Value	
Polystyrene 800 nm	1.05	0.01	-3.3×10^{-2}	0.999
Polystyrene 1 µm	1.05	0.01	-1.8×10^{-3}	0.994
Polystyrene 2 µm	1.04	0.01	-2.3×10^{-3}	0.997
Polymethacrylate 1 µm	1.19	0.01	-1.4×10^{-3}	0.995
Melamine 2 µm	1.50	0.01	-1.4×10^{-3}	0.995
BSA - heat	1.33	0.01	-2.8×10^{-2}	0.998
BSA - stirring	1.31	0.01	-2.4×10^{-2}	0.983
mAb1 - heat	1.28	0.01	-8.8×10^{-2}	0.992
mAb1 - solvent-induced precipitation	1.28	0.01	-6.2×10^{-3}	0.995
mAb1 - shaking stress	1.28	0.01	-7.0×10^{-3}	0.995
mAb1 - stirring	1.28	0.01	-9.0×10^{-3}	0.998
mAb2 - heat	1.28	0.01	-8.3×10^{-3}	0.994
mAb2 - solvent-induced precipitation	1.29	0.01	-9.0×10^{-3}	0.990
mAb2 - stirring	1.28	0.01	-9.2×10^{-3}	0.999

Density determination for protein samples

A number of samples containing artificially generated proteinaceous particles were prepared using three different model proteins – BSA, mAb1 and mAb2 (see Materials and Methods for experimental details). The different stress conditions (heat, solvent-induced precipitation, stir and shaking) resulted in different amounts of precipitated protein (data not shown). The presence of residual monomers bears the risk for potential analytical artefacts, such as further aggregation upon contact with high concentrations of cesium chloride and consequent undesirable particle formation. To mitigate this risk, the impact of every different medium used in these experiments on the mAb solutions regarding particle formation under the method conditions was investigated before actually measuring buoyant mass of spiked protein

particles in the different media. The protein solutions were diluted 10-fold with each medium, and the particle formation was assessed one hour after mixture using flow imaging and RMM techniques. It was observed that any aggregation under experimented conditions was negligible when pure protein solution was diluted with all media, except for 50% and 55% CsCl solutions, where relevant particle formation was observed during RMM and MFI measurements (data not shown). Therefore, in order to avoid measurement artifacts, measurements of buoyant masses for proteinaceous particles resuspended in 50% or 55% CsCl solutions were not performed. In addition, the impact of dilution regarding particle morphological parameters for particles obtained following each stress conditions was assessed using flow imaging. No impact on any of morphological parameters measured by flow imaging was detected upon dilution of protein particles into the media used in the study (data not shown).

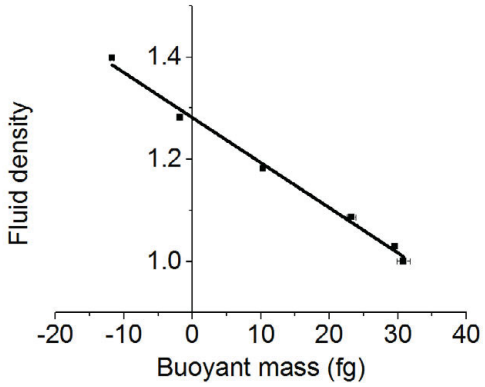

Figure 4: Particle density of artificially stressed mAb1. Density of mAb1 particles (heat stress) was determined by measuring the buoyant mass of each sample in 6 different surrounding media (water, PBS, D_2O, CsCl 20%, CsCl 30%, CsCl 40%).

To determine the density of the different populations of stressed model proteins, particles were spiked from stock solutions in six different solutions with densities varying from 1.00 to 1.45 g/cm^3 (using water, PBS, D_2O, CsCl solutions – for more details see Materials and Methods) and the mean buoyant mass of each population was measured in triplicate using RMM (maximum one hour measurement time). The mean buoyant mass over a selected size range obtained from the iterative calculation as described by Patel *et al.* was used to plot the Figure 4, supplementary Figure 2 for mAb1, Figure 5, supplementary Figure 3 for mAb2 and

Figure 6 for BSA particles.[9] The size restriction was employed to ensure that the same population of particles is analyzed in media of different densities. This size restriction had a considerable effect on the standard deviation between triplicate measurements which was significantly reduced after application of this procedure. The summary of the linear fit results is presented in Table 1 for the three model proteins.

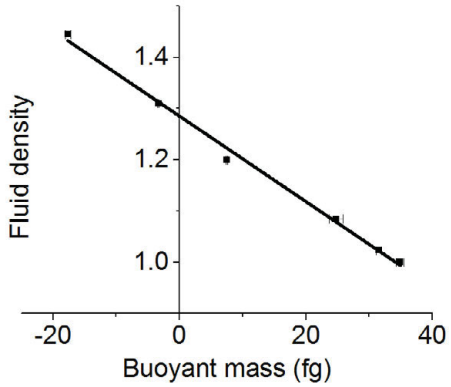

Figure 5: Particle density of artificially stressed mAb2. Density of mAb2 particles (heat stress) was determined by measuring the buoyant mass of each sample in 6 different surrounding media (water, PBS, D_2O, CsCl 20%, CsCl 30%, CsCl 40%).

It is important to note that the good linear fit to all of the experimental values described above, including H_2O, PBS and D_2O particle dispersions as well as these in increasing concentration of CsCl excludes the possibility that changes induced by higher concentrations of CsCl (e.g. particle dehydration) have influenced the measurements. In case such influence would have been present, a significant deviations from linearity would have been expected, which was not the case. This conclusion was also confirmed by the lack of any discernible effects on the protein hydrodynamic radius (Rh) upon resuspension into differently concentrated CsCl solutions, clearly indicating the absence of potential salt-induced swelling or compaction of the protein itself (Supplementary Figure 4). Similar results were described in literature by Parmar et al for lysozyme.[19]

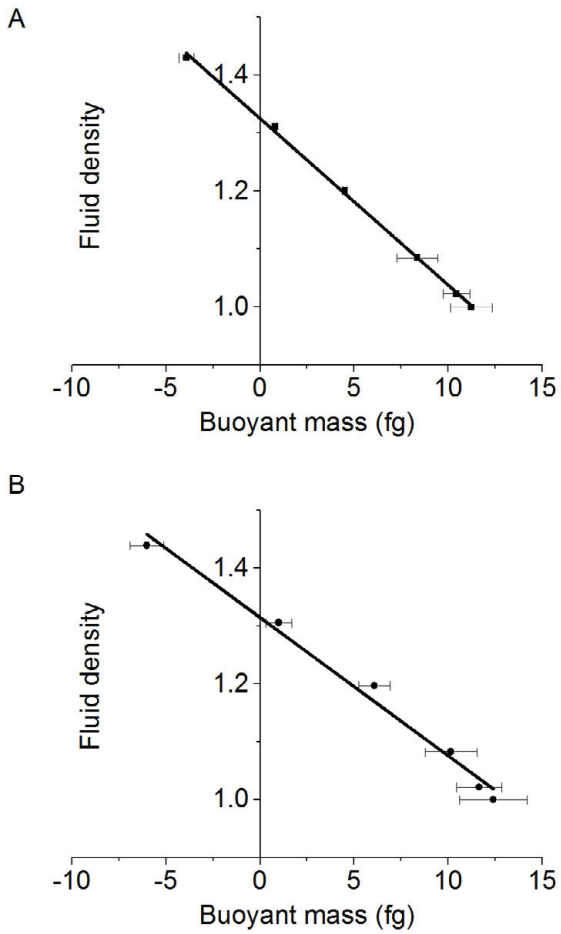

Figure 6: Particle density of artificially stressed BSA. Densities of BSA particles ((A) heat, (B) stirring) were determined by measuring the buoyant mass of each sample in 6 different surrounding media (water, PBS, D_2O, CsCl 20%, CsCl 30%, CsCl 40%) with increasing densities.

Previous estimates of the density of protein particles were largely based on the mean protein density calculated from large crystallographic datasets and arbitrary estimation of the likely water content of protein particles. These estimates have arrived at average densities of proteinaceous particles of about 1.32-1.35 g/cm^3.[13,18,20,21] Now we offer for the first time experimentally measured values for proteinaceous subvisible particles. The experimental values that we report here range between 1.28 g/cm^3 for immunoglobulin particles and 1.33 g/cm^3 for BSA particles, which on average is lower than the estimated values reported previously. Interestingly, we did not observe significant density disparities between the particles generated using different stress conditions; however, protein-to-protein differences were more substantial. The latter observation likely reflects the strong influence of the

molecular geometry on the packing of protein monomers in an aggregate. For example, the measured density of BSA (relatively more compact molecular structure) particles generated using different stress conditions were between 1.31 g/cm^3 and 1.33 g/cm^3, whereas the density of IgG (relatively more extended molecular structure) particles were between 1.28 g/cm^3 and 1.29 g/cm^3. It is reasonable to assume that proteins with more extended structures would pack into less dense aggregates – assumption which correlates well with the results reported in this manuscript. Of course, in order to make a general conclusion regarding the relationship of structure and molecular packing, a much more extensive dataset would be needed. One important implication of the results reported here is the apparent necessity to measure the density of aggregates when these values are used for calculations (e.g. calculating particle size distributions from RMM measurements or calculation of the mass contained in particles measured using other methods), particularly when a new structural class of protein is studies. The method reported here provides a simple and easy to use tool for such measurements.

In order to determine the impact of the discrepancy between the newly determined experimental density values for protein particles and the density estimation used in the literature, the size distribution of the particles in a stressed mAb sample were measured and re-calculated using previously estimated values and the newly determined density values. Using the newly determined density value of 1.28 g/cm^3 for mAb-derived particles instead of previously suggested 1.32 or 1.35 g/cm^3 has a slight impact on the particle size measured by RMM. The impact is different in the different particle size bins as depicted in Figure 7.

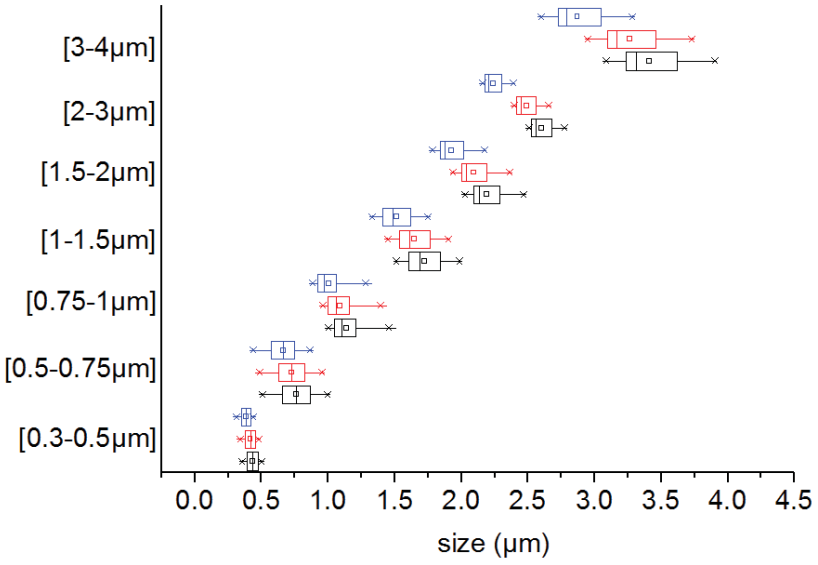

Figure 7: Impact of protein particle densities on size bins for a proteinaceous sample (mAb1-heat). The impact of protein particles densities of 1.28 g/cm^3 (black), 1.32 g/cm^3 (red) and 1.35 g/cm^3 (blue) was investigated. Horizontal box plots show 25/75% (box), mean values (squares), median (vertical line) and min/max (whisker).

It is important to note, that the method for density determination reported here is only suitable to measure the density of particles smaller than 5 µm due to limitations in the current RMM instrumentation. Further studies will be needed to measure the density of larger particles. The development of a new type of RMM sensor adapted for larger particles might help to answer this question.

Conclusion

We report for the first time the direct measurement of the density of proteinaceous subvisible particles (of sizes between 200 nm and 5 μm) using a new, RMM method. Interestingly, the measured densities for proteinaceous particles (1.28-1.33 g/cm^3) originating from three different proteins and four different stress conditions were lower than previous calculations. Whereas relatively small differences were observed between the densities of particles generated using different stress conditions, protein-to-protein particle density differences were more pronounced. The new method presented here can be easily applied to any system and would allow researchers to accurately measure the density of the subvisible particles present in their samples, enabling improved sizing of RMM measurements.

Acknowledgements

The authors thank Stefan Fischer for helpful discussions and suggestions.

References

(1) Singh, S. K.; Afonina, N.; Awwad, M.; Bechtold-Peters, K.; Blue, J. T.; Chou, D.; Cromwell, M.; Krause, H. J.; Mahler, H. C.; Meyer, B. K.; Narhi, L.; Nesta, D. P.; Spitznagel, T. *J Pharm Sci* **2010**, *99*, 3302.

(2) Mahler, H. C.; Friess, W.; Grauschopf, U.; Kiese, S. *J Pharm Sci* **2009**, *98*, 2909.

(3) Zolls, S.; Tantipolphan, R.; Wiggenhorn, M.; Winter, G.; Jiskoot, W.; Friess, W.; Hawe, A. *J Pharm Sci* **2012**, *101*, 914.

(4) Hamrang, Z.; Rattray, N. J.; Pluen, A. *Trends Biotechnol* **2013**, *31*, 448.

(5) Demeule, B.; Messick, S.; Shire, S. J.; Liu, J. *Aaps J* **2010**, *12*, 708.

(6) Narhi, L. O.; Jiang, Y.; Cao, S.; Benedek, K.; Shnek, D. *Curr Pharm Biotechnol* **2009**, *10*, 373.

(7) Nishi, H.; Mathas, R.; Furst, R.; Winter, G. *J Pharm Sci* **2014**, *103*, 90.

(8) Mahler, H. C.; Jiskoot, W. *Analysis of aggregates and particles in protein pharmaceuticals*; Wiley ed. Hoboken NJ, 2011

(9) Patel, A. R.; Lau, D.; Liu, J. *Anal Chem* **2012**, *84*, 6833.

(10) Panchal, J.; Kotarek, J.; Marszal, E.; Topp, E. M. *Aaps J* **2014**, *16*, 440.

(11) Burg, T. P.; Godin, M.; Knudsen, S. M.; Shen, W.; Carlson, G.; Foster, J. S.; Babcock, K.; Manalis, S. R. *Nature* **2007**, *446*, 1066.

(12) Weinbuch, D.; Zolls, S.; Wiggenhorn, M.; Friess, W.; Winter, G.; Jiskoot, W.; Hawe, A. *J Pharm Sci* **2013**, *102*, 2152.

(13) Kalonia, C.; Kumru, O. S.; Kim, J. H.; Middaugh, C. R.; Volkin, D. B. *J Pharm Sci* **2013**, *102*, 4256.

(14) Depaz, R. A.; Chevolleau, T.; Jouffray, S.; Narwal, R.; Dimitrova, M. N. *J Pharm Sci* **2014**, *103*, 1384.

(15) Christie, M.; Torres, R. M.; Kedl, R. M.; Randolph, T. W.; Carpenter, J. F. *J Pharm Sci* **2014**, *103*, 128.

(16) Barnard, J. G.; Singh, S.; Randolph, T. W.; Carpenter, J. F. *J Pharm Sci* **2011**, *100*, 492.

(17) Dextras, P.; Burg, T. P.; Manalis, S. R. *Anal Chem* **2009**, *81*, 4517.

(18) Nejadnik, M. R.; Jiskoot, W. *J Pharm Sci* **2014**.

(19) Parmar, A. S.; Muschol, M. *Biophys J* **2009**, *97*, 590.

Associated content - Supporting information

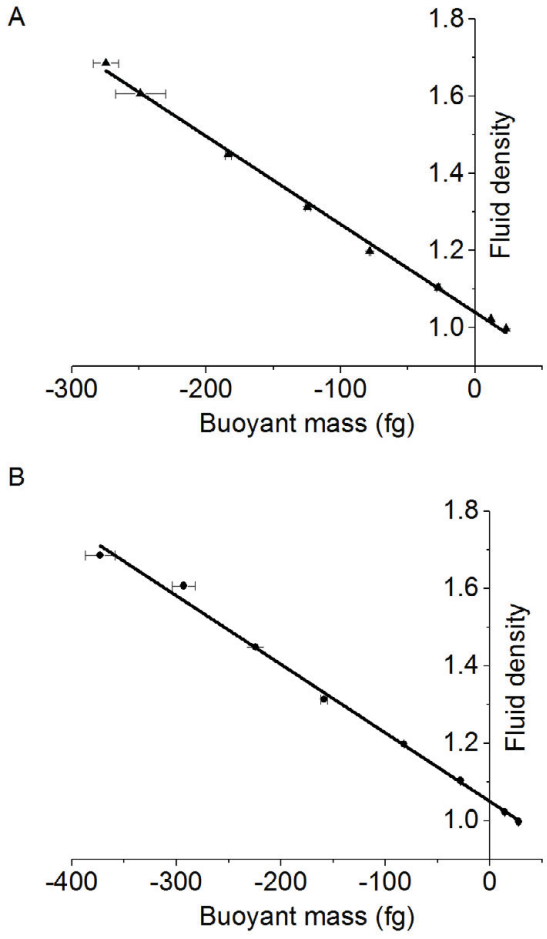

Supplementary Figure 1: Particle density of polystyrene microspheres (A) 1 µm, (B) 2 µm. Measurement of the microsphere buoyant mass in 6 different surrounding media (buffer, CsCl 20%, CsCl 30%, CsCl 40%, CsCl 50% and CsCl 55%) with increasing densities allow to find the polystyrene particle density.

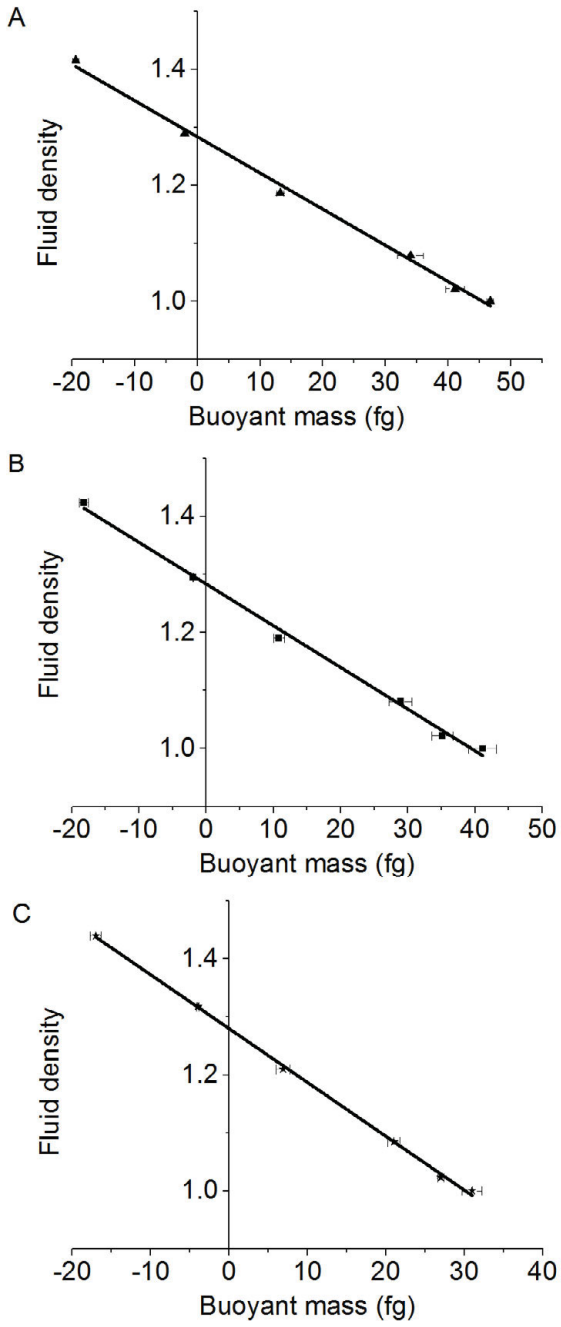

Supplementary Figure 2: Particle density of artificially stressed mAb1. Densities of mAb1 particles ((A) solvent-induced precipitation, (B) shaking stress, (C) stirring) were determined by measuring the buoyant mass of each sample in 6 different surrounding media (water, PBS, D_2O, CsCl 20%, CsCl 30%, CsCl 40%).

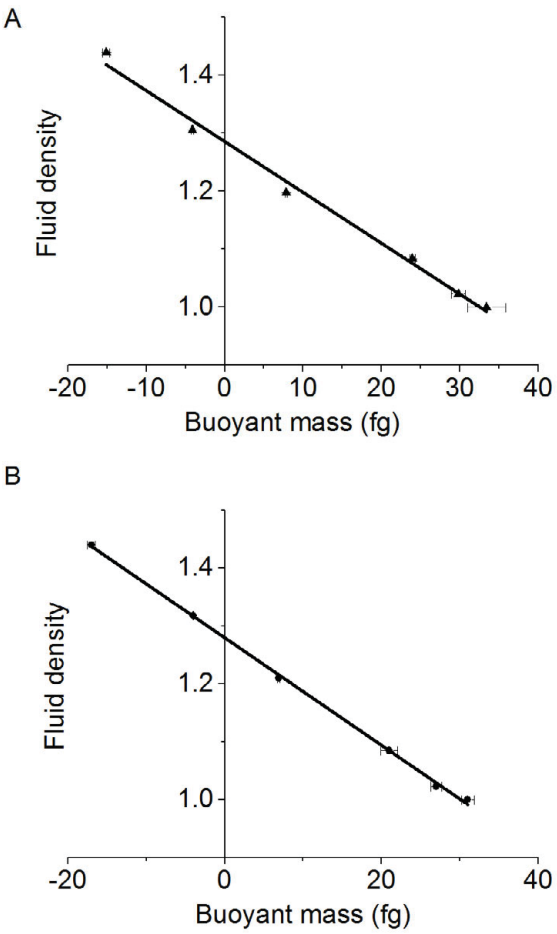

Supplementary Figure 3: Particle density of artificially stressed mAb2. Densities of mAb2 particles ((A) solvent-induced precipitation, (B) stirring) were determined by measuring the buoyant mass of each sample in 6 different surrounding media (water, PBS, D_2O, CsCl 20%, CsCl 30%, CsCl 40%).

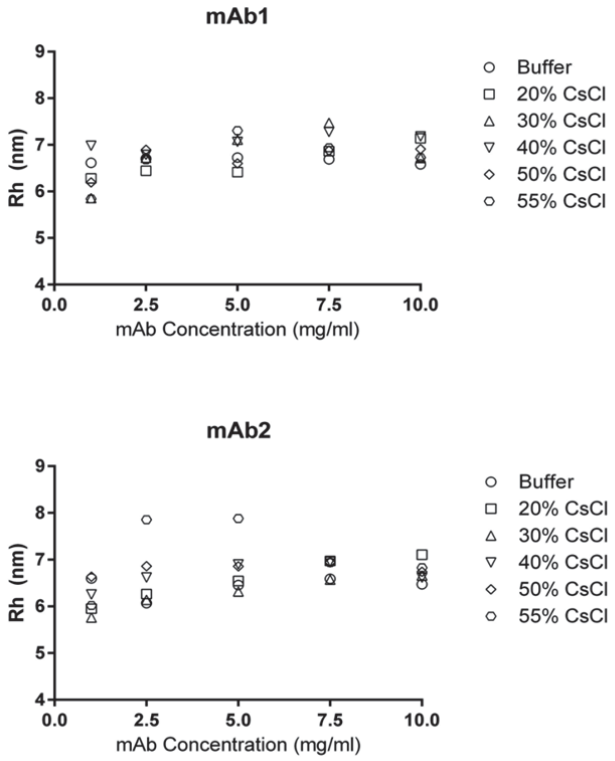

Supplementary Figure 4: Hydrodynamic diameter measured by DLS. The measurements were performed in 8 different surrounding media (water, PBS, D_2O, CsCl 20%, CsCl 30%, CsCl 40%, CsCl 50%, CsCl 55%) at 5 different protein concentration (1, 2.5, 5, 7.5 and 10 mg/ml) for mAb1 and mAb2.

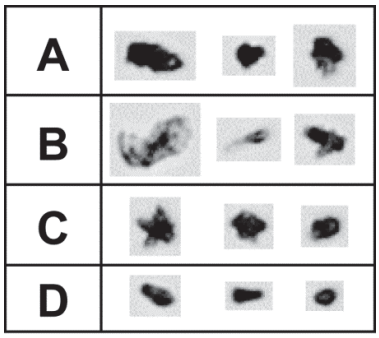

Supplementary Figure 5: Representative Flow Microscopy images of mAb1 particles. Those particles were generated using different types of stress. A) heat stress B) solvent precipitation, C) shaking stress, D) stirring.

CHAPTER 2

COMPARATIVE EVALUATION OF TWO METHODS FOR PREPARATIVE FRACTIONATION OF PROTEINACEOUS SUBVISIBLE PARTICLES – DIFFERENTIAL CENTRIFUGATION AND FACS

Pharmaceutical Research

Research Article

Keywords:
subvisible particles
particle fractionation
particle size
protein aggregation
proteinaceous particles

Authors:
Emilien FOLZER
Björn BOLL
Christof FINKLER
Jörg HUWYLER
Hanns-Christian MAHLER
Roland SCHMIDT
Atanas KOULOV

Abstract:

Purpose: The goal of this study was to compare and evaluate two preparative techniques for fractionation of proteinaceous subvisible particles. This work enables future studies to address the potential biological consequences of proteinaceous subvisible particles in protein therapeutic products.

Methods: Particles were generated by heat stress and separated by size using differential centrifugation and FACS (Fluorescence-activated cell sorter). Resulting fractions were characterized by size-exclusion chromatography, light obscuration, flow imaging microscopy and resonant mass measurement.

Results: Here we report the optimization and comprehensive evaluation of two methods for preparative fractionation of subvisible proteinaceous particles into distinct size fractions in the range between 0.25 μm and 100 μm: differential centrifugation and FACS. Using these methods, well-defined size fractions were prepared and characterized in detail. Critical assessment and comparison of the two techniques demonstrated their complementarity and for the first time – their relative advantages and drawbacks.

Conclusions: FACS and differential centrifugation are valuable tools to prepare well-defined size-fractions of subvisible proteinaceous particles. Both techniques possess unique and advantageous attributes and will likely find complementary application in future research on the biological consequences of proteinaceous subvisible particles.

Introduction

Protein aggregation takes place to a certain extent in all biotherapeutic formulations. Concerns are often raised and debated with regards to the theoretical potential for aggregates to cause an immune response in patients.[1,2] Because of possible biological consequences, such as immunogenicity or altered bioactivity and pharmacokinetics, particles of proteinaceous origin have recently received increased interest from industry, academia and regulators.[1,3-6] However, an undisputed general link between relevant clinical endpoints such as immunogenicity and subvisible particles in biotherapeutic preparations is still elusive. To date, the available data from *in vitro* and *in vivo* experiments are often conflicting and fragmented, which impedes coming to sound general conclusions. A major caveat of the published studies to date is the use of complex mixtures of therapeutic protein monomer, various aggregates and particle populations spanning a large range of sizes and possibly including a variety of chemical variations. However, potential effects generated by individual species (*i.e.* different size or modification) are difficult to delineate in such complex mixtures, as individual species are not easy to obtain. Studies using human interferon beta show that particles exposed to extreme artificial conditions e.g. metal oxidation or adsorption to glass induced an immune response in a transgenic mouse model.[7,8] Clinical data with different interferon beta products show an increased anti-drug antibody formation which cannot solely attributed to aggregates but also to formulation (can contain HSA), modifications in the primary sequence and impurities acting as adjuvants.[9] Furthermore, a sound characterization of complex mixtures used in these and other studies is often technically difficult or not feasible. Additionally, it has not been routinely employed by many groups studying the effects of subvisible particles generated by artificial stress conditions in various biological *in vitro* or *in vivo* models.

Thus, the reliable preparation of particles of such discrete sizes and their detailed characterization may provide significant advantage in further researching distinct species of proteinaceous subvisible particles in relevant *in vivo* or *in vitro* test systems, possibly being able to identify specific subvisible species primarily relevant for a potential biological consequence, if occurring.

Aggregation can be induced by a wide variety of stress conditions (especially, when protein is not adequately stabilized), including temperature stress, mechanical stress such as shaking and stirring, pumping, pH stress and freezing and/or thawing stress.[10] Such stresses can also lead to proteinaceous particles, which can be in the visible or subvisible size range.[10] The effect of different types of stress on the induction of protein particles and aggregates has been investigated extensively.[6,11-14] Depending on the protein and applied stress the resulting proteinaceous particles can range in size from nanometers to hundreds of micrometers. To characterize (subvisible) particle sizes, several methods have been applied to date and are in further assessment. Size exclusion chromatography is usually used for separation of soluble oligomeric (*i. e.* dimeric up to tetrameric) protein aggregates in the nanometer range[15,16], and is incapable to measure protein particles. For larger protein aggregates (nanometers and submicron), the use of asymmetrical flow field-flow fractionation (AF4) has been employed to measure proteinaceous particles with sizes between 50 and 250 nm.[17-19] However, the separation with AF4 and size exclusion chromatography leaves room for improvement in terms of size range and partition of protein aggregation. The separation of proteinaceous particles in a size range of 1 to 50 μm which was reported recently, utilized a fluorescence-activated cell sorter (FACS).[20] Centrifugation for fractionation has been used in various fields such as cell biology, bacteriology. or in the soil industry where species in the nm-, μm- and mm-size range have been successfully separated.[21-23] Commonly used centrifugation methods to fractionate nanoparticles, blood leukocytes, blood plasma and erythrocytes, cells, bacteria, DNA or soils implement sucrose gradient, cesium chloride gradient, iodixanol gradients or the use of Ficoll/Percoll.[24-30] However, the use of gradients has been shown to lead to contamination with new chemicals or residuals in the sample.[27]

FACS and centrifugation are two of the most promising techniques for fractionation of proteinaceous particles and a most recent report utilized versions of the two approaches to enrich proteinaceous particles for follow-up biological characterization.[31]. However, to date these methods have not been comprehensively studied and optimized protocols are not available. Here we report the production of several distinctly sized protein nano- and micrometer subvisible particle fractions using the methods: a) differential centrifugation separation and b) fractionation of particles using a FACS. Both methods enabled preparation

of well-defined size fractions of proteinaceous subvisible particles using a model mAb, as well as their detailed characterization. The two approaches were examined in detail and the experimental parameters that influence particle isolation, fractionation resolution, fraction purity, yield and other attributes were carefully evaluated, which allowed for the first time detailed characterization and optimization of these two particle separation strategies. Finally, we provide an assessment of the relative advantages and shortcomings of the two techniques.

Materials and Methods

Materials

One Roche proprietary IgG1 monoclonal antibody (mAb1) was used as model protein for these studies. The solution was filtered using 0.22 mm Millex GV (PVDF) syringe filter units (Millipore, Bedford, MA) before use.

Dulbecco's phosphate-buffered saline (DPBS) from GIBCO (Invitrogen, San Diego, California) was used when PBS is mentioned. Glycerol (for molecular biology, ≥99 %) was purchased from Sigma Aldrich (St. Louis, Missouri, USA).

Stress condition: heat stress

Thermal/shaking stress was applied using a Thermomixer fitted for 1.5 ml-tubes (Thermomixer Comfort, Eppendorf, Germany). 1 ml of the 25 mg/ml mAb1 solution was incubated for 3 min at 80 °C with 1400 rpm shaking. The temperature was chosen as being way beyond the melting temperature of the mAb1 (data not shown). The sample was then resuspended by drawing in and emptying out using a disposable Norm-inject 5 ml luer lock silicone free syringe (HENKE SASS WOLF, Tuttlingen, Germany) with attached 27 G x $1^{1/2}$" needle (0.40 × 40 mm) (Braun, Melsungen, Germany) for 20 consecutive times, in order to homogenize the solution and the generated insoluble matter. The bulk solution was stored at -80 °C after stressing. The sample was diluted with PBS to an optimal concentration of particles before fractionation using FACS.

Preparation of subvisible particles by differential centrifugation

A 5810R table-top centrifuge (Eppendorf, Germany) with a swing-bucket angle A-4-81 rotor (R=180 mm) was used for all centrifugation experiments.

1) *Empirical approach: selection of centrifuge time/acceleration/volume/media, multi-step preparation*

For fraction 1 (centrifugation-F1), 100 μl of initial stressed sample was overlaid on the top of 1.7 ml glycerol solution (25 % w/w) using a pipette. The eppendorf tube was then centrifuged for 180 sec at 25 × g. The supernatant was discarded, whereas the pellet was resuspended in PBS for analysis.

For the preparation of fraction 2 (centrifugation-F2) 100 μl of initial stressed sample was overlaid on the top of 1.7 ml glycerol solution (25 % w/w) using a pipette. The first centrifugation step was performed for 240 sec at 50 × g. The supernatant was collected in an eppendorf tube and centrifuged again for 220 sec at 50 × g. The resulting pellet was resuspended in PBS.

For the preparation of fraction 3 (centrifugation-F3), 1 ml of the initial stressed sample was centrifuged for 60 sec at 805 × g. After centrifugation the supernatant was collected and analyzed.

Fraction 4 (centrifugation-F4) was obtained by centrifuging 1 ml of centrifugation-F3 for 7 min at 1811 × g. The supernatant was then collected for analysis.

2) *Design Of Experiments: Optimizing empirical parameters and refining fractionation*

The experimental parameters to obtain fraction 1-4 were refined using Central Composite Face-Centered Designs (CCF) of experiment. The optimization for each fraction is described in detail in the supporting information.

Preparation of subvisible particles by preparative flow cytometry (FACS)

A BD FACS Aria IIu preparative cell sorter (BD Biosciences, San Jose, California) was used with BD FACSDiva v 6.1 software, applying the low-angle FSC detector equipped with a 488/10 band pass filter for the 488 nm laser. A flow cytometry size calibration kit (1, 2, 4, 6 10, and 15 μm) from Molecular Probes (#F-13838; Life Technologies, Zug, Switzerland) with non-fluorescent microspheres was used for the calibration and definition of the sorting gates. For all experiments, autoclaved PBS (pH 7.2) was used as sheath fluid, prepared using 10× stock solutions and deionized water. To eliminate contaminating particles from the sheath

fluid, the sheath line was equipped with 0.22 μm filter. Five milliliter 12 x 75 mm polypropylene round-bottom tubes (#352063, Corning Inc.) were used for fraction collection. All samples were filtered through 40 μm cell strainer (#352235, Corning Inc.) before sorting.

Size exclusion chromatography (SE-HPLC)

Samples were analyzed by UV absorbance detection at 280 nm. A TSK G3000 SWXL column (5 μm, 250 Å, 7.8 x 300 mm) from Tosoh was used for separation. The mobile phase (200 mM sodium phosphate, 250 mM KCl, pH 7.0) was pumped at a flow rate of 0.5 ml/min. Sample size for analysis was 25 μg. The stationary phase was kept at 25 ± 2 °C. 1 ml of each sample was centrifuged for 10 min at 14000 rpm before injection of the obtained supernatant. For each sample 25 μl was injected.

Light obscuration

A HIAC ROYCO instrument model 9703 (Pacific scientific, New Jersey, USA) was used for all light obscuration (LO) measurements. A small volume method using a rinsing volume of 0.4 ml and 4 runs of 0.4 ml each was applied, as described previously[14]. Flow rate was set to 10 ml/min. The first run was discarded and the average ± standard deviation of the last 3 runs was reported for each sample. Blank measurements were performed at the beginning of the measurements and in between samples using fresh particle-free water. The acceptance criterion for blanks was: "less than 5 particles > 1 μm". The system suitability test consisted of the measurement of count standards of 5 μm (Thermo Fisher count standards) with acceptance limits of ± 10 % the reported concentration for particles bigger than 3.0 μm was performed in the beginning of each measurement day.

Flow imaging microscopy

The initial samples as well as all collected fractions were analyzed by flow imaging microscopy (FI) using a MFI DPA4200 series instrument (ProteinSimple, Santa Clara, California) equipped with a 470 nm LED light source. All particles larger than 1 μm in equivalent circular diameter were reported, considering the lower limit of detection of equipment. Size and count standards (ThermoFisher, Reinach, Switzerland) were used to check consistency of the sizing

and counting accuracy of the instrument on the day of each measurement. The system was cleaned (before each measurement day) using 1 % (w/v) Tergazyme® (Sigma Aldrich, St. Louis, Missouri), followed by rinsing with water for 10 min. For these flushing steps, the flow rate was set to "maximum speed". Flushing with water was repeated after each sample. The "optimization of illumination" routine was performed prior to analysis, using filtered sample or PBS matching the buffer composition of the sample to be analyzed (*e.g.* filtered sample for measuring after heat stress or PBS to measure FACS fractions). For measuring, 1 ml of sample was placed in a 1 ml dual-filter tip on the inlet port.

Resonant mass measurement (RMM, Archimedes)

Resonant Mass Measurements (RMM) were performed using Archimedes system (RMM0017, generation 2) from Malvern instruments LTD (Malvern, United Kingdom). Micro sensor chips with internal microchannel dimensions of 8 μm × 8 μm were used for all the experiments. The calibration of the sensor was done using 1 μm Duke polystyrene size standards (Waltham, Massachusetts, USA) diluted in water to approximately 10^6 part/ml. The calibration was finalized after 300 particles were detected as recommended by the manufacturer. The particle density for proteinaceous particles was defined as 1.28 g/ml. Before measurement, one ml of the sample to be analyzed was centrifuged 5 min at 1258 ×g in order to remove large particles that could block the sensor during RMM. The influence of the additional centrifugation step on the particle concentration can be seen in Supplementary Figure 7. Measurements were performed in triplicates and the sensor was filled with fresh sample during 40 sec before each measurement. The limit of detection (also called threshold) was manually set to 0.015 Hz for each analysis. Each measurement stopped either after one hour of measurement or when a total of 4000 particles were detected. During measurement, the "autoreplenish" function was automatically activated every 500 sec for 5 sec to load fresh sample and avoid settling down of particles in the sensor and tubings.

Results

The aim of this study was the development, comprehensive evaluation and comparison of methods for the preparative fractionation of proteinaceous subvisible particles, with diameters ranging from hundreds of nanometers to approximately hundred micrometers. Two different methods were evaluated. Besides the two reported methods, other techniques such as sequential filtration, gravitation, asymmetrical flow field-flow fractionation or gel chromatography were initially also tested for their applicability to isolate different size fractions. However, these methods had limitations in their usable size range or sample amount.

First, a differential centrifugation fractionation of proteinaceous particles was developed and carried out to obtain a number of discrete fractions of various sizes spanning the range mentioned earlier. In order to optimize the method and process parameters, a statistical design of experiments approach (DoE) was applied. Second, fractionation of proteinaceous particles using preparative FACS strategy, comparable to the method reported elsewhere, was applied.[20] The factors influencing the quality of separation in both methods were examined in detail. Light obscuration (LO), Flow Imaging (FI), flow cytometry and Resonant Mass Measurements (RMM) were used to measure the particle size distributions of the resulting fractions. The digital images generated by the FI measurements allowed an approximate calculation of ratio of protein particles contained in these fractions. RMM was used for the detection and quantification of submicron particles.

Generation and characterization of subvisible proteinaceous particles

In order to generate sufficient amounts of proteinaceous particles for method assessment, a starting solution of therapeutic IgG1 protein product with concentration of 25 mg/ml was heated to 80 °C for 3 min which lead to the extensive particle formation. After this treatment, the relative protein monomer content in the supernatant was below 0.05 % and no nanometer aggregate formation could be detected by size exclusion chromatography. After heat stress, the resulting samples contained particles in a broad size range (see Figure 1A). The harsh treatment described above generated numerous very large particles which were broken up

into smaller species by drawing and pushing these through a 27G x 1.5“ needle mounted on a 5 ml disposable syringe, resulting in a typical decay distribution with increasing size (see also Figure 1B). The proteinaceous particles prepared using this technique demonstrated adequate stability upon dilution in PBS and in the media used in all experiments (measured by flow imaging microscopy – see Supplementary Figure 8). Furthermore, the particles produced using the procedure described above were sufficiently stable upon freeze/thaw and storage at -80 °C (Supplementary Figure 8), to allow sample storage.

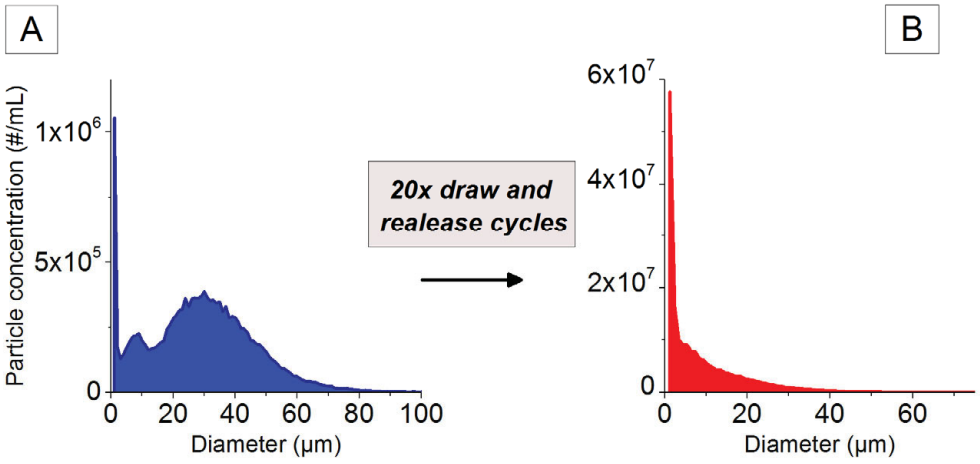

Figure 1: Size-distribution obtained suing MFI of the sample after heat/shake stress (A) and consequent application of 20 syringe draw and release cycles (B).

Fractionation of subvisible proteinaceous particles using differential centrifugation

An empirical approach for centrifugation using adapted Stokes law [$T = 9\ln/(2r^2(\rho_p-\rho_s)\omega^2R]$ where T represents the centrifugation time, r is the radius of a sphere, ρ_p is the density of the particle, ρ_s stands for the density of the solution, ω is the angular velocity of the centrifuge and R is the rotor radius, was used to isolate four different fractions of high purity (approximate mean diameters; 0.4 µm, 1.5 µm, 15 µm and 40 µm). These experiments informed the definition of the critical experimental parameters that might have an impact on the fractionation performance.

In order to extend centrifugation times to practical length, to slow down the sedimentation of large particles and prevent co-sedimentation of particles of different sizes, we noticed that it

was necessary to increase the viscosity of the medium. This was achieved by the addition of glycerol to varying concentrations (see Table 1). A content of 25 % glycerol (w/w) was sufficient to maintain large particles (>15 μm) in suspension and avoid rapid sedimentation. To verify that the use of glycerol did not impact the morphology of the particles flow imaging microscopy measurements were carried out. Indeed, particles which were in contact with glycerol during the fractionation procedure and consequently resuspended in PBS did not show any measurable difference in their size, circularity, aspect ratio and object intensity parameters in comparison to particles that did not have contact with glycerol (data not shown). Moreover, the amount of glycerol remaining after centrifugation and resuspension of pellets in PBS was estimated (based on pellet/fraction volumes) to be relatively low (approximately 2.5 % (w/w)). To arrive at these initial parameters for the empirical approach, a broad screen was carried out in a large number (~1000) of experiments which explored the following parameter ranges: centrifugation time in the range of 30 seconds to 6 hours, acceleration in the range of 8 ×g to 3226 ×g, and glycerol concentrations from 0 to 100 % . As a guide to future experiments, we would suggest the user to begin with the parameters outlined in Table 2 and adapt them in order to fulfill their requirements.

Table 2: Centrifugation parameters to obtain four different fractions, including final results obtained with empirical approach and optimized results using a DoE. Techniques used to measure individual fractions: Microflow Flow Imaging (MFI) and Resonance Mass Measurement (RMM)

Name	Target/ mean size expected	Process	Variables for centrifugation: time, acceleration, and glycerol concentration	Particle concentration [#/ml]	Mean diameter measured in µm	Comments
centrifugation-F1	Larger than 40 µm	empirical	180 sec-25 ×g-25 %	1.5 x 10^5 (MFI)	38.1 (MFI)	Higher particle concentration and larger mean diameter
		optimized by DoE	200 sec-48 ×g-26.8 %	1.6 x 10^5 (MFI)	42.3 (MFI)	
centrifugation-F2	15 µm	empirical	240 sec-50 × g-25 % + 220sec-50×g	1.5 x 10^5 (MFI)	17.8 (MFI)	Lower particle concentration for particle larger than 25 µm
		optimized by DoE	260 sec-72 ×g-25 % + 180 sec-72×g	1.5 x 10^5 (MFI)	15.3 (MFI)	
centrifugation-F3	Close to 1 µm	empirical	60 sec-805 ×g	8.0 x 10^5 (MFI)	1.33 (MFI)	Lower particle concentration but smaller mean diameter (*i.e.* lower amount of bigger particles)
		optimized by DoE	160 sec-846 ×g	4.2 x 10^5 (MFI)	1.25 (MFI)	
centrifugation-F4	Smaller than 0.5 µm	empirical	7 min-2051 ×g	4.1 x 10^6 (RMM)	0.43 (RMM)	Lower particle concentration but smaller mean diameter (*i.e.* lower amount of bigger particles)
		optimized by DoE	11 min-2465 ×g	2.1 x 10^6 (RMM)	0.36 (RMM)	

In a second step, a design of experiments (DoE)-approach was used to further optimize and refine the fractionation parameters. For this approach a response surface methodology (RSM) and a Central Composite Face-Centered Designs (CCF) were utilized due to their flexibility, efficiency and the fact that the experiments could be run sequentially. The empirically optimized fractionation parameters in the first step of the method development served as center points of each DoE. The aims of the DoE optimization (optimal responses) were high purity and high particle concentration in the desired size range. Therefore, the variables (*i.e.* acceleration, centrifugation time and glycerol concentration) and responses were selected in each case as described in Table . Each optimal point was confirmed experimentally to verify the predicted optimal conditions. After each successful confirmatory run the respective fractionation using those optimal conditions was repeated in larger scale in order to perform the full analytical characterization (SE-HPLC, RMM, FI, LO).

Using the DoE optimization it was possible to refine the experimental parameters in order to obtain higher particle concentration and/or reach size targets for four different fractions as described in Table and Figure 2. The proportion of the variation of the response described by the model (R2) shows in all the cases that the data was accurately modeled (see Supplementary Figure 2B, Supplementary Figure 3B, Supplementary Figure 4B, and Supplementary Figure 5B). The high values obtained for the proportion of the variation of the response predicted by the model according to cross validation (Q2) allow good model prediction in each case. Moreover, the models were deemed to be valid as demonstrated by validity values larger than 0.25 for each model (indicating no lack of fit) as depicted in Supplementary Figures 2B to 5B.

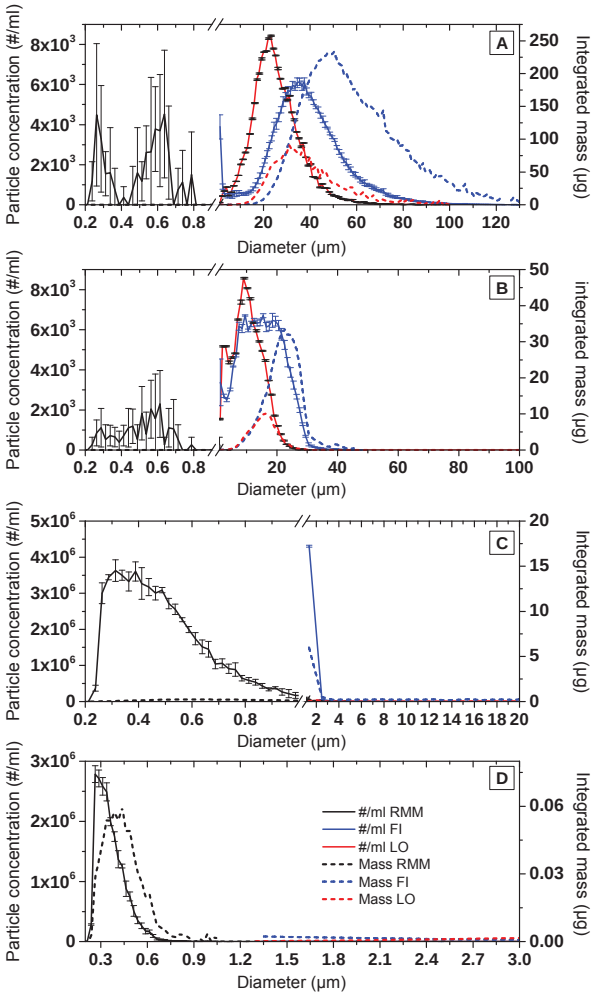

Figure 2: Particle concentration (solid lines) and integrated mass (dashed lines; see Materials and Methods for detailed description of the calculations) for fraction 1 (A), fraction 2 (B), fraction 3 (C), fraction 4 (D) obtained by centrifugation with optimized conditions. Results from RMM are shown in black, FI measurements in blue and LO - in red.

The size distributions of the four DoE optimized fractions described above were measured using LO and the additional characterization methods FI and RMM (see Figure 2). Besides the minor discrepancy between the distributions reported by LO and flow imaging microscopy (observations also previously reported in literature).the results presented in Figure 2 demonstrate that the resulting fractions had high particle concentrations in the targeted size ranges, high purity as indicated by low content of small particles in large fractions (centrifugation-F1 and centrifugation-F2) and low content of large particles in the small

fractions (centrifugation-F3 and centrifugation-F4).[32,33] Representative FI images of particles from the different fractions can be found in Supplementary Figure 6.

As seen in Figure 2, defining features (and major advantages) of the differential centrifugation approach were: a) the relatively high concentrations of particles that can be achieved in the final fractions and b) the broad size range that can be accessed using this method. Resuspension of the pellet (for fractions containing large particles) allowed adjusting the particle concentration and the buffer composition to user requirements. Moreover, contamination of large size fraction with nanoparticles was nearly completely eliminated by adding glycerol during the centrifugation process.

Fractionation of subvisible proteinaceous particles using FACS

For the preparation of micrometer-sized subvisible proteinaceous particles, the same starting material was used as for the centrifugation approach (see Materials and Methods section). In principle, preparation of nanometer-sized particle fractions by FACS is also possible, although using this approach restricts the sample to low final protein concentrations. These low concentrations may present challenges for follow-up biological characterization studies. The sizes of the target fractions were estimated using a FACS size calibration kit containing beads with an approximate diameter of 2, 4, 6 and 15 μm and the Forward Scatter (FSC-A) signal. The cell sorter used in this study (see Materials and Methods section) allows simultaneous sorting of four different size-fractions. The position and the broadness of gates were set to achieve very narrow size-fractions (see Figures 3 and Figure 4.). However, it needs to be pointed out that narrow gates require more material and longer sorting times (see Supplementary Figure 1). The particles were sorted (with settings “4-way purity”) applying the gate limits defined above. After sorting, all fractions were measured using flow cytometry (see Figure 3) The polystyrene beads, as well as the sorted proteinaceous particles where measured using FI (for representative images see Figure 3 B and C). As seen in Figures 3 and 4 all fractions were in excellent agreement with the polystyrene beads of similar size and the final size distributions matched the pre-determined gates which was confirmed by the additional analytical methods applied.

The first experimental parameter explored in detail was the nozzle size. Using different nozzle sizes influenced the particle concentration of the sorted fractions. As expected, larger nozzle sizes lead to larger drops containing more sheath fluid (PBS) and sample buffer (also PBS). Thus, the risk of coincidence of two or more particles per drop is higher for larger drops and the drop frequency is much lower compared to streams from smaller nozzles. In addition, larger nozzle sizes require less pressure and exert a less harsh mechanical treatment to particles. Conversely, some of the disadvantages of smaller nozzle size are the higher tendency for clogging of the orifice and also spraying of the stream by partial blocking and the resulting diversion of the stream. Larger particles may cause a deflection of the stream by partial blocking the nozzle and therefore mis-sorting when passing through the nozzle. After testing all three available nozzles, the 100 μm nozzle was chosen as optimal for the target fractions, because it applied the softest conditions in matters of pressure and mechanical stress from passing the nozzle.

The optimal number of events per second (*i.e.* number of particles) in FACS is a quarter of the overall drops per second (manufacturer's recommendation). Therefore, in the case of the 70 μm nozzle with a drop rate of 90 kHz, the optimal rate is ~22000 events/sec and for the 100 μm nozzle with a drop rate of 30 kHz the optimal rate is ~7500 events/sec. In cases where higher concentrations of particles in the starting solution were used, a higher discard rate of drops by the instrument was observed, which resulted in an increased probability of coincidence of two or more particles in one drop (not separated). Therefore, the concentrations of particles in the starting material were adjusted below 7500 events/sec by dilution with PBS (sheath fluid). It needs to be pointed out that using a buffer different from the sheath fluid may lead to false positive results due to differences in the refractive indices or in rare cases foaming.

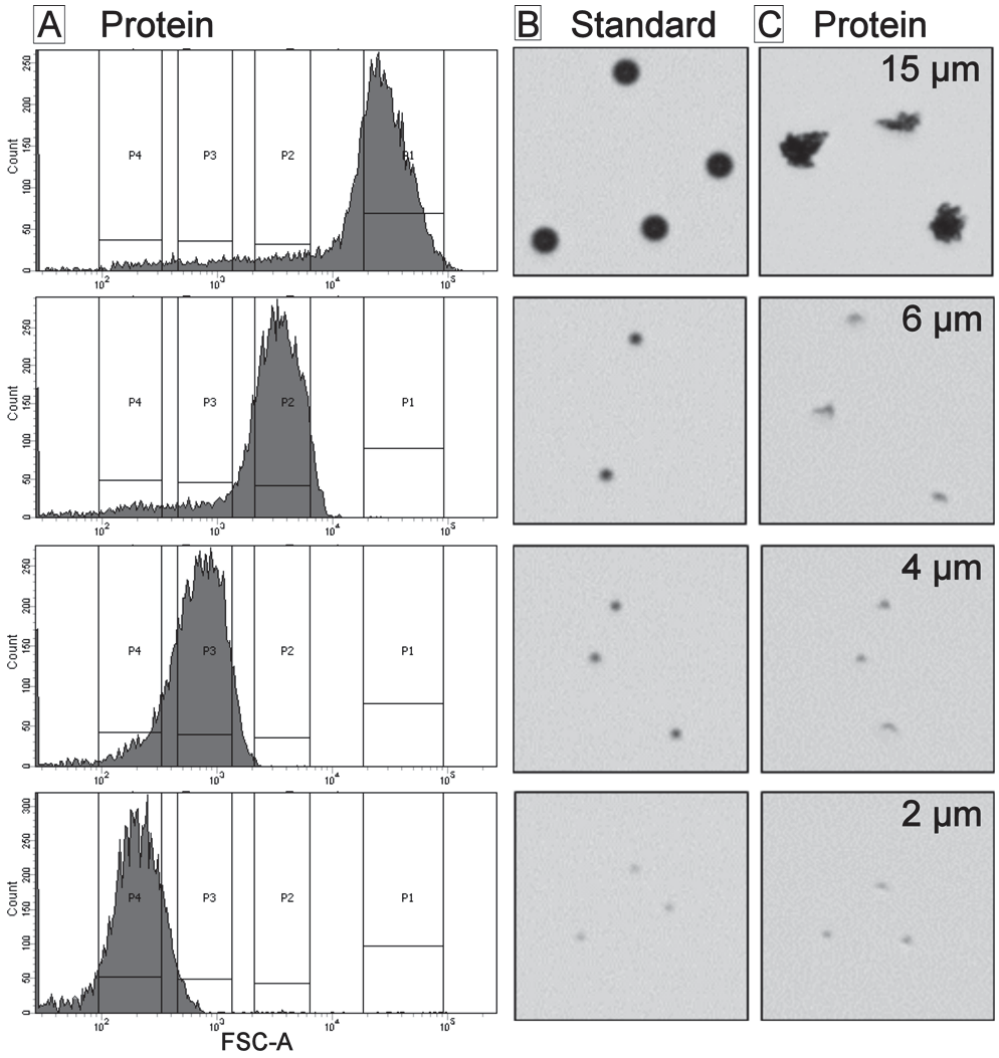

Figure 3: Fractions sorted using FACS and re-analyzed with flow cytometry (A). Flow imaging microscopy images of the size-standards used in the FACS experiments for gate determination (B). Representative FI images of protein fractions after FACS sorting (C).

The resulting sorted fractions were analyzed using flow cytometry (Figure 3A), LO and FI (to quantify the particles larger than 1 µm) and RMM for submicrometer particles (Figure 4A-D). The results from all size-distribution measurements were consistent between all methods with a small shift to smaller sizes in the case of LO measurements. This minor undersizing effect has been described previously in reports that have reported smaller and fewer particles in LO as compared to flow imaging microscopy.[32,33] The content of submicrometer particles in all four FACS fractions determined by RMM was several million particles per ml (Figure 4). These smaller particles could not be measured and fractionated by FACS due to the technical

limitation of this method to detect only scattered light of particles larger than the laser wavelength. All particles smaller than this threshold cannot be detected and end up in all FACS-sorted fractions. Therefore, after sorting, the samples did contain not only particles of the desired size but also a small amount of “contaminating” particles of smaller (submicrometer-sized) and larger sizes. This can be attributed either to a) the possible break-up or aggregation of particles upon sorting due to the mechanical forces that are applied apart, b) coincidence of two particles in one drop or c) partial blocking of the nozzle by large particles causing diversion of the stream. One strategy to increase the purity of the fractions is by resorting the already sorted fractions[20]. However, it was found that resorting only led to a small increase in the purity, but in a large decrease in the concentration of particles. In comparison to a previous study[20], the purity of the individual initial fractions in the current report was very high and therefore, a resorting was not justified. The relatively high purity after the first sort was attributed to the higher stability of the particles as compared to the previous report. Data regarding the stability (reversibility) of fractions after freeze/thaw can be found in Supplementary Figure 8 (FACS fraction 1 and fractions generated by differential centrifugation given as examples). A comparison of the fractions generated by centrifugation and FACS can be found in Table 3.

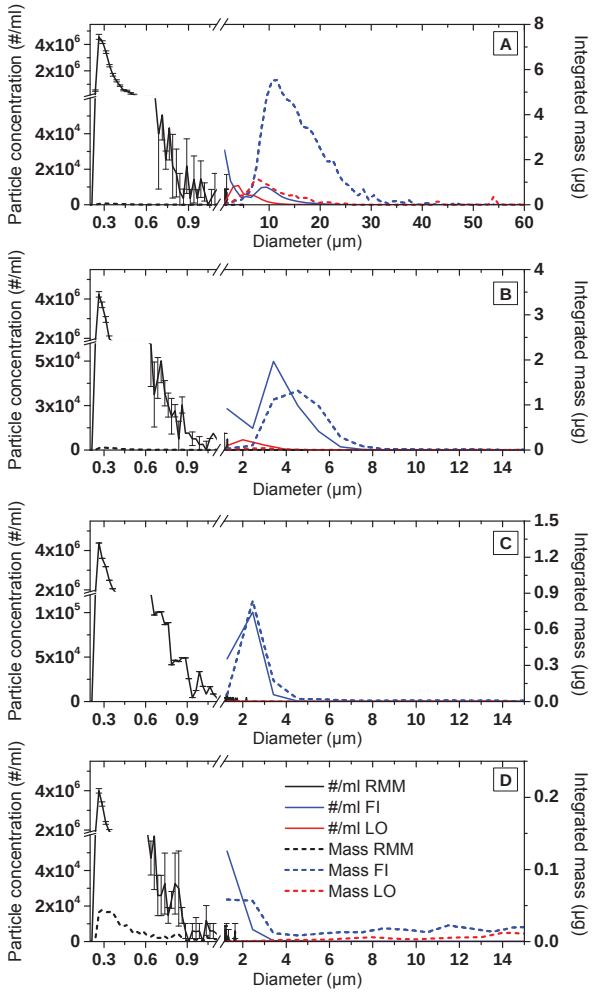

Figure 4: Particle concentration (solid lines) and integrated mass (dashed lines; see Materials and Methods for details on calculation) for fraction 1 (A), fraction 2 (B), fraction 3 (C), fraction 4 (D) isolated by FACS. Results from RMM are shown in black, FI measurements in blue and LO - in red.

Table 3: Summary for fractions isolated via centrifugation or FACS

Parameters	*centrifugation-F1*	*centrifugation-F2*	*centrifugation-F3*	*centrifugation-F4*	*FACS-F1*	*FACS-F1*	*FACS-F3*	*FACS-F4*
Flow imaging microscopy particles/ml (1-200 µm) ± SD	2.0×10^5 $\pm 4.0 \times 10^3$	1.5×10^5 $\pm 3.6 \times 10^3$	4.4×10^6 $\pm 2.4 \times 10^4$	1.6×10^3 $\pm 1.2 \times 10^1$	1.3×10^5	1.2×10^5	1.6×10^5	0.6×10^5
Light obscuration particles/ml (1.3-100 µm) ± SD	1.7×10^5 $\pm 2 \times 10^3$	1.1×10^5 $\pm 4.5 \times 10^2$	1.0×10^5 $\pm 2.4 \times 10^3$	1.5×10^2 $\pm 1.4 \times 10^1$	6.8×10^4 $\pm 6 \times 10^2$	1.2×10^5 $\pm 1.8 \times 10^2$	6.7×10^2 $\pm 2.9 \times 10^1$	5.1×10^2 $\pm 2.7 \times 10^1$
RMM particles/ml (0.2-5 µm) ± SD	4.0×10^4 $\pm 1.6 \times 10^4$	2.0×10^4 $\pm 1.5 \times 10^4$	1.0×10^8 $\pm 1.6 \times 10^4$	2.1×10^7 $\pm 2.8 \times 10^5$	1.7×10^7 $\pm 5.9 \times 10^5$	2.4×10^7 $\pm 8.3 \times 10^5$	1.9×10^7 $\pm 5.4 \times 10^5$	2.1×10^7 $\pm 3.5 \times 10^5$
Mean diameter (µm) + (instrument used to measure)	38.8 µm (FI)	15.3 µm (FI)	1.25 µm (FI)	0.36 µm (RMM)	13.1 µm (FI)	4.5 µm (FI)	2.3 µm (FI)	1.6 µm (FI)
Working fluid	PBS or placebo buffer	PBS or placebo buffer	PBS or placebo buffer	PBS or placebo buffer	PBS	PBS	PBS	PBS
Additives	Glycerol	Glycerol	none	none	none	none	none	none

Discussion

In this study a number of method attributes were evaluated in order to understand the applicability of the individual methods and define a toolkit for characterization of proteinaceous subvisible particles that researchers can use in future studies. The size-range, resolution, purity and yield and some additional factors were systematically assessed.

Size-range

Naturally, both methods examined in this study are restricted in their working size-range by physical limitations related to the separation principle or the instrumentation used. For example, the smallest particles that FACS can theoretically separate have a diameter of 0.5 μm. The lower detection limit could in principle be improved by increasing the angle of the forward scattering (FSC) detectors because particles with sizes near and below the laser wavelength (nanometer-sized particles) scatter proportionally more light at larger angles.[34] The limit is also dependent on the instruments settings for the detector voltage of the forward and side scatter detectors. It has been shown that detector voltage settings for detection of very small particles (0.5 to 3 μm) are not suitable to distinguish between larger sizes (larger than 3 μm) and settings for larger particles (larger than 1 μm) results in the loss of sensitivity for particles smaller than 1 μm[35]. The upper size-limit of FACS instruments is dependent on the nozzle size. As a general recommendation the manufacturer suggests not to exceed an object size of 50 μm for this specific instrument.

In contrast to FACS, centrifugation-based separations are less restricted in their working size-range. As a consequence, the differential centrifugation method described here can be used to preparatively separate a much broader size range of particles as compared to FACS-particles between the sizes of 0.2 μm and 100 μm can be easily separated. Therefore, one major advantage of differential centrifugation is its suitability for preparation of submicrometer particle fractions. In addition, as demonstrated in this study (see Figure 2A.), particles larger than 40 μm can be easily separated as well. The possibility to obtain particle fractions of different sizes ranging from low-nanometer to larger than 100 μm in the same experiment is a major advantage of differential centrifugation. However, it needs to be mentioned that

obtaining multiple size-fractions in a single experiment requires the use of an additive to increase the viscosity of the medium (*i.e.* glycerol or sucrose) in order to avoid cross-contamination of the different fractions.

Resolution

A major difference between both methods is the resolution of prepared fractions. With flow cytometry it was possible to prepare particles in a very narrow size window, *e.g.* 2 μm (Figure 4). The differential centrifugation method allowed isolating fractions with approximate mean diameters of 0.4 μm [0.2-0.8 μm], 1.5 μm [0.2-2.5 μm], 15 μm [1-30 μm] and 40 μm [10-60 μm], whereas FACS fractionation method separated fractions with mean diameters of 2 μm, [1-3 μm] 4 μm [3-5 μm], 6 μm [5-7 μm] and 15 μm [5-25 μm]. With exception for submicron fractions, the centrifugation method generated rather broad size distributions. For example, comparison of the 15 μm fractions generated by FACS (Fraction 1, Figure 4A) and differential centrifugation (Fraction 2, Figure 2B) show a very broad distribution for the fraction using the second method. In contrast, the 15 μm fraction generated by flow cytometry was much narrower in size range. Very narrow fractions of 2, 4 or 6 μm mean particle diameter have also been generated using FACS, which was not possible with the centrifugation method. Whereas obtaining fractions of discrete sizes using centrifugation was challenging and might need further development. In principle, the FACS method can be used to generate even more narrow fractions than the ones reported here. Naturally, one drawback associated with such efforts would be the requirement for more material and longer fractionation run times. The time for sample preparation with both methods is very different and depends highly on the initial sample and its preparation. As stated in Table 3, differential centrifugation uses more time than FACS mainly because of the higher sample amount requirements. The fractionation run time (*i.e.* the instrument time that was needed for either centrifugation or FACS, not counting the time for sample preparation or setup of the instrument) for 1 ml of both 15 μm fractions is 8 min for centrifugation and 5 min with FACS. Any changes in size range of the desired fraction and particle concentration of the initial sample can significantly change these time frames.

Table 4: Comparison of the attributes of FACS and differential centrifugation methods with respect to the generation of micrometer-sized subvisible particle fractions

Attribute	Method	
	Differential centrifugation	***FACS***
Presence of nanoparticles	low	high
Resolution	medium	high
Yield	high	low
Size range	large	medium
Preparation time	long	medium
Additives needed	yes	no

Purity and yield

One drawback of the FACS fractionation method is the inability to detect particles smaller than 0.5 μm due to physical limitations in the detection with laser light scattering. This leads to contamination of all FACS fractions with small particles which can be detected using alternative methods (*e.g.*, RMM, FI). Indeed, RMM confirmed the presence of nanoparticle contaminants in the FACS fractions (Figure 4A-D). Although, resorting of the initial fractions did minimize the nanoparticle contamination, the improvement was attributed largely to the dilution effect rather than specific removal of submicrometer particles. More importantly, the differential centrifugation method does not have this limitation. Figures 2A and 2B show a very low content of submicrometer particles in the micrometer fractions (Fraction 1 and 2). This also suggests an interesting approach to achieve very pure and also narrowly sized fractions – a combination between FACS and centrifugation fractionation. More specifically, a first-pass centrifugation step could be applied to remove the nanoparticles present in a sample. As a second step the micrometer centrifugation fractions can be separated using FACS to generate well-defined fractions of specific sizes. Alternatively, the approach can be reversed centrifuging FACS-generated fractions to separate micrometer from nanometer particles. However, the latter approach may be impractical due to the necessity for viscosity additives (*e.g., g*lycerol).

Although some of the fractions generated in this study did contain certain amounts of "contaminating" nanoparticles, if calculated in terms of protein mass the impact of this

contamination was negligible. Flow imaging microscopy and RMM data can be used to perform such calculations of the total protein mass of the particles present in every sample based on the digital image analysis (taken in Flow imaging microscopy) or on the buoyant mass (RMM).[36-37] Such calculations for the fractionation experiments presented here showed practically no influence of the submicrometer particles on the protein content of micrometer fractions generated by FACS and centrifugation (Figure 4A-D and Figure 2A-B). However, the mass calculations reveal an important practical aspect of the fractionation of subvisible particles – *i.e.* the fractions of the smaller-sized particles contain much less protein than the larger-sized fractions. This effect is a natural consequence of the power relationship between size and volume (*e.g.* sphere=$\frac{4}{3}\pi r^3$). Interestingly, the impact of this effect seems to be larger in the FACS fractionation method, which can be attributed to the higher purity of the individual fractions.

The particle concentration generated by FACS is limited by the fact that the flow cytometer sorts drops of buffer and sheath fluid of the same size. Drops with smaller particles therefore, contain relatively more sample fluid than large drops that almost fill out the whole drop. This can also be seen at the particle concentration measured by FI of the FACS fractions 1 to 3 indicating that the same number of particles is present in the same volume. Fraction 4 has a lower particle concentration due to the detection limit of the FI instrument. Therefore, FACS cannot be used to create concentrated fractions, but might be combined with centrifugation to concentrate and also to remove submicron contamination from the fractions as described above. Using centrifugation it would possible to reach even larger protein concentrations (than those presented here) for fractions including the resuspension of a pellet (Fraction 1 and 2). Indeed, each pellet was resuspended in 1 ml of PBS in our study but for some other purposes the number of pellets or the initial volume could have been increased and resuspended in smaller volumes (data not shown). Although the primary target was purity of the fractions, we calculated the recovery yield for both 15 μm fractions generated with FACS and centrifugation. The initial sample contains 86 million particles/ml in the size range between 5 and 25 μm which is diluted 1 to 5. The FACS fraction 1 contains only 60000 particles/ml, *i.e.* 0.35 %. For centrifugation fraction 2 the initial sample was diluted 1 to 10 and

contains 150 000 particles/ml, *i.e.* 1.75 %. However it needs to be pointed out that 1 ml of initial sample yields more than 1 ml after FACS sorting.

Other factors

An important consideration in setting up fractionation of subvisible particles using the methods described in this study is the particle concentration in the samples. For example, in flow cytometry the number of particles should not exceed the number of drops per second (*e.g.* 7500 events per sec with the 100 μm nozzle) in order to avoid coincidence of two or more particles in the same drop. Thus, high particle concentrations can lead to either mis-sorting and/or to slower sorting rates because of discarded drops containing multiple particles. In the case of centrifugation we only tested experiments using protein solutions with concentrations of up to 25 mg/ml. It is conceivable, that higher concentrations might need to be diluted before centrifugation to prevent an interaction between large and small particles.

The centrifugation-based approach to fractionation of particles larger than 5 μm requires the addition of viscosity modifiers (*e.g.,* glycerol) to reduce the sedimentation speed and improve the fraction purity. In fact, it is exceedingly difficult to isolate proteinaceous particle fractions of large mean diameter (*e.g.* 30-40 μm) without the use of glycerol. Our first attempts to generate such fractions without glycerol always contained a large number of smaller particles (0.2 to 2 μm). Of course, the use of glycerol may potentially result in additional complications – for example, the addition of glycerol may induce changes in the particle size- or morphology distributions. This was not the case in the experiments reported here and such changes were not observed or reported in the literature, but it remains a theoretical possibility which needs to be carefully controlled. A further practical aspect of the use of glycerol for fractionation by centrifugation is the fact that small amounts of glycerol are carried over after resuspension of the fraction pellet into working medium (buffer) resulting in the presence of glycerol in the final fractions (albeit in very low concentrations, *i.e.* 2.5 % w/w). Conversely, for the preparation of FACS fractions no additives are necessary, which may be an additional factor in choosing a fractionation method. The dilution of the samples fractioned by FACS can be done using any buffer, which in turn can be used as a sheath fluid in the FACS instrument

with the only caveats that the buffer should not foam and needs to contain a sufficient amount of ions for charging and deflection.

Another major difference between both methods is the type of physical stress that is applied to the particles during the fractionation process. During centrifugation the samples experience centrifugal forces and perhaps shear stress; during flow cytometry fractionation several different types of stress are present. For example, in the flow cell a pressure of up to 70 psi (4.82 bar) is applied (depending on the nozzle size), which could impact the sample in either way. It has been reported that high pressure can be used to dissociate aggregates and refold protein, however, the pressure used in that study was significantly higher (2000 bar) and therefore such effect is likely irrelevant.[38] In the flow cell of the flow cytometer the particles pass through laser beams and the surrounding liquid is repeatedly charged negative and positive using electrical potential of ± 40 to 80 V. After exiting the flow cell, the particles pass through a small orifice and return to atmospheric pressure, experiencing shear and cavitational forces. Afterwards, the sample is accelerated to 20 m/sec and passes through an electric field of 3 to 5 kV/cm before hitting a liquid surface or a solid tube wall. There are alternative cell sorters available that divert the particles mechanically or by an air stream instead of electrostatics, but these instruments have a maximal drop rate of 2 kHz and therefore 10 fold slower than the instrumentation used in this study. As a side note an instrument using air stream (Union Biometrica, Inc.) for sorting is capable to sort particles up to 1,500 μm as advertised by the manufacturer. In relation to the physical stress it needs to be mentioned that the stability of the particles to be fractionated (their ability to remain intact, *i.e.* irreversibility) is important. Although particle stability in FACS sorting was shown for stir stress[31] as well as syringe shear-cavitation stress[20], particles generated under different conditions with other proteins might demonstrate different stability behavior. For example, our experience with particles of the same IgG used in this study produced by stir stress was that they were not suitable to create fractions larger than 5 μm because these particles were fragile for this particular protein and this particular stress condition.

All technical challenges of mechanical, electrical or chemical nature mentioned above may have impact on the proteinaceous particles. Depending on the further use of the generated

fractions, (*e.g. in vivo* or *in vitro* biological assays) it might be necessary to assess possible physico-chemical changes induced by the separation process, particularly if the protein is sensitive to the types of stress exerted during fractionation. In such cases, additional investigations should be taken into consideration. It is recommended to consider CE-SDS to check degradation and covalent linkage, and RP-HPLC and peptide mapping to check for modifications like oxidation or deamidation of amino acid residues.[39] Furthermore, it may be relevant to assess potential changes in the secondary and tertiary structure using spectroscopic techniques such as circular dichroism (CD), Fourier transform infrared- (FTIR), and Fluorescence- or Raman spectroscopy. For the subsequent use in *in vivo* or *in vitro* assays it may also be important to check the endotoxin content. In principle both methods can produce fractions that have low endotoxin content if the necessary precautions are taken. A procedure to prepare a FACS for endotoxin-free sorting has been published recently[31] and is also available from some instrument manufacturers (*e.g.* BD: prepare for aseptic sort). Finally, it should be pointed out that irrespective of the separation method particle size-fractions though enriched in size may still contain conformational or chemically heterogeneous populations.

Conclusions

Here we report a comprehensive evaluation and optimization of the experimental parameters of two new methods for fractionation of proteinaceous subvisible particles of sizes between approximately 0.2 μm and 100 μm: differential centrifugation and FACS. Applying the optimized method parameters size-fractions of proteinaceous subvisible particles were isolated using both techniques and the methods' attributes such as size-range, resolution, fraction purity and yield were assessed. It was found that both techniques present advantages and disadvantages (see Table for a summary) and will likely find complementary use in the research practice. Further research will focus on assessing immunogenicity in *in vitro* models of various fractions of protein aggregates and particles.

Acknowledgements

We thank Tarik Khan for editorial help, Gabriela Quebatte and Adeline Boillon for helpful discussions and Marc Bedoucha for providing access to instrumentation and technical assistance.

Associated content - Supporting information: Optimizing fraction 1-4 (obtained by centrifugation) with a Design of Experiments

Fraction 1:

The time length (60 to 300 sec), the acceleration (8 × g to 50 × g) and the glycerol concentration (10-40 % w/w), were identified as critical parameters for this single centrifugation step, based on previous experience. A Central Composite Face-Centered Design (CCF) of experiment was used including three center point experiments which resulted in 17 runs (see Supplementary Table 1). After each run, the pellet was resuspended in 1 ml of PBS and analyzed.

Fraction 2:

Fraction 2 was obtained in two steps that were evaluated separately in two separated designs of experiments (DoE). For the first centrifugation step the time length (60 to 420 sec), the acceleration (8 to 129 × g) and the glycerol concentration (10 to 40 % w/w) were considered in a CCF design including three center point experiments, resulting in a total of 17 experiments. Once the optimum was set for step 1, supernatant of different tubes were pooled in order to optimize step 2.

Development for step 2 also utilized a CCF design (2 parameters, 11 experiments including three center point experiments). The time-length (60 to 300 sec) and the acceleration (8 to 129 × g) were considered for the experiments. After each run, the pellet was resuspended in 1 ml of PBS and analyzed.

Fraction 3:

One single centrifugation step using a CCF design (11 experiments including three center point experiments) with variation of the time length (60 to 180 sec) and of the acceleration (453 to1258 × g) was used to obtain fraction 3. After each run, the supernatant was analyzed.

Fraction 4:

An additional centrifugation step was performed using fraction 3 as starting material in order to obtain fraction 4. CCF design (11 experiments including 3 center point experiments) with changes in time length (3 to 11 min) and acceleration (805 to 3220 × g) was used for this optimization. Resonant Mass Measurements (RMM) were performed on the supernatant after each run.

For each fraction, optimal points were defined using the optimizer function of the DoE-software Modde (Version 10) but also the presented contour plots (manually chosen).

Description of DoE results:

As seen in Supplementary Figure 2A for centrifugation- fraction 1 the optimal conditions (regions in red) for the total particle concentration and for the mean diameter did not overlap when superimposing the contour plots, *i.e.* no conditions can be found to satisfy both requirements. Therefore, the obtained particle size and concentration requirements were balanced. The particle concentration of the resuspended pellets was measured using FI, (see Supplementary Table 1). Additionally, the contents of particles in the submicron size-range were measured using RMM. These measurements demonstrated that the content of nanometer-sized particles was very low (4×10^4 particle/ml) when using the optimal conditions.

To obtain the second fraction (centrifugation fraction 2) with a targeted mean diameter of 15 μm, particles between 10 and 25 μm were enriched, particles larger than 40 μm or smaller 2 μm eliminated. In summary, two centrifugation steps were needed for this and treated in two different DoE assessments. The first step (for details, see

Supplementary Table **2**) was implemented to discard the largest particles. The optimum conditions for step 1 to obtain the supernatant maximized concentration of particle between 10-25 μm and minimized the concentration of larger particles than 40 μm. After setting the optimum for step 1 (centrifugation for 240 sec with an acceleration of 50 × g using a glycerol solution of 25 %), the experiments for the second DoE were performed as described in Supplementary Table 3 in order to get rid of particles in the low submicrometer range. The short centrifugation time (180 sec) at a high acceleration (72 × g) resulted in fraction containing (after reconstitution of the pellet) high number of particles between 10-25 μm and a mean diameter around 15 μm as depicted in Figure2B. In addition, only 2×10^4 particle/ml in the low micrometer size range were measured after optimization in fraction 2 using RMM.

One single centrifugation step was sufficient to generate centrifugation fraction 3 (approximate mean size of 1.5 μm) from the initial stock solution. The total particle concentration and the mean diameter of the resulting supernatant were selected as responses for the DoE. Using the contour plots, optimal conditions were found in order to reduce the mean diameter (from 1.33 to 1.25 μm). However, the longer centrifugation time implemented after optimization (160 sec against 60 sec before optimization) induced a decrease of the particle concentration present in the supernatant by two times. The total particle concentration below 3 μm measured by FI and RMM remains reasonably high as depicted Figure 2C.

To obtain a fraction with a diameter smaller than 0.5 μm (centrifugation fraction 4), an additional centrifugation step was performed using fraction 3 as a starting material in order to remove the largest particles present in this fraction. This optimal centrifugation run using a higher acceleration and a longer centrifugation time allowed a decrease of the mean diameter from 0.43 to 0.36 μm but induced a decrease from 4.1×10^6 to 2.1×10^6 particles per ml. The presence of particle in the μm-range is relatively low as expected (see Figure 2D).

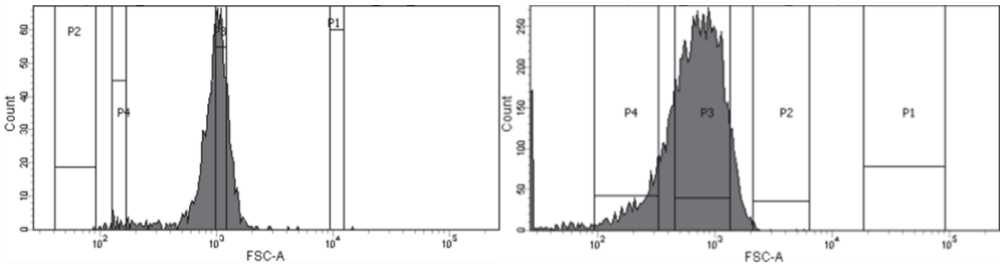

Supplementary Figure 1: Influence of smaller gate sizes on size distribution of particle fractions

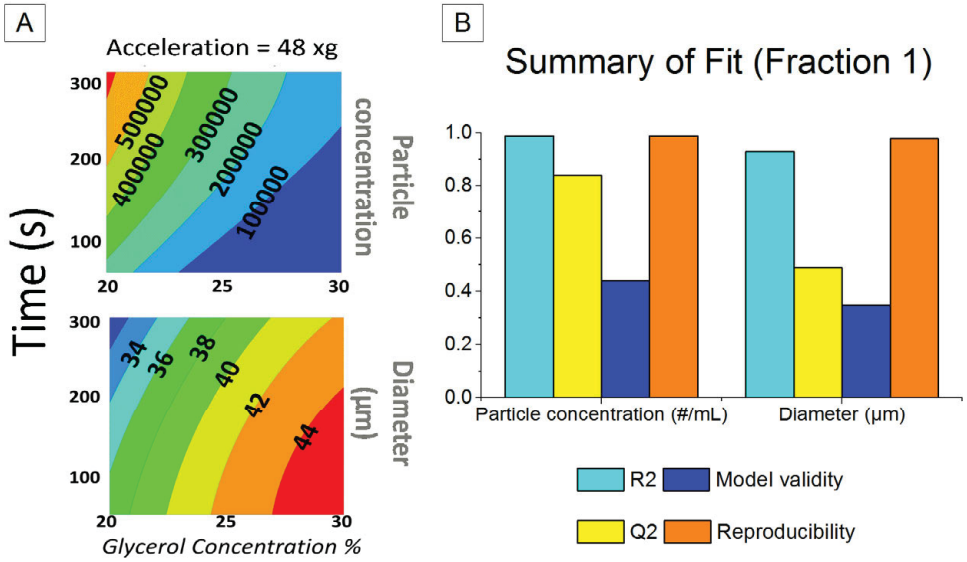

Supplementary Figure 2: Fraction 1 DoE Contours plots at 48 × g for the particle concentration and mean diameter measured by flow imaging microscopy as a function of centrifugation time and glycerol concentration in specific ranges (A). Summary of fit for fraction 1 response surface methodology (RSM) obtained model (B).

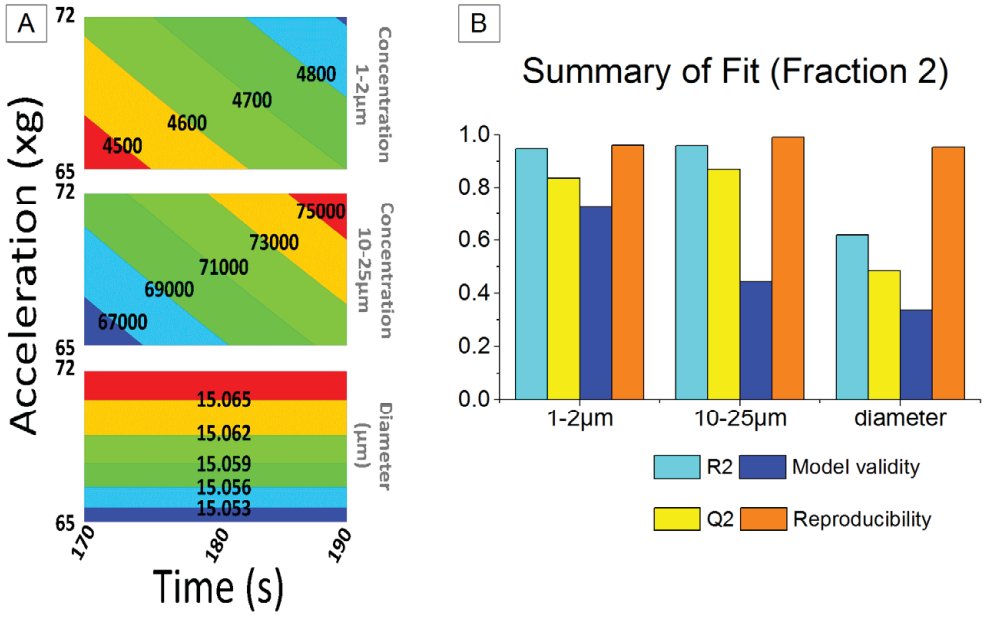

Supplementary Figure 3 Fraction 2 DoE Contours plots for the particle concentration 1-2 µm and 10-25 µm and also for the mean diameter given by flow imaging microscopy analysis in function of centrifugation time and acceleration (A). Summary of fit for fraction 2 RSM obtained model (B).

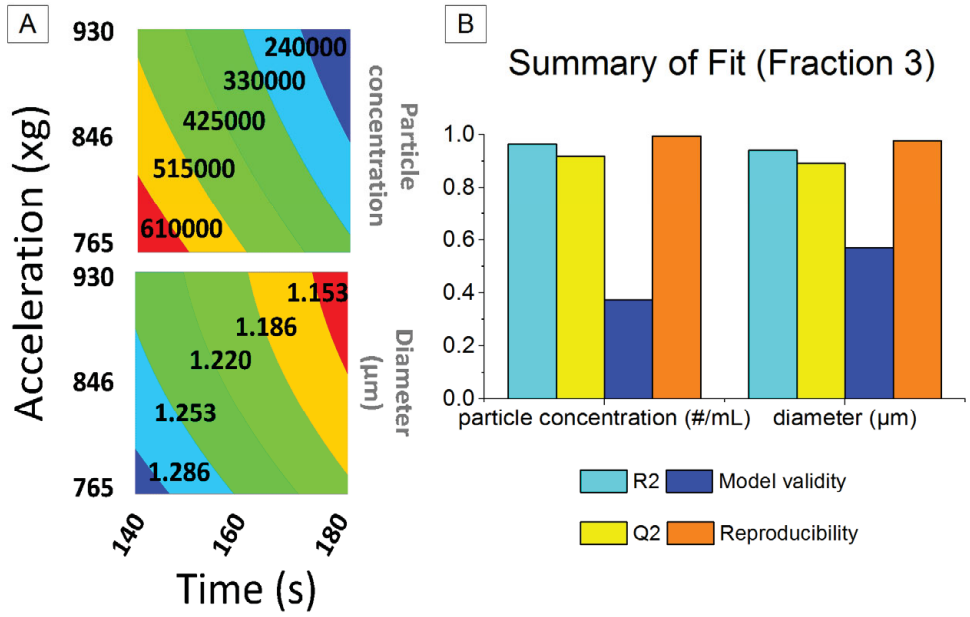

Supplementary Figure 4: Fraction 3 DoE Contours plots for the total particle concentration 1-100 µm and for the mean diameter given by flow imaging microscopy analysis in function of centrifugation time and acceleration (A). Summary of fit for fraction 3 RSM obtained model (B).

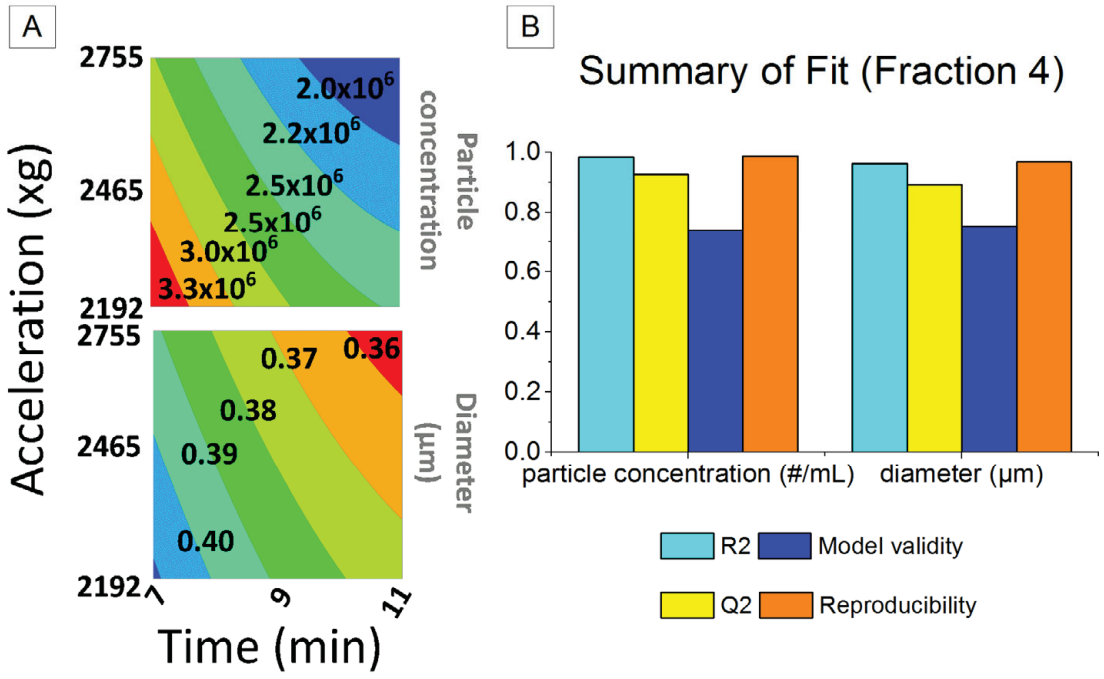

Supplementary Figure 5: Fraction 4 DoE Contours plots for the total particle concentration 0.2-5 µm and for the mean diameter given by RMM analysis in function of centrifugation time and acceleration (A). Summary of fit for fraction 4 RSM obtained model (B).

Fraction F1 (40 µm)

Fraction F2 (15 µm)

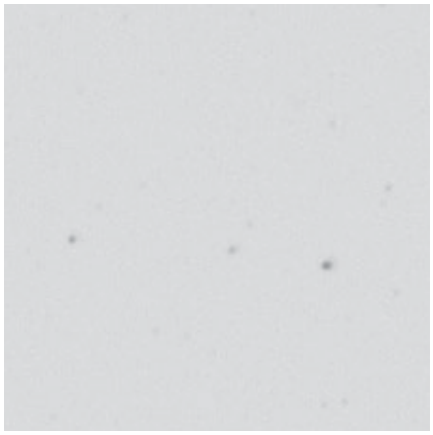

Fraction F3 (1 µm)

Supplementary Figure 6: FI pictures of the three different fractions generated by differential centrifugation.

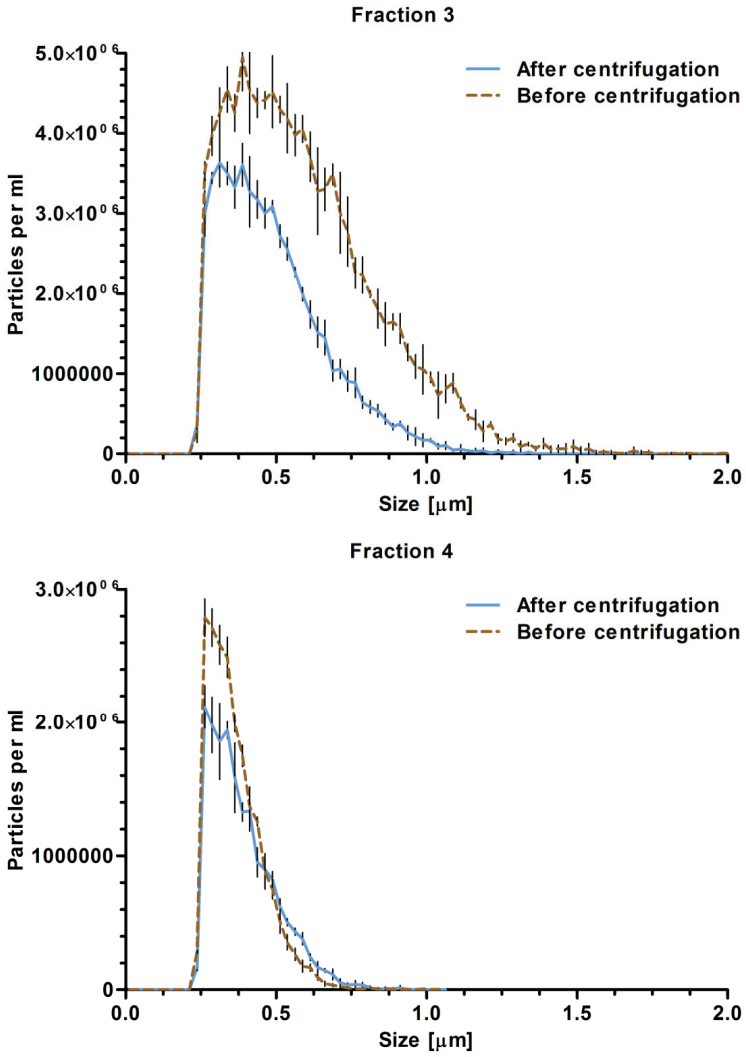

Supplementary Figure 7: Influence of sample preparation (centrifugation for 5 min at 1258 × g) on the particle concentration measured by RMM.

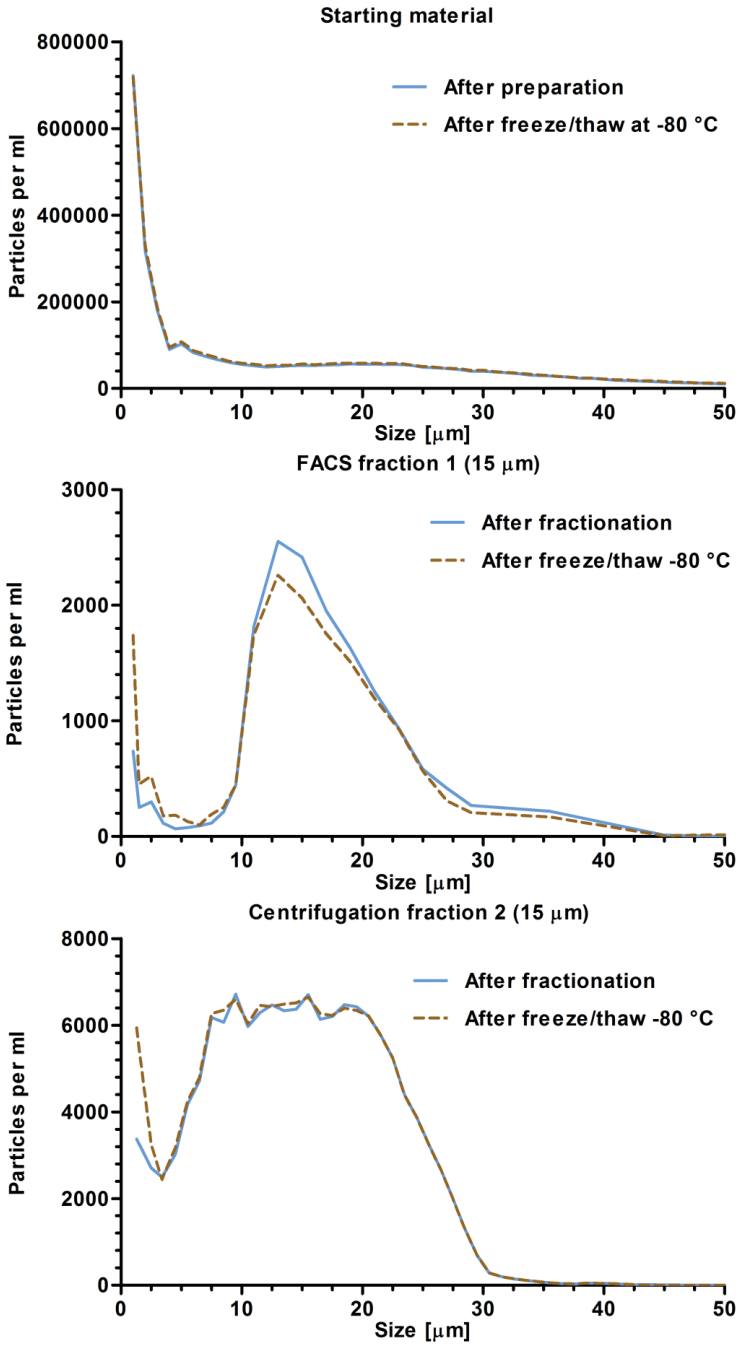

Supplementary Figure 8:Stability of starting material (diluted) that was used for fractionation and of the 15 µm FACS and centrifugation fractions sorting after freezing at -80 °C and thawing measured with FI.

Supplementary Table 1: Experimental design for optimization of fraction 1 obtained by centrifugation.

Run Order	Time (sec)	Acceleration (× g)	Glycerol concentration (%)	Particles/ml (1-100 µm)	Mean diameter (µm)
11	60	8	10	7.8×10^5	10.7
6	300	8	10	1.3×10^6	14.1
13	60	50	10	1.1×10^6	13.0
10	300	50	10	1.6×10^6	10.5
16	60	8	40	5.7×10^2	15.7
12	300	8	40	1.9×10^4	40.1
9	60	50	40	2.0×10^4	42.5
1	300	50	40	2.0×10^5	38.8
3	60	25	25	5.7×10^4	42.7
2	300	25	25	1.8×10^5	38.0
5	180	8	25	5.8×10^4	41.6
17	180	50	25	1.8×10^5	39.1
15	180	25	10	1.4×10^6	10.8
14	180	25	40	4.0×10^4	41.8
7	180	25	25	1.7×10^5	36.2
8	180	25	25	1.6×10^5	39.2
4	180	25	25	1.1×10^5	38.9

Supplementary Table 2: Experimental design for optimization of fraction 2 obtained by centrifugation (step 1/2).

Exp No	Run Order	Time (sec)	Acceleration (× g)	Glycerol concentration (%)	Particles/ml 10-25 µm	Particles/ml 40-100 µm
1	9	60	8	10	1.6×10^5	2.3×10^4
2	6	420	8	10	6.5×10^5	2.7×10^4
3	8	60	129	10	1.1×10^6	3.0×10^5
4	13	420	129	10	3.2×10^4	2.3×10^5
5	3	60	8	40	3.2×10^5	3.3×10^5
6	1	420	8	40	2.8×10^5	1.3×10^5
7	2	60	129	40	2.7×10^5	2.1×10^5
8	12	420	129	40	2.0×10^5	4.9×10^4
9	7	60	50	25	2.6×10^5	6.4×10^4
10	11	420	50	25	1.5×10^5	1.1×10^4
11	14	240	8	25	2.6×10^5	9.0×10^4
12	16	240	129	25	1.3×10^5	1.4×10^4
13	15	240	50	10	6.8×10^4	5.7×10^4
14	4	240	50	40	2.2×10^5	5.0×10^4
15	17	240	50	25	1.8×10^5	1.2×10^4

Supplementary Table 3: Experimental design for optimization of fraction 2 obtained by centrifugation (step 2/2).

Exp No	Run Order	Time (sec)	Acceleration (× g)	Particles/ml (FI) 10-25 µm	Mean diameter (µm)	Particles/ml 1-2 µm
1	8	60	8	1.1×10^4	13.2	1.9×10^3
2	6	300	8	2×10^4	14	2.6×10^3
3	3	60	129	4×10^4	15.1	3.0×10^3
4	11	300	129	1.5×10^5	14.2	8.3×10^3
5	2	60	50	2.3×10^4	13.7	3.2×10^3
6	5	300	50	9.4×10^4	15	5.2×10^3
7	1	180	8	8.1×10^3	12.8	1.7×10^3
8	7	180	129	1.3×10^5	14.8	7.0×10^3
9	10	180	50	5.3×10^4	15.3	4.5×10^3
10	9	180	50	5.8×10^4	15.1	4.0×10^3
11	4	180	50	6.2×10^4	15.5	3.7×10^3

Supplementary Table 4: Experimental design for optimization of fraction 3 obtained by centrifugation.

Exp No	Run Order	Time (sec)	Acceleration (× g)	Particles/ml (FI)	Diameter (µm)
1	3	60	454	2.3e+6	1.94
2	10	180	454	1.2e+6	1.51
3	7	60	1260	1.3e+6	1.58
4	5	180	1260	3.2e+5	1.25
5	2	60	806	1.3e+6	1.47
6	6	180	806	3.5e+5	1.24
7	9	120	454	1.8e+6	1.81
8	8	120	1260	4e+5	1.27
9	1	120	806	7.7e+5	1.33
10	4	120	806	8.5e+5	1.29
11	11	120	806	7.6e+5	1.36

Supplementary Table 5: Experimental design for optimization of fraction 4 obtained by centrifugation.

Exp No	Run Order	Time (min)	Acceleration (× g)	Particles/ml (RMM)	Diameter (µm)
1	5	3	806	8.6e+6	0.537
2	8	11	806	4.7e+6	0.432
3	7	3	3226	5e+6	0.455
4	2	11	3226	1.5e+6	0.345
5	1	3	1814	6.7e+6	0.503
6	4	11	1814	3e+6	0.392
7	3	7	806	6.6e+6	0.482
8	10	7	3226	1.9e+6	0.352
9	11	7	1814	3.8e+6	0.427
10	9	7	1814	4.2e+6	0.427
11	6	7	1814	4.3e+6	0.445

Supplementary Table 6: Parameters and responses selected for the optimization of fractions obtained by centrifugation.

Fractions	Selected variables for the DoE	Selected responses for the DoE
centrifugation-F1	Acceleration, Centrifugation time, Glycerol concentration	Particles per ml total (1-100 µm) Mean diameter (µm)
centrifugation-F2	Acceleration, Centrifugation time Glycerol concentration	<u>Step1:</u> Particles per ml 10-25 µm Particle concentration 40-100 µm
	Acceleration, Centrifugation time	<u>Step2:</u> Particles per ml 10-25 µm Mean diameter (µm) Particles per ml 1-2 µm
centrifugation-F3	Acceleration, Centrifugation time	Particles per ml total(1-100 µm) Mean diameter (µm)
centrifugation-F4	Acceleration, Centrifugation time	Particles per ml (RMM) Mean diameter (µm)

References

(1) Rosenberg, A. S. *Aaps J* **2006**, *8*, E501.

(2) Singh, S. K.; Afonina, N.; Awwad, M.; Bechtold-Peters, K.; Blue, J. T.; Chou, D.; Cromwell, M.; Krause, H. J.; Mahler, H. C.; Meyer, B. K.; Narhi, L.; Nesta, D. P.; Spitznagel, T. *J Pharm Sci* **2010**, *99*, 3302.

(3) Carpenter, J. F.; Randolph, T. W.; Jiskoot, W.; Crommelin, D. J.; Middaugh, C. R.; Winter, G.; Fan, Y. X.; Kirshner, S.; Verthelyi, D.; Kozlowski, S.; Clouse, K. A.; Swann, P. G.; Rosenberg, A.; Cherney, B. *J Pharm Sci* **2009**, *98*, 1201.

(4) den Engelsman, J.; Garidel, P.; Smulders, R.; Koll, H.; Smith, B.; Bassarab, S.; Seidl, A.; Hainzl, O.; Jiskoot, W. *Pharm Res* **2011**, *28*, 920.

(5) Singh, S. K. *J Pharm Sci* **2011**, *100*, 354.

(6) Joubert, M. K.; Hokom, M.; Eakin, C.; Zhou, L.; Deshpande, M.; Baker, M. P.; Goletz, T. J.; Kerwin, B. A.; Chirmule, N.; Narhi, L. O.; Jawa, V. *J Biol Chem* **2012**, *287*, 25266.

(7) van Beers, M. M.; Sauerborn, M.; Gilli, F.; Brinks, V.; Schellekens, H.; Jiskoot, W. *Pharm Res* **2011**, *28*, 2393.

(8) van Beers, M. M.; Gilli, F.; Schellekens, H.; Randolph, T. W.; Jiskoot, W. *J Pharm Sci* **2012**, *101*, 187.

(9) van Beers, M. M.; Jiskoot, W.; Schellekens, H. *J Interferon Cytokine Res* **2010**, *30*, 767.

(10) Mahler, H. C.; Friess, W.; Grauschopf, U.; Kiese, S. *J Pharm Sci* **2009**, *98*, 2909.

(11) Joubert, M. K.; Luo, Q.; Nashed-Samuel, Y.; Wypych, J.; Narhi, L. O. *J Biol Chem* **2011**, *286*, 25118.

(12) Mahler, H. C.; Müller, R.; Friess, W.; Delille, A.; Matheus, S. *Eur J Pharm Biopharm* **2005**, *59*, 407.

(13) Kiese, S.; Pappenberger, A.; Friess, W.; Mahler, H. C. *J Pharm Sci* **2008**, *97*, 4347.

(14) Kiese, S.; Pappenberger, A.; Friess, W.; Mahler, H. C. *J Pharm Sci* **2010**, *99*, 632.

(15) Kükrer, B.; Filipe, V.; van Duijn, E.; Kasper, P. T.; Vreeken, R. J.; Heck, A. J.; Jiskoot, W. *Pharm Res* **2010**, *27*, 2197.

(16) Paul, R.; Graff-Meyer, A.; Stahlberg, H.; Lauer, M. E.; Rufer, A. C.; Beck, H.; Briguet, A.; Schnaible, V.; Buckel, T.; Boeckle, S. *Pharm Res* **2012**, *29*, 2047.

(17) Hawe, A.; Romeijn, S.; Filipe, V.; Jiskoot, W. *J Pharm Sci* **2012**, *101*, 4129.

(18) John, C.; Langer, K. *J Chromatogr A* **2014**, *1346*, 97.

(19) Freitag, A. J.; Shomali, M.; Michalakis, S.; Biel, M.; Siedler, M.; Kaymakcalan, Z.; Carpenter, J. F.; Randolph, T. W.; Winter, G.; Engert, J. *Pharm Res* **2014**.

(20) Rombach-Riegraf, V.; Allard, C.; Angevaare, E.; Matter, A.; Ossuli, B.; Strehl, R.; Raulf, F.; Bluemel, M.; Egodage, K.; Jeschke, M.; Koulov, A. V. *J Pharm Sci* **2013**, *102*, 2128.

(21) Lee, Y. H.; Tan, H. T.; Chung, M. C. *Proteomics* **2010**, *10*, 3935.

(22) Cahn, F. H.; Fox, M. S. *J Bacteriol* **1968**, *95*, 867.

(23) Moni, C.; Derrien, D.; Hatton, P. J.; Zeller, B.; Kleber, M. *Biogeosciences* **2012**, *9*, 5181.

(24) Novak, J. P.; Nickerson, C.; Franzen, S.; Feldheim, D. L. *Anal Chem* **2001**, *73*, 5758.

(25) Sun, X.; Tabakman, S. M.; Seo, W. S.; Zhang, L.; Zhang, G.; Sherlock, S.; Bai, L.; Dai, H. *Angew Chem Int Ed Engl* **2009**, *48*, 939.

(26) Noble, P. B.; Cutts, J. H. *Can Vet J* **1967**, *8*, 110.

(27) Lu, Y.; Ahmed, S.; Harari, F.; Vahter, M. *J Trace Elem Med Biol* **2014**.
(28) Jaatinen, T.; Laine, J. *Curr Protoc Stem Cell Biol* **2007**, *Chapter 2*, Unit 2A 1.
(29) Lueders, T.; Manefield, M.; Friedrich, M. W. *Environ Microbiol* **2004**, *6*, 73.
(30) Sohi, S. P.; Mahieu, N.; Arah, J. R. M.; Powlson, D. S.; Madari, B.; Gaunt, J. L. *Soil Science Society of America Journal* **2001**, *65*, 1121.
(31) Telikepalli, S.; Shinogle, H. E.; Thapa, P. S.; Kim, J. H.; Deshpande, M.; Jawa, V.; Middaugh, C. R.; Narhi, L. O.; Joubert, M. K.; Volkin, D. B. *J Pharm Sci* **2015**, *104*, 1575.
(32) Werk, T.; Volkin, D. B.; Mahler, H. C. *Eur J Pharm Sci* **2014**, *53*, 95.
(33) Zhao, H.; Diez, M.; Koulov, A.; Bozova, M.; Bluemel, M.; Forrer, K. In *Analysis of Aggregates and Particles in Protein Pharmaceuticals*; John Wiley & Sons, Inc.: 2012, p 133.
(34) Nolte-'t Hoen, E. N.; van der Vlist, E. J.; Aalberts, M.; Mertens, H. C.; Bosch, B. J.; Bartelink, W.; Mastrobattista, E.; van Gaal, E. V.; Stoorvogel, W.; Arkesteijn, G. J.; Wauben, M. H. *Nanomedicine* **2012**, *8*, 712.
(35) Nishi, H.; Mathäs, R.; Fürst, R.; Winter, G. *J Pharm Sci* **2014**, *103*, 90.
(36) Barnard, J. G.; Singh, S.; Randolph, T. W.; Carpenter, J. F. *J Pharm Sci* **2011**, *100*, 492.
(37) Weinbuch, D.; Zölls, S.; Wiggenhorn, M.; Friess, W.; Winter, G.; Jiskoot, W.; Hawe, A. *J Pharm Sci* **2013**, *102*, 2152.
(38) Seefeldt, M. B.; Rosendahl, M. S.; Cleland, J. L.; Hesterberg, L. K. *Curr Pharm Biotechnol* **2009**, *10*, 447.
(39) Chirino, A. J.; Mire-Sluis, A. *Nat Biotechnol* **2004**, *22*, 1383.

CHAPTER 3

SELECTIVE OXIDATION OF METHIONINE AND TRYPTOPHAN RESIDUES IN A THERAPEUTIC IgG1 MOLECULE

Pharmaceutical Research

Research Article

Keywords:
therapeutic proteins
protein oxidation
methionine
tryptophan
mass spectrometry
protein A binding

Authors:
Emilien FOLZER
Katharina DIEPOLD
Katrin BOMANS
Christof FINKLER
Roland SCHMIDT
Patrick BULAU
Jörg HUWYLER
Hanns-Christian MAHLER
Atanas KOULOV

Abstract

Oxidation of methionine and tryptophan are common degradation pathways for monoclonal antibodies (mAbs) and present major analytical challenges in biotechnology. Generally, protein oxidation is detectable in stability and/or stressed samples (e.g., exposed to hydrogen peroxide, UV light or metal ions). The induced chemical modifications may impact the biological activity of antibodies and may have biological consequences. However, these effects and the contribution of individual protein modifications are difficult to delineate as different amino acids are often oxidized simultaneously and accompanied by other degradants such as aggregates, especially in forced degradation studies. Here, we report a new method to obtain selective oxidation of methionine or tryptophan by using oxidation reagents combined with large excess of free tryptophan or methionine, correspondingly. More specifically, using hydrogen peroxide (H_2O_2) or tert-butyl hydroperoxide (t-BHP) in combination with addition of free tryptophan allowed for selective oxidation of methionine. Conversely, the use of 2,2-azobis(2-amidinopropane) dihydrochloride (AAPH) in combination with free methionine resulted in selective tryptophan oxidation whilst methionine oxidation was not significantly altered. This novel stress model system may prove to be valuable tool in future mechanistic studies of oxidative degradation of protein therapeutics.

Introduction

Oxidation is a common degradation pathway that may occur during the life cycle of proteins and peptides.[1-5] The resulting chemical modifications may affect *in vitro* stability and *in vivo* biological functions.[5-17] The position of oxidized amino acids in the protein sequence is crucial for their impact on protein structure, function and biological response, especially in the case of monoclonal antibodies where binding properties are essential to reach target antigen. It has been previously reported that oxidation of methionine from the Fc region can reduce binding to the neonatal Fc receptor and biological half-life of the concerned mAb.[8,10,11] Such a change in the pharmacokinetic profile is highly dependent on the position of the oxidation. A recent study, reported that M252 oxidation was the dominant contributor to PK impairment observed in mice transgenic for the human FcRn receptor. In this study, an increased plasma clearance was only observed if both IgG HCs were oxidized at M252.[17] Moreover, the formation of oxidized methionine or tryptophan in the complementary-determining regions (CDRs) may induce loss of potency and antigen binding capabilities.[14,15]

During the last thirty years cysteine, histidine, methionine, phenylalanine, tryptophan and tyrosine residues were identified as major oxidation sites in proteins due to the high reactivity of sulfur atoms and aromatic rings towards various reactive oxygen species.[5,18] Oxidation might be induced during production, processing or storage, e.g. due to the possible reactive impurities present or formed in excipients (e.g. polyethylene glycol or polysorbate).[19,20] The generation of peroxides through auto-oxidation of these polymeric compounds might favor oxidation of these amino acid residues. The presence of transition metals may also lead to oxidation, e.g. via the Fenton reaction.[21,22] One option to minimize or prevent oxidation of the active protein is the addition of antioxidants, chelating agent or radical scavengers to the formulation buffer, if acceptable from a toxicological and regulatory perspective and thus, if considered acceptable and safe to clinical use.[20,22,23]

In order to assess the potential susceptibility of protein products to oxidation, different oxidation stress conditions have been studied, such as H_2O_2, t-BHP, AAPH, transition metal ions, or UV exposure. [15,22-25] Such relatively harsh treatments often result in a myriad of modifications on several amino-acid residues like histidine, phenylalanine, and tyrosine, for

example.[5,22,26] However, methionine and tryptophan are the residues that are oxidized most commonly and to the highest extent when exposed to such conditions.[23,24,27-29]

In recent investigations, antibody samples containing both methionine and tryptophan oxidation products were used to draw conclusions regarding impact on target binding and reduced binding affinity.[14-16] Still, one major impediment to the interpretation of such studies is the fact that frequently both methionine and tryptophan residues are oxidized concurrently, making the definition of the individual contribution of these residues to the overall effects difficult to delineate. Thus, the preparation of proteins in which methionine and tryptophan have been selectively oxidized would be very helpful, in order to improve the understanding of the relationship between structure and functional consequences.

In a recent report it has been demonstrated that the addition of free L-methionine and L-tryptophan to forced oxidation reactions of parathyroid hormone can effectively limit the oxidation of methionine and tryptophan residues, respectively.[22] However, so far this observation has not been further tested and reported when mAbs are used. In the present study we demonstrate the utility of this competition approach using a new method for selective oxidation of methionine or tryptophan residues in a model monoclonal antibody from the IgG1 subclass (the experimental strategy is depicted in Figure 1). In order to achieve this aim, a large excess of free amino acids was added to the reaction conditions, in order to protect the corresponding amino acid in the mAb when applying different oxidants (t-BHP, H_2O_2, AAPH). Different reaction conditions such as incubation temperature, reaction time and oxidant concentration were evaluated. Oxidation products in the model IgG1 were characterized using size-exclusion chromatography, Protein A-based affinity chromatography, reversed phase-HPLC and mass spectrometry.

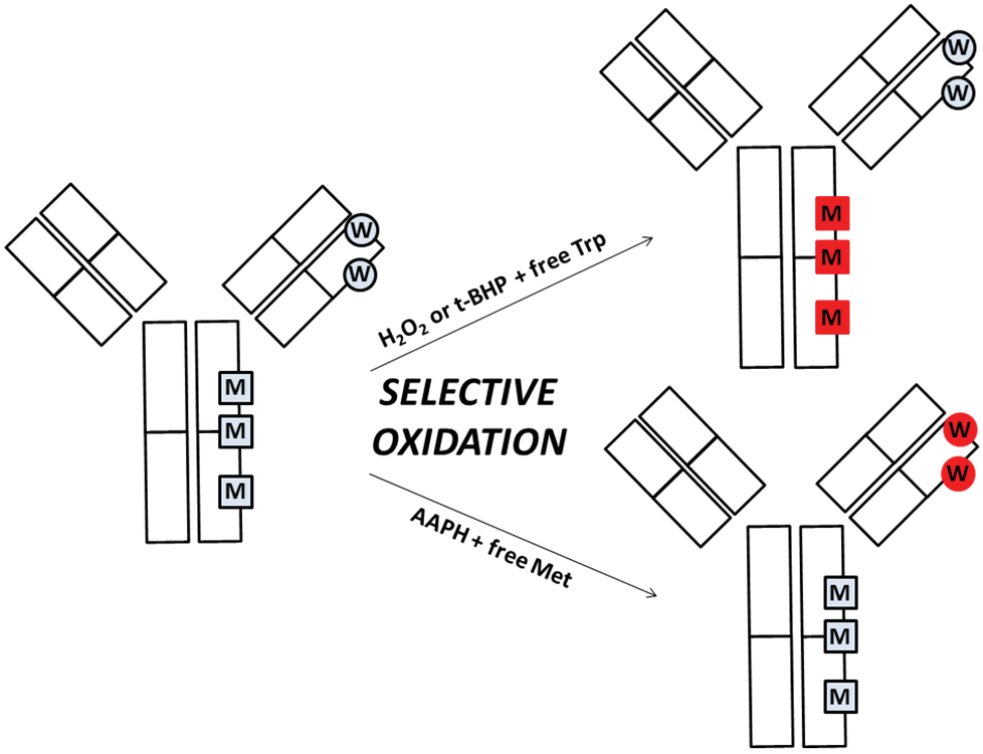

Figure 1: Schematic representation of experimental strategy to generate selectively oxidized antibody species. Combination of hydrogen peroxide (H_2O_2) or tert-butyl hydroperoxide (t-BHP) with addition of free tryptophan under well-defined experimental conditions leads to selective oxidation of methionine residues. Combination of 2,2-azobis(2-amidinopropane) dihydrochloride (AAPH) with addition of free methionine allows to selective tryptophan oxidation under well-defined experimental conditions.

Materials and Methods

An IgG1 therapeutic monoclonal antibody (mAb) was chosen as a model protein for the present study. The mAb (IgG1) solution was provided at 25 mg/ml in 51 mM sodium phosphate, 6 % trehalose, and 0.04 % polysorbate 20 (pH 6.2) by F. Hoffmann-LaRoche Ltd, Basel, Switzerland.

H_2O_2, t-BHP, AAPH, EDTA, DTT (dithiothreitol), iodoacetic acid, cysteine were purchased from Sigma–Aldrich (St. Louis, Missouri) and Dulbecco's phosphate-buffered saline (DPBS) 10× from GIBCO (Invitrogen, San Diego, California). Guanidine hydrochloride (Gdn-HCl) from AppliChem (Darmstadt, Germany) was used during the study.

Trifluoroacetic acid (TFA), formic acid (FA), acetic acid (AcOH), acetonitrile, hydrochloric acid (HCl), potassium chloride (KCl) and sodium chloride (NaCl) were purchased from Merck (Whitehouse Station, New Jersey). Tris(hydroxymethyl)-aminomethan (Tris) was used from Ajinomoto (Raleigh, North Carolina).

Papain from Carica papaya (10 mg/ml) was delivered by Roche Diagnostic (Indianapolis, Indiana). Trypsin Proteomics grade was provided by Roche Diagnostics GmbH (Penzberg, Germany).

L-tryptophan was purchased from Sigma–Aldrich (St. Louis, Missouri) and was dissolved directly in mAb solution to reach a final tryptophan concentration of 4 mg/ml in solution (19.6 mM). H_2O_2 or t-BHP were used as oxidants and added into the mAb solution with or without prior addition of free tryptophan to obtain final concentrations of oxidants between 0% and 5%.

L-methionine was purchased from Sigma–Aldrich (St. Louis, Missouri) and was dissolved directly in mAb solution to reach a final methionine concentration of 40 mg/ml in solution (0.26 M). As oxidant, AAPH was then added into the mAb solution in presence or absence of free methionine to final oxidant concentrations between 0% and 5% (see Table 1).

Table 1: Experimental parameters for artificial oxidation of model IgG1. The oxidant, oxidant concentration, antioxidant, incubation temperature and time were varied to find optimal condition for selective oxidation of methionine or tryptophan respectively. The mAb concentration was kept constant for the complete set of samples.

Parameter	Value/range
Oxidant	H_2O_2, t-BHP, AAPH
Oxidant concentration	0.0, 0.05, 0.1, 0.2, 0.5, 1.0, 2.0, 5.0%
Antioxidant	None L-methionine (0.26M) L-tryptophan (19.6mM)
Incubation temperature	5, 25, 40°C
Incubation time	1, 6, 24, 120h
model mAb concentration	18.5 mg/ml

The final mAb concentration for each prepared sample was 18.5 mg/ml. Samples were incubated under protection from direct light at 5°C, 25°C or 40°C and aliquots were collected at 1, 6, 24 or 120 h. A control sample, without oxidant, was also incubated and analyzed for each time point and temperature. The oxidation was stopped by buffer exchange using disposable PD-10 desalting columns (GE Healthcare, Buckinghamshire, UK).

Instrumentation and Sample analysis

A Waters Alliance 2695 high-pressure liquid chromatographic (HPLC) system equipped with a 2487 UV detector and Empower2 software (version 7) (Waters, Milford, Massachusetts) was used throughout the study. The determination of protein concentration before injection was performed on a SoloVPE spectrometer from C-Technologies (Bridgewater, New Jersey).

SE-HPLC (Size-Exclusion Chromatography)

Samples were analyzed by UV absorbance detection at 280 nm. A TSK G3000 SWXL column (5 μm, 250A, 7.8 x 300mm) from Tosoh was used for separation. The mobile phase (200 mM phosphate, 250 mM KCl, pH 7.0) was pumped at a flow rate of 0.5 ml/min. Sample size for analysis was 25 μg. The stationary phase was kept at 25 ± 2°C.

Protein A Chromatography

Analytical Protein A chromatography was performed, as described previously on a POROS® A (4.6 × 50 mm) column (Applied Biosystems, Foster City, California).[12] The stationary phase was kept at 23 ± 2°C.

RP-HPLC (Reversed-Phase Chromatography)

Protein samples were diluted to a final concentration of 1 mg/ml in Tris buffer (0.1 M Tris, 4 mM EDTA, and 1 mM cysteine, pH 7.4). 50 µl of 0.1 mg/ml papain was added to 500 µl of the mAb1 solution before incubation at 37°C for 2 h. Following incubation, 11 µl of 1 M DTT was added to each tube and samples were incubated for another 30 min at 37°C. Analysis of oxidized and intact mAb was carried out using a BioBasic Phenyl column (5 µm, 300A, 2.1 x 250 mm) from Thermo Fischer Scientific. Mobile phase A was 0.09% TFA in water. Mobile phase B was 0.08% TFA in acetonitrile. Flow rate was 0.45 ml/min. The chromatography was performed using a linear gradient from 35 to 40% solvent B in 16 min. 40% of mobile phase B was maintained during 4 minutes and finally 35% solvent B was pumped during 10 min. Sample size for analysis was 8 µg. The fragment elution was monitored by UV absorption at 215 nm. As the method described above cannot be used to identify the tryptophan oxidation site in the protein sequence, it was utilized only as a rapid screening tool for tryptophan oxidation present in the fragment antigen-binding part of the heavy chain (HC-Fab). The tryptophan oxidation fraction was calculated by dividing the area of the pre-peak by the total peak area of the HC-Fab peaks.

Proteolytic digest of mAb

For detection and quantification of oxidized amino acids, the mAb was digested with trypsin. First, the protein was denatured in 0.4 M Tris-HCl, 8 M Gdn-HCl, at pH 8.5 by diluting 350 µg of oxidized mAb in a total volume of 300 µl. For reduction, 10 µl of 100 mg/ml DTT were added and incubated at 50°C for 1 h. After alkylation of free cysteines by adding 10 µl of 330 mg/ml iodoacetic acid and incubation at room temperature in the dark for 30 min, the buffer was exchanged to digestion buffer (0.1 M Tris-HCl, pH 7.0) by using a NAP5 gel filtration column. Subsequently, NAP5-eluate (500 µl) was mixed with 10 µl of a solution of 0.25 mg/ml

trypsin in 10 mM HCl and incubated at 37°C for 18 h. The digestion reaction was stopped by adding 50 µl of a 10% TFA solution.

The tryptic peptide mixture was separated by reversed phase-UPLC (ACQUITY, Waters, Manchester, UK) on a C18 column (BEH C18 1,7 µm, 2,1 x 150 mm; Waters, Manchester, UK) and the eluate online analyzed on a Q-TOF SYNAPT G2 instrument (Waters, Manchester, UK). The mobile phases of RP-HPLC consisted of 0.1% FA in water (solvent A) and 0.1% FA in acetonitrile (solvent B). The chromatography was performed using a linear gradient from 1 to 35% solvent B in 45 min and finally from 35 to 80% solvent B in 3 min using a flow rate of 300 µl/min. 3 µg digested protein was applied. UPLC-system and mass spectrometer were connected by PEEK capillary tubes. Data acquisition was controlled by MassLynx^{TM} software (Waters, Manchester, UK).

MS/MS experiments were performed on a LTQ Orbitrap Velos electrospray mass spectrometer (Thermo Scientific, Dreieich, Germany) using the chromatographic system described above in order to identify the oxidized peptides. The fragmentation was induced by low-energy CID using helium as collision gas ("top5" mode). Data acquisition was controlled by Xcalibur software (Thermo Fisher Scientific) using a manual acquisition mode. Oxidized amino acids were identified from the MS/MS-data using the software Proteomics Discoverer (Thermo Fisher Scientific). The collision energy was adjusted according to stability and mass of the parent ion.

Peptides of interest were identified manually by searching for their theoretical m/z-values within the experimental mass spectrum. For their quantification, specific ion current (SIC) chromatograms of peptides of interest were generated on the basis of their monoisotopic mass and detected charge states using GRAMS AI software (Thermo Fisher Scientific). Relative amounts of non-oxidized and oxidized peptides were calculated by manual integration of the corresponding peaks.

Besides the summarized large number of methionine and tryptophan oxidation sites (see Table 2 and Tables S1 and S2) no significant levels of additional amino acid oxidations events

(e.g. at histidine residues) were detected by careful inspection of the experimental mass spectra.

Table 2: LC-MS results for the oxidation with H_2O_2 or t-BHP with or without addition of free tryptophan. The mAb was denatured and the disulfide bridges were reduced using DTT. Alkylation of free cysteines was performed using iodoacetic acid. After a buffer exchange, the mAb was finally digested with trypsin. LC stands for light chain, HC stands for heavy chain. Methionine (M) and tryptophan (W) oxidation levels were quantified.

OXIDATION WITH/WITHOUT TRYPTOPHAN PROTECTION					
Modified Amino Acids	**Control**	**1% H_2O_2 5°C 24h**	**1% H_2O_2 5°C 24h with tryptophan**	**2% t-BHP 25°C 120h**	**2% t-BHP 25°C 120h with tryptophan**
LC M4ox	0.3	4.4	0.9	4.1	3.8
HC M34ox	0.7	7.4	2.5	6.9	7.4
HC M83ox	0.6	4.1	0.7	4.2	4.0
HC M258ox	4.4	99.6	99.6	99.7	99.7
HC M364ox	0.4	90.8	92.9	91.0	91.6
HC M434ox	1.2	96.1	96.1	96.1	96.7
LC W35ox+4	0.2	0.6	0.5	0.6	0.5
LC W35ox+16	0.0	0.0	0.0	0.0	0.0
LC W96ox+4	0.1	0.3	0.2	0.4	0.2
LC W96ox+16	0.1	0.2	0.1	0.2	0.2
HC W50ox+4	0.1	0.2	0.2	0.2	0.2
HC W50ox+16	0.2	0.3	0.2	0.3	0.3
HC W50ox+32	0.0	0.0	0.0	0.0	0.0
HC W108ox+4	0.0	0.0	0.0	1.5	0.3
HC W108ox+16	0.2	0.3	0.2	2.6	0.6
HC W108ox+32	0.1	0.1	0.1	0.1	0.1
HC W283ox+4	0.1	0.1	0.1	0.2	0.1
HC W283ox+16	0.1	0.2	0.2	0.2	0.2
HC W319ox+4	0.1	0.2	0.1	0.2	0.2
HC W319ox+16	0.4	0.8	0.6	0.8	0.7
HC W319ox+32	0.0	0.0	0.0	0.0	0.0

Results and discussion

In forced oxidation studies of therapeutic proteins widely varying extents of methionine oxidation (from 0% to 100%) were reported. In these reports the most commonly used oxidative reagents were H_2O_2 and t-BHP with reaction conditions spanning a broad range, including different temperatures (room temperature or 40°C), different concentrations of the oxidative agent (0.0005% to 0.2% for H_2O_2, 0.05% to 5% for t-BHP) and different reaction times (6 h to 7 days).[12-14,22] One drawback of such oxidation studies is the possible co-oxidation of tryptophan and methionine. This effect was reported for the oxidation of a recombinant antibody performed with 0.05% t-BHP at room temperature for 7 days where 65% methionine oxidation and 25% tryptophan oxidation were detected in the same sample.[14] One other example of co-oxidation of tryptophan and methionine was shown during the reaction of parathyroid hormone with AAPH. Indeed, incubation of 0.1mg/ml parathyroid hormone with 0.1 M AAPH at 40°C for 24 h resulted in 84% of tryptophan oxidation and 58% of methionine oxidation.[22] After reacting human growth hormone with AAPH, Steinmann *et al*. reported a multitude of oxidized residues, including 20% tryptophan oxidation and significant methionine oxidation (100% M14; 80% M125; 70% M170).[30]

Indeed, the use of established conditions for forced oxidation available in literature did not allow us to selectively oxidize neither methionine nor tryptophan amino acids in a monoclonal antibody model protein as depicted in Figure 2, 3 and 4, and Supplementary Table 1 and 2. Instead, extensive co-oxidation of both methionine and tryptophan was present under these conditions.

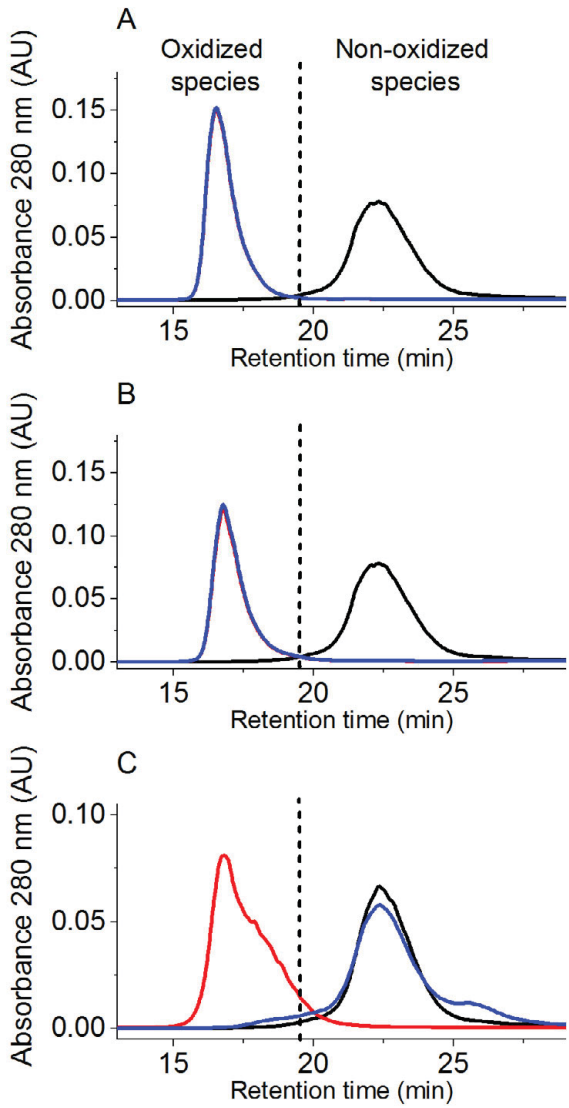

Figure 2: Analysis of oxidized and non-oxidized mAb species by analytical Protein A chromatography. (A) The chromatogram overlay shows the elution profile of control material (black), mAb oxidized in the presence of 1% H_2O_2 for 24 h at 5°C with (blue) or without addition of free tryptophan (red). The red and blue curves are perfectly overlapping. (B) The chromatogram overlay shows the elution profile of control material (black), mAb oxidized in the presence of 2% t-BHP for 120 h at 25°C with (blue) or without addition of free tryptophan (red). The red and blue curves are perfectly overlapping. (C) The chromatogram overlay shows the elution profile of control material (black), mAb oxidized in the presence of 5% AAPH with (blue) or without addition of free methionine (red) for 120 h at 40°C.

To identify optimal conditions leading to selective oxidation of methionine or tryptophan in a mAb, a large set of parameters were evaluated based on published studies and previous in-house experiments (data not shown).[12,14,22] A model IgG1 was incubated with different

oxidants while the reaction times and incubation temperatures were varied as described in Table 1. To curtail oxidation of the amino acids methionine or tryptophan, the corresponding free amino (L-methionine or L-tryptophan) acids were added to the reaction mixtures. After completion of all reactions, samples were screened for total oxidation levels using Protein A analytical chromatography and RP-HPLC. Selected samples were further analyzed using LC-MS and LC-MS/MS in order to identify and semi-quantify the methionine and tryptophan oxidation sites in the amino-acid sequence.

In the model IgG1 used in this study several methionine residues were identified as susceptible to oxidation (M4, M34, M83, M258, M364 and M434). Basal levels of oxidation of these susceptible residues were identified in the starting material (see Table 2). From the oxidized tryptophan identified by LC-MS/MS (W35, W50, W96, W108, W283, W319) only surface exposed W50 and W108 showed significant changes between unstressed and stressed samples.

Selective methionine oxidation

Oxidation levels of Fc methionine were first quantified by Protein A chromatography. The non-oxidized antibody species eluted at 23 min (Figure 2). The oxidized species formed upon incubation with oxidant eluted earlier (before 19.8 min) because of the lower affinity of oxidized Fc methionine to Protein A.[7,12] As depicted in Figure 2A and 2B, the incubation of the mAb with 1% H_2O_2 for 24 h at 5°C as well as the incubation with 2% t-BHP for 120 h at 25°C allowed for the nearly complete oxidation of the methionine residues from the Fc region.

The extent of methionine oxidation was also determined by selected ion current chromatogram analysis of the oxidized peptides (see Table 2). We found more than 91% oxidation for M364, 96% oxidation for M434 and 99% oxidation for M258 according to LC-MS results.

In order to assess the total tryptophan oxidation of the HC-Fab, the oxidized samples were first digested with papain and then the disulfide bridges were reduced with DTT. The generated LC, HC-Fc and HC-Fab were then separated by RP-HPLC (for details see Materials and Methods) as presented in Figure 3A and the tryptophan oxidation of the HC-Fab was

quantified. The oxidized species due to tryptophan oxidation elute before the HC-Fab peaks. The peak with a retention time of 19.5 min represents in that case mainly oxidized tryptophan W108 of the HC-Fab (Figure 3B and 3C, signal labeled as “Trp-ox”).

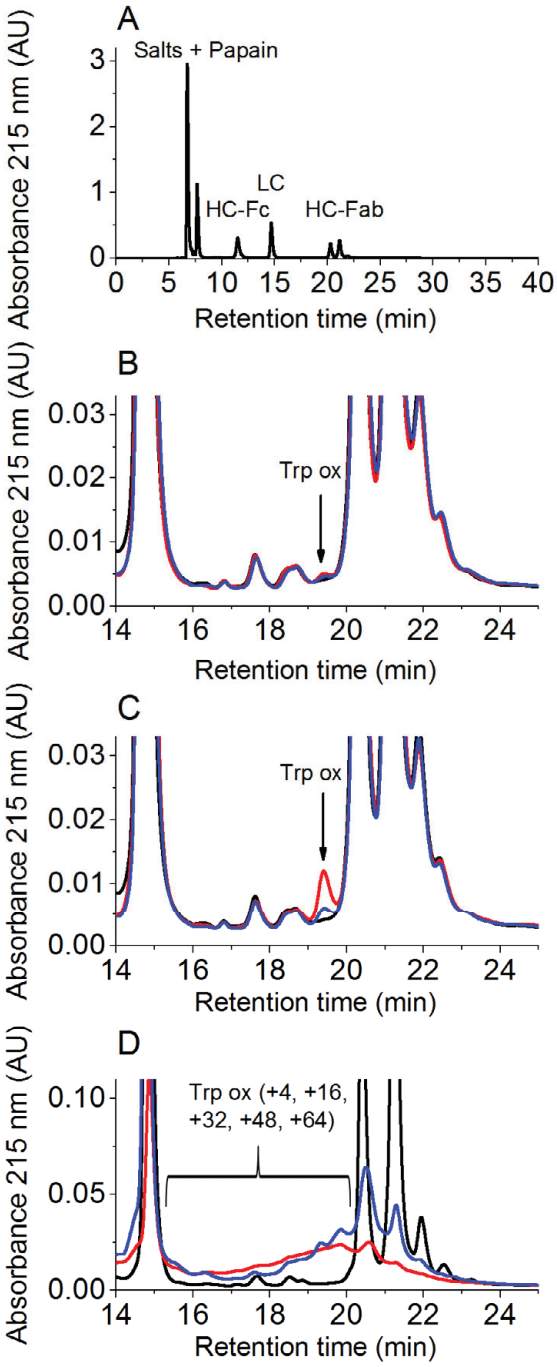

Figure 3: Overlay of RP-HPLC chromatograms used to quantify tryptophan oxidation present in the heavy chain Fab part (HC-Fab) of studied IgG1 for control material vs oxidized samples. The analyses were

performed after papain digest followed by DTT reduction. (A) Complete RP-HPLC chromatogram for control material (black). (B) Zoom in of HC-Fab region; control material (black), 1% H_2O_2 oxidation for 24 h at 5°C with (blue) or without addition of free tryptophan (red). (C) Zoom in of HC-Fab region; control material (black), 2% t-BHP oxidation 120 h at 25°C with (blue) or without addition of free tryptophan (red). (D) Zoom in of HC-Fab region; control material (black), 5% AAPH oxidation for 120 h at 40°C with (blue) or without addition of free methionine (red).

As previously reported, the oxidation of mAb with H_2O_2 or t-BHP induced relatively low tryptophan oxidation levels (please, see Figure 3B and 3C).[22] The well-resolved signal with a retention time of 19.5 min (corresponding to tryptophan oxidation products) increased not only with increasing H_2O_2 or t-BHP concentrations but also when increasing the reaction time and the temperature of incubation (data not shown). In order to exclude the possibility of metal ion contamination resulting in Fenton-like reactions, protein oxidation reactions were carried out in the presence and absence of EDTA. As no differences in the oxidation levels of Trp were detected (data not shown) the mechanism of Trp oxidation in these reactions remains unclear. To avoid this unwanted tryptophan oxidation, reaction conditions were set as H_2O_2 oxidation at 5°C for 24 h and t-BHP oxidation at 25°C for 120 h. Moreover, the tryptophan oxidation could be inhibited using addition of free tryptophan at concentrations of 19.6 mM during the incubations as depicted in Figure 3B and 3C (for detailed LC/MS results see Table 2).

LC-MS analyses confirmed the low abundance of tryptophan oxidation (see Table 2), and as a consequence the protective effect of free tryptophan against tryptophan oxidation. According to LC-MS results, the total oxidation of W50 and W108 was lower than 1% when adding free tryptophan before oxidation with t-BHP (2%-25°C-120 h). In the case of H_2O_2 oxidation (1%-5°C-24 h), where tryptophan oxidation products were present at very low level (< 1%), the addition of free tryptophan could not protect against the formation of low levels of residual tryptophan oxidation products (see Table 2).

In addition to free tryptophan, which has been shown to protect tryptophan residues in proteins from oxidation, other antioxidants could potentially be used to avoid tryptophan oxidation.[20,21] However, the addition of antioxidant should be investigated in detail before use to avoid unexpected effects.[31]

SE-HPLC was used to assess the sample integrity after oxidation. Both H_2O_2 (1%-5°C-24 h with free tryptophan) or t-BHP (2%-25°C-120 h with free tryptophan) oxidation induced only minimal changes in aggregate and fragment formation. In comparison to the reference material, the incubation with 1% H_2O_2 induced 0.8% soluble aggregates, whereas the oxidation with 2% t-BHP induced 1.4% soluble aggregates (Figure 5A). Thus, the application of the developed model stress system does not significantly impact molecular integrity and the biological consequences of selective methionine oxidation could be further analyzed by functional testing.

Selective tryptophan oxidation

AAPH is a reagent that has been used for forced tryptophan oxidation studies.[22] In our hands the simultaneous oxidation of several tryptophan residues upon stress (mass additions of +4, +16, +32, +48, +64) resulted in a complex mixture of reaction products that were difficult to separate well by RP-HPLC (Figure 3D). The pre-peaks were broad and poorly resolved. Nevertheless, it was possible to detect tryptophan oxidized species in the oxidized sample as early-eluting peaks (retention times from 16 to 19.6 min in Figure 3D) and to identify the different tryptophan oxidation sites by subsequent LC-MS analyses. Upon incubation at 40°C for 120 h with AAPH (0-5%) a considerable tryptophan oxidation (between 12 and 95%) was observed, as seen in Supplementary Table 2 and 3.

As reported in previous studies, the reaction of proteins with alkyperoxyl radicals (generated by AAPH that reacts with oxygen) induced also methionine oxidation.[22,32] As seen in Figure 2C and 4A, oxidation with 5% AAPH lead to almost complete oxidation of Fc methionine measured by Protein A chromatography and LC-MS peptide mapping.

The addition of a large excess of free methionine into solution before oxidation at 40°C for 120 h, allowed protection of Fc methionine as seen in the Protein A chromatogram (Figure 2C). As depicted in Supplementary Figure 1 and 2, the low levels or absence of peptide signal in the TIC plots and extracted ion chromatograms for M258ox (RT=12.65 min), M364ox (RT=1.78 min) and M434ox (RT=18.45 min) when adding free methionine into the mAb

solution before oxidation with 5% AAPH (at 40°C for 120 h) is a clear confirmation of the protective effect of free methionine against methionine oxidation.

The results from LC-MS analyses of AAPH oxidized samples are presented in Table 1 and 2 of the Supplementary material. These results clearly demonstrate that methionine residues otherwise susceptible to oxidation by AAPH can be selectively protected by addition of free methionine, even in the harshest reaction conditions used in this study (longest incubation time [120 h], highest oxidant concentration [5%] and highest temperature of incubation [40°C]). This specific sample showed 10.3% oxidation for M258 whereas the same sample without methionine addition showed oxidation of 99.7%. Similarly 6.3% versus 98.8% M434ox was verified by LC-MS. The oxidation of M364 was lower than 1% in the protected sample (99% oxidation in the sample without addition of free methionine). It has to be mentioned that 4.5% M258ox, 0.4% M364ox and 1.1% M434ox were found in the non-stressed reference material (Figure 4A).

Figure 4A, 4B and 4C show a comparison of the methionine (M258, M364 and M434) and tryptophan (W50 and W108) distribution between AAPH stressed samples with and without addition of free methionine. Over and above the decrease of methionine oxidation, the presence of free methionine in the mAb solution for AAPH incubation slightly changed the oxidation profile of tryptophan residues as seen in Figure 4B and 4C. As already observed in the RP-HPLC data, the total amount of tryptophan oxidation (as quantified by LC-MS) slightly decreased but remained considerable when adding free methionine to the solution (Figure 8 and 9). On the one hand a higher percentage of hydroxytryptophan (+16) for W50 and W108 was measured in the samples containing free methionine. A lower percentage of N-formylkynurenine (+32) was found for W50 and W108 when adding free methionine (Supplementary Figure 3 and 4). Presumably, this effect is related to shift in the equilibrium between reaction intermediates caused by the addition of the antioxidant. Further elucidation of this mechanism may be of interest as a topic of future studies.

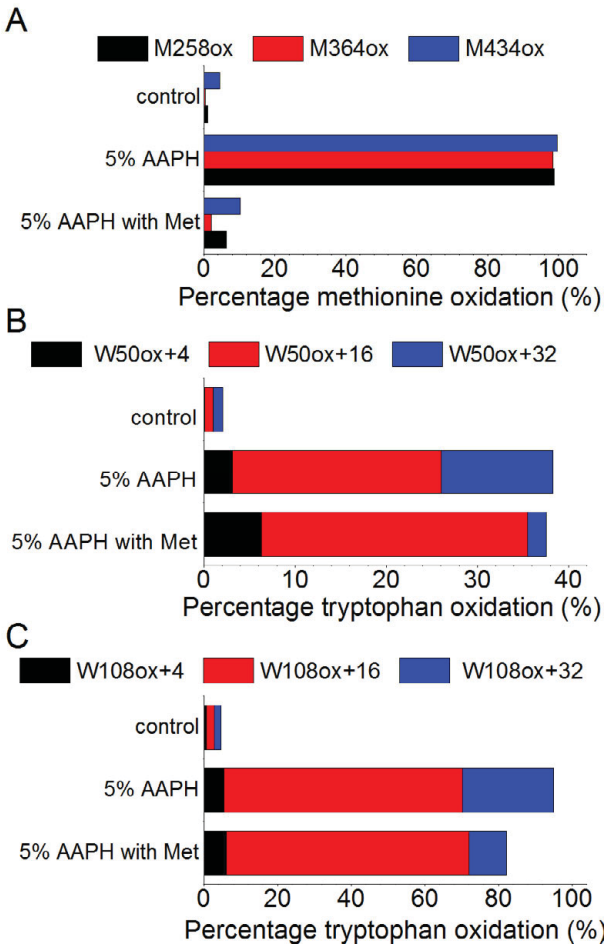

Figure 4: Comparison of the relative abundance of methionine and tryptophan residues susceptible to oxidation quantified by LC/MS peptide map. The oxidation was performed with 5% AAPH at 40°C for 120 h with or without addition of free methionine. Relative abundance is calculated as relative % using specific ion current chromatogram analysis of tryptic peptides for M258, M364 and M434 (panel A), W50 (panel B) and W108 (panel C). The tryptophan modifications kynurenine (+4), hydroxytryptophan (+16) and N-formylkynurenine (+32) are represented in panel B and C.

Significant formation of soluble aggregates was detected by size exclusion chromatography (SEC) correlating well with the increase in AAPH concentration. The addition of free methionine however, had a protective effect against aggregation as seen in Figure 5B. This effect correlates well with overall reduction on oxidation. The monomer content represented 30% of the total area in the AAPH sample without methionine addition whereas 65% of monomers were still present in the sample containing free methionine during incubation with 5% AAPH for 120 h at 40°C. The content of soluble fragments remained below 0.3% for the control and the stressed samples in all studies. The correlation between Met oxidation and

protein aggregation observed in this study was not unexpected, as such correlation has been reported previously by others and studied in some detail.[11,33] These studies have demonstrated that Met oxidation in mAbs may result in changes of the secondary and tertiary structure and in turn affect significantly the physical stability of the protein resulting in increased aggregation propensity. Thus, the decrease of aggregation upon the addition of free Met can be attributed to the oxidation protective effect of Met.

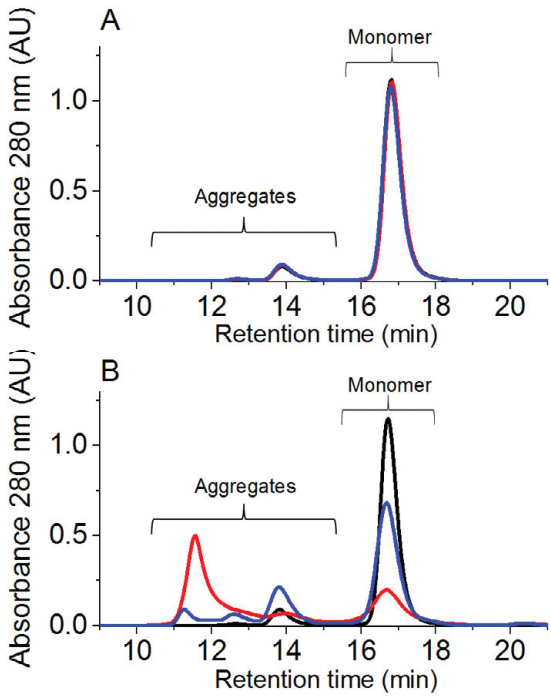

Figure 5: SE-HPLC chromatograms of control material vs. oxidized samples. Monomer peak elutes at 17 min. The aggregated species elute below 15.5 min. (A) The chromatogram overlay shows the elution profile of control material (black), 1% H_2O_2 oxidized sample for 24h at 5°C with tryptophan addition (blue) and 2% t-BHP oxidized sample for 120h at 25°C with tryptophan addition (red). The blue and red curves overlap the black curve. (B) The elution profile of control material (black) is represented with the aggregation profile of 5% AAPH oxidation for 120 h at 40°C with (blue) or without addition of free methionine (red).

The experimental approach of using combinations of oxidative reagents and antioxidants presented here provided an efficient strategy for selective oxidation of Met and Trp residues in therapeutic IgG molecules. Although residual low levels of undesirable oxidation were detected in some cases (which presumably would need to be accounted for follow-up biological studies), we believe that this approach will find broad application in studying the biological effects of protein oxidation.

Conclusions

Free methionine and/or tryptophan are used as pharmaceutical antioxidants due to their protective action against oxidation of amino acids in protein therapeutics. In the present report, we explore the potential of these antioxidants to selectively generate methionine- or tryptophan oxidized residues. A combination of oxidative (H_2O_2, t-BHP and AAPH) and protective (free tryptophan or methionine) components will serve as a strategy to address questions related to the impact of oxidation-induced changes on the biological properties of protein therapeutics (e.g., bioactivity, PK/PD, immunogenicity etc.). Such mechanistic studies will be instrumental to better understand and control oxidative degradation of antibodies.

Acknowledgments

We thank Y. John Wang, Ulla Grauschopf and Kishore Ravuri, for insightful discussions and comments on the manuscript.

Associated content - Supporting information

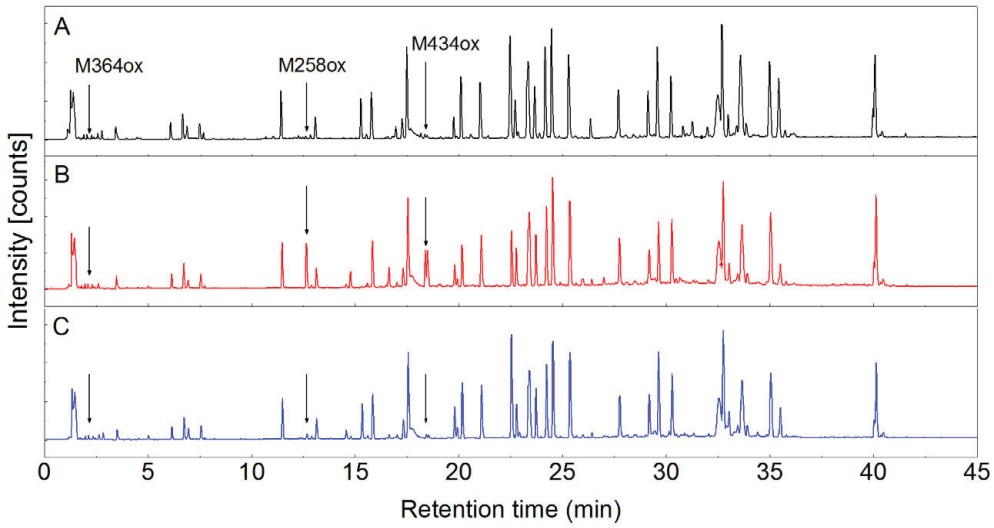

Supplementary Figure 1: Comparison of total ion current chromatogram. LC-MS analysis performed after tryptic digest, of control material (black), 5% AAPH oxidation for 120 h at 40°C with addition of free methionine (blue) or without (red). Arrows show the corresponding peak for oxidation product of M258, M364 and M434.

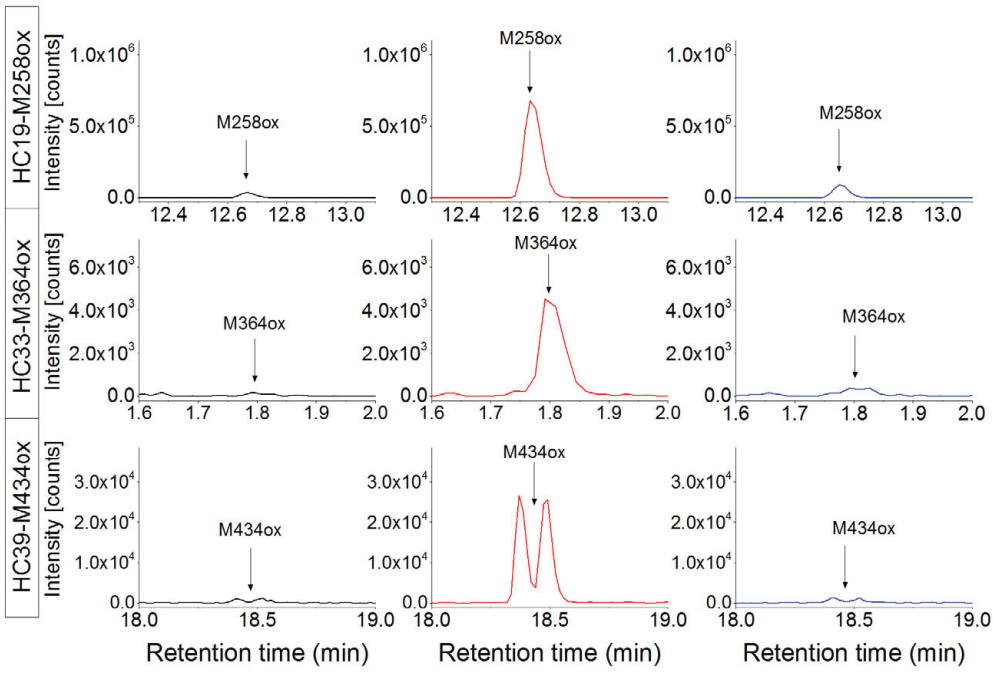

Supplementary Figure 2: LC-MS peptide map extracted ion chromatograms for oxidation product (+16) of M258, M364 and M434. The control material (black) is compared with the 5% AAPH oxidized samples for 120 h at 40°C with (blue) or without addition of free methionine (red).

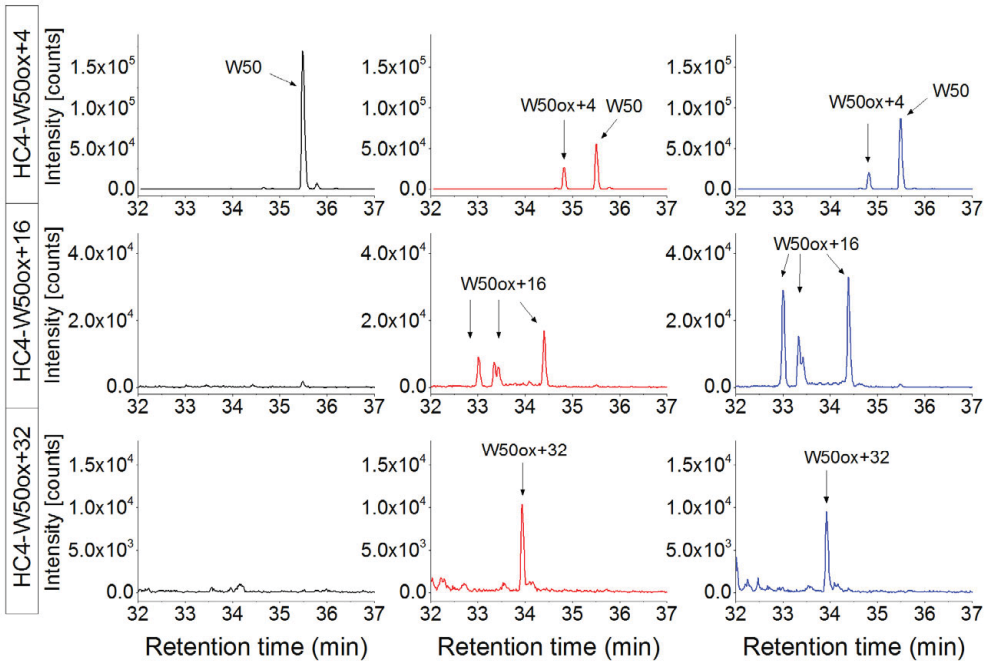

Supplementary Figure 3: LC-MS peptide map extracted ion chromatograms for oxidation residues of W50 (+4, +16, +32). The control material (black) is compared with the 5% AAPH oxidized samples for 120 h at 40°C with (blue) or without addition of free methionine (red).

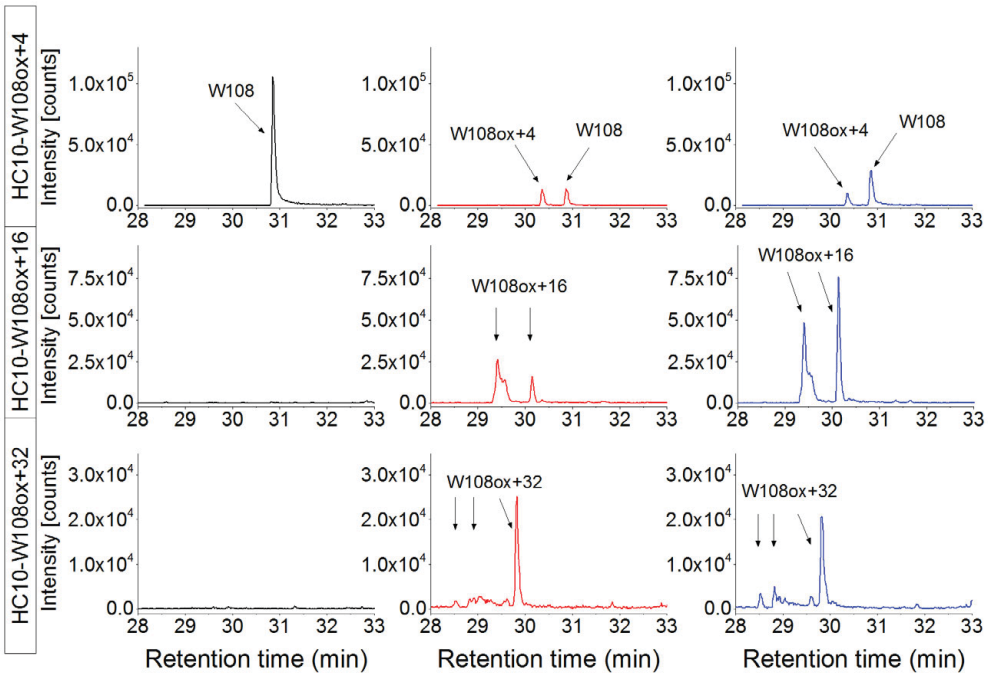

Supplementary Figure 4: LC-MS peptide map extracted ion chromatograms for oxidation residues of W108 (+4, +16, +32). The control material (black) is compared with the 5% AAPH oxidized samples for 120 h at 40°C with (blue) or without addition of free methionine (red).

Supplementary Table 1: LC-MS results for the oxidation of mAb with AAPH (0-5%) without addition of free methionine. The mAb was denatured and the disulfide bridges were reduced using DTT. Alkylation of free cysteines was performed using iodoacetic acid. After a buffer exchange, the mAb was finally digested with trypsin. LC stands for light chain, HC stands for heavy chain. Methionine (M) and tryptophan (W) oxidation levels were quantified.

AAPH OXIDATION WITHOUT METHIONINE PROTECTION						
Modified Amino Acids	**Control**	**0.05% AAPH 40°C 120h**	**0.5% AAPH 40°C 120h**	**1% AAPH 40°C 120h**	**2% AAPH 40°C 120h**	**5% AAPH 40°C 120h**
LC M4ox	0.3	1.6	2.3	6.1	8.1	23.3
HC M34ox	0.6	10.7	16.8	23.3	24.1	26.7
HC M83ox	0.7	6.6	7.9	12.0	14.4	28.3
HC M258ox	4.5	98.4	99.7	99.7	99.7	99.7
HC M364ox	0.4	43.1	98.8	99.2	98.9	98.5
HC M434ox	1.1	93.8	97.3	95.9	97.3	98.8
LC W35ox+4	0.2	0.6	1.1	2.2	3.2	3.2
LC W35ox+16	0.0	1.0	2.1	4.9	7.2	9.9
LC W96ox+4	0.3	0.9	0.8	2.1	2.6	2.6
LC W96ox+16	0.1	5.0	5.6	5.1	5.4	9.0
HC W50ox+4	0.1	1.4	3.5	5.0	4.6	3.2
HC W50ox+16	0.9	7.7	15.1	19.1	22.1	22.9
HC W50ox+32	1.1	4.2	11.6	12.8	13.0	12.3
HC W108ox+4	0.7	3.7	7.4	6.0	8.3	5.4
HC W108ox+16	2.1	47.4	47.7	55.1	52.6	64.9
HC W108ox+32	1.8	22.5	26.2	30.2	31.8	24.7
HC W283ox+4	< 1					
HC W283ox+16	0.0	0.4	2.3	3.6	2.9	5.8
HC W319ox+4	< 1					
HC W319ox+16	0.4	0.5	1.3	2.4	2.6	5.7
HC W319ox+32	< 1					

Supplementary Table 2: LC-MS results for the oxidation of mAb with AAPH (0-5%) with addition of free methionine. The mAb was denatured and the disulfide bridges were reduced using DTT. Alkylation of free cysteines was performed using iodoacetic acid. After a buffer exchange, the mAb was finally digested with trypsin. LC stands for light chain, HC stands for heavy chain. Methionine (M) and tryptophan (W) oxidation levels were quantified.

AAPH OXIDATION WITH METHIONINE PROTECTION						
Modified Amino Acids	**Control**	**0.05% AAPH 40°C 120h with methionine**	**0.5% AAPH 40°C 120h with methionine**	**1% AAPH 40°C 120h with methionine**	**2% AAPH 40°C 120h with methionine**	**5% AAPH 40°C 120h with methionine**
LC M4ox	0.3	1.5	0.9	0.8	0.9	2.0
HC M34ox	0.6	2.5	1.9	1.4	1.7	2.6
HC M83ox	0.7	1.5	0.9	0.7	0.9	1.8
HC M258ox	4.5	7.7	8.2	8.5	8.7	10.3
HC M364ox	0.4	0.4	0.5	0.7	0.9	2.1
HC M434ox	1.1	5.1	3.0	2.7	3.5	6.3
LC W35ox+4	< 1					
LC W35ox+16	< 1					
LC W96ox+4	< 1					
LC W96ox+16	0.1	0.6	0.9	0.9	0.9	1.3
HC W50ox+4	0.1	2.2	4.7	5.3	5.8	6.3
HC W50ox+16	0.9	8.9	21.7	25.9	28.3	29.2
HC W50ox+32	1.1	2.8	3.2	2.4	2.8	2.1
HC W108ox+4	0.7	2.9	6.7	6.6	6.9	6.1
HC W108ox+16	2.1	45.5	57.6	61.1	60.9	65.8
HC W108ox+32	1.8	6.5	8.0	10.4	11.1	10.2
HC W283ox+4	< 1					
HC W283ox+16	< 1					
HC W319ox+4	< 1					
HC W319ox+16	< 1					
HC W319ox+32	< 1					

References

(1) Mohammadian-Mosaabadi, J.; Naderi-Manesh, H.; Maghsoudi, N.; Khalilzadeh, R.; Shojaosadati, S. A.; Ebrahimi, M. *Biotechnol Appl Biochem* **2005**, *41*, 37.

(2) Krishnamurthy, R.; Madurawe, R. D.; Bush, K. D.; Lumpkin, J. A. *Biotechnol Progr* **1995**, *11*, 643.

(3) Kerwin, B. A. *J Pharm Sci* **2008**, *97*, 2924.

(4) Takenawa, T.; Yokota, A.; Oda, M.; Takahashi, H.; Iwakura, M. *J Biochem* **2009**, *145*, 517.

(5) Torosantucci, R.; Schoneich, C.; Jiskoot, W. *Pharm Res* **2014**, *31*, 541.

(6) Khor, H. K.; Jacoby, M. E.; Squier, T. C.; Chu, G. C.; Chelius, D. *MAbs* **2010**, *2*, 299.

(7) Gaza-Bulseco, G.; Faldu, S.; Hurkmans, K.; Chumsae, C.; Liu, H. *J Chromatogr B Analyt Technol Biomed Life Sci* **2008**, *870*, 55.

(8) Pan, H.; Chen, K.; Chu, L.; Kinderman, F.; Apostol, I.; Huang, G. *Protein Sci* **2009**, *18*, 424.

(9) Bertolotti-Ciarlet, A.; Wang, W.; Lownes, R.; Pristatsky, P.; Fang, Y.; McKelvey, T.; Li, Y.; Drummond, J.; Prueksaritanont, T.; Vlasak, J. *Mol Immunol* **2009**, *46*, 1878.

(10) Wang, W.; Vlasak, J.; Li, Y.; Pristatsky, P.; Fang, Y.; Pittman, T.; Roman, J.; Wang, Y.; Prueksaritanont, T.; Ionescu, R. *Mol Immunol* **2011**, *48*, 860.

(11) Liu, D.; Ren, D.; Huang, H.; Dankberg, J.; Rosenfeld, R.; Cocco, M. J.; Li, L.; Brems, D. N.; Remmele, R. L., Jr. *Biochemistry* **2008**, *47*, 5088.

(12) Loew, C.; Knoblich, C.; Fichtl, J.; Alt, N.; Diepold, K.; Bulau, P.; Goldbach, P.; Adler, M.; Mahler, H. C.; Grauschopf, U. *J Pharm Sci* **2012**, *101*, 4248.

(13) Schlothauer, T.; Rueger, P.; Stracke, J. O.; Hertenberger, H.; Fingas, F.; Kling, L.; Emrich, T.; Drabner, G.; Seeber, S.; Auer, J.; Koch, S.; Papadimitriou, A. *MAbs* **2013**, *5*, 576.

(14) Hensel, M.; Steurer, R.; Fichtl, J.; Elger, C.; Wedekind, F.; Petzold, A.; Schlothauer, T.; Molhoj, M.; Reusch, D.; Bulau, P. *Plos One* **2011**, *6*.

(15) Wei, Z. P.; Feng, J. H.; Lin, H. Y.; Mullapudi, S.; Bishop, E.; Tous, G. I.; Casas-Finet, J.; Hakki, F.; Strouse, R.; Schenerman, M. A. *Anal Chem* **2007**, *79*, 2797.

(16) Haberger, M.; Bomans, K.; Diepold, K.; Hook, M.; Gassner, J.; Schlothauer, T.; Zwick, A.; Spick, C.; Kepert, J. F.; Hienz, B.; Wiedmann, M.; Beck, H.; Metzger, P.; Molhoj, M.; Knoblich, C.; Grauschopf, U.; Reusch, D.; Bulau, P. *MAbs* **2014**, *6*, 327.

(17) Stracke, J.; Emrich, T.; Rueger, P.; Schlothauer, T.; Kling, L.; Knaupp, A.; Hertenberger, H.; Wolfert, A.; Spick, C.; Lau, W.; Drabner, G.; Reiff, U.; Koll, H.; Papadimitriou, A. *MAbs* **2014**, *6*.

(18) Li, S.; Schoneich, C.; Borchardt, R. T. *Biotechnol Bioeng* **1995**, *48*, 490.

(19) Wu, Y.; Levons, J.; Narang, A. S.; Raghavan, K.; Rao, V. M. *AAPS PharmSciTech* **2011**, *12*, 1248.

(20) Wang, W. *Int J Pharm* **1999**, *185*, 129.

(21) Mozziconacci, O.; Ji, J. A.; Wang, Y. J.; Schoneich, C. *Mol Pharmaceut* **2013**, *10*, 739.

(22) Ji, J. A.; Zhang, B.; Cheng, W.; Wang, Y. J. *J Pharm Sci* **2009**, *98*, 4485.

(23) Lam, X. M.; Yang, J. Y.; Cleland, J. L. *J Pharm Sci* **1997**, *86*, 1250.

(24) Keck, R. G. *Anal Biochem* **1996**, *236*, 56.

(25) Wasylaschuk, W. R.; Harmon, P. A.; Wagner, G.; Harman, A. B.; Templeton, A. C.; Xu, H.; Reed, R. A. *J Pharm Sci* **2007**, *96*, 106.

(26) Luo, Q.; Joubert, M. K.; Stevenson, R.; Ketchem, R. R.; Narhi, L. O.; Wypych, J. *J Biol Chem* **2011**, *286*, 25134.

(27) Qi, P.; Volkin, D. B.; Zhao, H.; Nedved, M. L.; Hughes, R.; Bass, R.; Yi, S. C.; Panek, M. E.; Wang, D.; Dalmonte, P.; Bond, M. D. *J Pharm Sci* **2009**, *98*, 3117.

(28) Liu, H.; Gaza-Bulseco, G.; Zhou, L. *J Am Soc Mass Spectrom* **2009**, *20*, 525.

(29) Rao, P. E.; Kroon, D. J. *Pharm Biotechnol* **1993**, *5*, 135.

(30) Steinmann, D.; Ji, J. A.; Wang, Y. J.; Schoneich, C. *Mol Pharmaceut* **2012**, *9*, 803.

(31) Grewal, P.; Mallaney, M.; Lau, K.; Sreedhara, A. *Mol Pharmaceut* **2014**, *11*, 1259.

(32) Werber, J.; Wang, Y. J.; Milligan, M.; Li, X.; Ji, J. A. *J Pharm Sci* **2011**, *100*, 3307.

(33) Zhang, A.; Hu, P.; MacGregor, P.; Xue, Y.; Fan, H.; Suchecki, P.; Olszewski, L.; Liu, A. *Anal Chem* **2014**, *86*, 3468.

CHAPTER 4

EVALUATION OF THE IMMUNOGENICITY OF PROTEINACEOUS SUBVISIBLE PARTICLES USING A TRANSGENIC MOUSE MODEL

Research Article

Keywords:
subvisible particles
particle fractionation
particle size
protein aggregation
proteinaceous particles
protein oxidation

Authors:
Emilien FOLZER
Björn BÖLL
Juliana BESSA
Christof FINKLER
Roland SCHMIDT
Patrick BULAU
Jörg HUWYLER
Hanns-Christian MAHLER
Antonio IGLESIAS
Atanas KOULOV

Abstract

Purpose: The formation of aggregates and particles may lead to an unwanted increase in immune response. The aim of this study was to find out which specific characteristics are needed for well-defined fractions to break tolerance in our transgenic mouse model.

Methods: Fractionation of proteinaceous subvisible particles in well-defined size fractions using differential centrifugation and fluorescence activated cell sorter (FACS) were executed. Each sample was extensively characterized using light obscuration, microflow imaging, resonant mass measurement, Fourier-transform infrared microscopy (FTIR) and LC/MS peptide mapping. In this study we investigated the immunogenic properties of subvisible particles (unfractionated material and well-defined size fractions) using a transgenic mouse model expressing a mini-repertoire of human IgG1.

Results: The immunization with proteinaceous subvisible particles generated by artificial stress (thermal stress) conditions demonstrated that only very extensive modifications within the primary amino acid structure of subvisible particles were able to induce a breakage of the immune tolerance in our mouse model.

Conclusions: Proteinaceous particles generated using specific IgG1 were not immunogenic in our transgenic mouse model unless highly chemically modified (*i.e.* following chemically induced oxidation or harsh UV exposure).

Introduction

Particles and aggregates are present in all biotherapeutic formulations in clinical trials or on the market. Protein aggregation can occur during many stages of production (*i.e*. purification, formulation, and filling), or during long-term storage and shipping.[1-6] Particles of proteinaceous origin have recently received increased interest from industry, academia and regulators due to possible biological consequences, such as immunogenicity or altered bioactivity and pharmacokinetics.[7-9] The current understanding of the immunogenicity of aggregates and particles is based on studies from vaccine development and on immunogenicity of protein assemblies.[10-12] Although there are theoretical concerns that proteinaceous particles are a potential risk factor for immunogenicity, their biological effects are still unclear. Immunogenic effects, after drug administration, refer to formation of anti-drug antibodies (ADAs) specific for the protein of interest.[13] The unwanted immunogenicity of a protein product might therefore induce inefficacy of the therapeutic drug.

However, a link between immunogenicity in the clinics and subvisible particle content in biotherapeutic preparations is still lacking. To date, the available data from *in vitro* and *in vivo* experiments is often conflicting and fragmented, which impedes the development of sound conclusions. A major caveat of the published studies is the use of not well-described mixtures of monomer, various aggregates and different particle populations.[10,14-17] More specific, studies with human interferon beta, where samples have been exposed to extreme artificial conditions (*e.g.* metal oxidation or adsorption to glass) lead to an increased immune response in a transgenic mouse model.[18,19] Interestingly, clinical data with different interferon beta products showed an increased anti-drug antibody formation, which cannot solely be attributed to aggregates but might be attributed also to formulation (can contain HSA), modifications in the primary sequence and impurities acting as adjuvants.[20] However, reduction or removal of protein aggregates has been claimed to reduce immunogenic effects.[9,21-23] A potential effect, if any, generated by an individual species, *i.e.* different size or chemical modification, cannot be isolated in these mixtures. To differentiate between the potential immunogenicity of aggregates and particles with different size, an increased interest and effort can be noticed in the field. Several studies describing methods for fractionation, which were subsequently used

for evaluation of immunogenicity in *in vitro* or *in vivo* model systems, were recently published.[24-28] While these studies are giving more insight about the impact of particle size, they neglect the influence of chemical modifications. Recently, an investigation using a novel human IgG1 transgenic mouse model and thoroughly characterized soluble IgG1 aggregates showed that the presence of neoepitopes is needed to observe immunogenic responses.[29] Moreover, the size of these soluble aggregates might be an enhancer of immunogenicity although only a small size range from dimers to large oligomers was investigated.

Here, we present the generation of well-defined size fractions with the recently reported methods; differential centrifugation and fluorescence activated cell sorter (FACS) that was recently published.[25,28] The mean size of these fractions ranged from 1 to 40 μm including chemically unmodified material as well as oxidized material obtained after different UV exposure and chemically induced oxidation (*i.e.* hydrogen peroxide and 2,2-azobis(2-amidinopropane) dihydrochloride). The samples prepared for immunization were extensively characterized regarding their particle size distribution, biochemical properties and chemical modifications using LC/MS peptide mapping and CE-SDS techniques. All samples were then tested in a human IgG1 transgenic mouse model.

Materials and Methods

An IgG1 therapeutic monoclonal antibody (mAb) was chosen as a model protein for the present study. The mAb solution was provided at 25 mg/ml in 51 mM sodium phosphate, 6 % trehalose, and 0.04 % polysorbate 20 (pH 6.2) by F. Hoffmann-LaRoche Ltd (Basel, Switzerland). The solution was filtered using 0.22 μm Millex GV (PVDF) syringe filter units (Millipore, Bedford, MA) before use.

H_2O_2, AAPH, EDTA, DTT (dithiothreitol), iodoacetic acid, cysteine were purchased from Sigma–Aldrich (St. Louis, Missouri) and Dulbecco's phosphate-buffered saline (DPBS) 10× from GIBCO (Invitrogen, San Diego, California). Guanidine hydrochloride (Gdn-HCl) from AppliChem (Darmstadt, Germany) was used during the study.

Trifluoroacetic acid (TFA), formic acid (FA), acetic acid (AcOH), acetonitrile, hydrochloric acid (HCl), potassium chloride (KCl) and sodium chloride (NaCl) were purchased from Merck (Whitehouse Station, New Jersey). Tris(hydroxymethyl)-aminomethan (Tris) was used from Ajinomoto (Raleigh, North Carolina).

Papain from Carica papaya (10 mg/ml) was delivered by Roche Diagnostic (Indianapolis, Indiana). Trypsin Proteomics grade was provided by Roche Diagnostics GmbH (Penzberg, Germany).

L-tryptophan was purchased from Sigma–Aldrich (St. Louis, Missouri) and was dissolved directly in mAb solution to reach a final tryptophan concentration of 4 mg/ml in solution (19.6 mM).

L-methionine was purchased from Sigma–Aldrich (St. Louis, Missouri) and was dissolved directly in mAb solution to reach a final methionine concentration of 40 mg/ml in solution (0.26 M).

Stress conditions

The thermal stress was applied with a thermomixer (Eppendorf, Germany). For mAb1 1 ml of the 25 mg/ml solution was incubated for 3 min at 80 °C with 1400 rpm shaking. The solution

was then resuspended by drawing in and emptying out for 20 consecutive times using a disposable Norm-inject 5 ml luer lock silicone free syringe (HENKE SASS WOLF, Tuttlingen, Germany) with attached 27 Gx1$^{1/2}$" needle (0.4 x 40 mm) (Braun, Melsungen, Germany). The bulk solution was stored at -80 °C after stressing.

For generating chemically modified samples, the protein solutions were treated with UV or chemicals before applying heat/thermal stress. For UV stress, glass vials containing 16 ml formulated antibody solution were kept under the UV–VIS light (Irradiance Energy 765 W/m^2) for 30 h using a SunTest XLS+ device. Chemical stress was applied by adding 2,2-azobis(2-amidinopropane) dihydrochloride (AAPH) or H_2O_2 to the mAb solution. Samples were incubated under protection from direct light with either 5 % AAPH at 40 °C for 120 h (with or without L-methionine addition) or 1 % H_2O_2 for 24 h at 5 °C with L-tryptophan addition. Incubation with H_2O_2 in combination with free tryptophan resulted in selective methionine oxidation. Incubation with AAPH in combination with free methionine resulted in selective tryptophan oxidation as described in detail by Folzer *et al*..[28]

Preparation of size fractions of mAb particles by preparative flow cytometry (FACS)

For the preparation of the subvisible particle fractions a BD FACS Aria III preparative cell sorter (BD Biosciences, San Jose, California) was used with BD FACSDiva v 6.1 software, applying the low-angle FSC detector equipped with a 488/10 band pass filter for the 488 nm laser. A flow cytometry size calibration kit (2, 4, 6 and 15 μm) from Molecular Probes (#F-13838; Life Technologies, Zug, Switzerland) with non-fluorescent microspheres was used for the calibration and definition of the sorting gates. For all experiments, autoclaved PBS (pH 7.2) was used as sheath fluid, prepared using 10× stock solutions and deionized water. To eliminate contaminating particles from the sheath fluid, the sheath line was equipped with 0.22 μm filter. All samples were filtered through 40 μm cell strainer (#352235, Corning Inc.) before sorting. The instrument was used with a 70 μm and the sheath pressure was set to 70 Psi (4.83 bar) and a drop rate of 90 kHz.

Preparation of size fractions of mAb particles by differential centrifugation

The different fractions were prepared using the optimized condition published earlier by our group.[28]

Light obscuration

A HIAC ROYCO instrument model 9703 (Pacific scientific, New Jersey, USA) was used for all light obscuration measurements. A small volume method using a rinsing volume of 0.4 ml and 4 runs of 0.4 ml each was applied. Flow rate was set to 10 ml/min. The first run was discarded and the average ± standard deviation of the last 3 runs was reported for each sample. Blank measurements were performed at the beginning of the measurements and in between samples using fresh particle-free water. The acceptance criterion for blanks was: "less than 5 particles > 1 μm". The system suitability test consisted of the measurement of count standards of 5 μm (Thermo Fisher count standards) with acceptance limits of ± 10% the reported concentration for particles bigger than 3.0 μm was performed in the beginning of each measurement day.

Flow imaging microscopy

The initial samples as well as all collected fractions were analyzed by flow imaging microscopy using a MFI DPA4200 series instrument (ProteinSimple, Santa Clara, California) equipped with a 470 nm LED light source. All particles larger than 1 μm in equivalent circular diameter were reported. Size and count standards (ThermoFisher, Reinach, Switzerland) were used to check the sizing and counting accuracy of the instrument on the day of each measurement. The system was cleaned (before each measurement day) using 1 % (w/v) Terg-a-zyme® (Sigma Aldrich, St. Louis, Missouri), followed by rinsing with water for 30 min. For these flushing steps, the flow rate was set to "maximum speed". Flushing with water was repeated after each sample. The "optimization of illumination" routine was performed prior analysis, using filtered sample or PBS matching the product to be analyzed. For measuring, 1 ml of sample was placed in a 1 ml dual-filter tip on the inlet port.

Resonant mass measurement (RMM, Archimedes)

Resonant mass measurements (RMM) were performed using Archimedes system (RMM0017, generation 2) from Malvern instruments LTD (Malvern, United Kingdom). Micro sensor chips with internal microchannel dimensions of 8 × 8 μm were used for all the experiments. The calibration of the sensor was done using 1 μm Duke polystyrene size standards (Waltham, Massachusetts, USA) diluted in water to approximately 10^6 particles/ml. The calibration was finalized after 300 particles were detected as recommended by the manufacturer. The particle density for proteinaceous particles was defined as 1.28 g/ml. Before measurement, one ml of the sample to be analyzed was centrifuged 5 min at 1258 × g in order to remove large particles that could block the sensor during RMM. Measurements were performed in triplicates and the sensor was filled with fresh sample during 40 s before each measurement. The limit of detection (also called threshold) was manually set to 0.015 Hz for each analysis. Each measurement stopped either after 1 h of measurement or when a total of 4000 particles were detected. During measurement, the "autoreplenish" function was automatically activated every 500 for 5 s to load fresh sample and avoid settling down of particles in the sensor and tubings.

LC/MS peptide mapping analysis, proteolytic digest of mAb

For detection and quantification of oxidized amino acids, the mAbs were digested with trypsin. First, the protein was denatured in 0.4 M Tris-HCl, 8 M Guanidinium-HCl, at pH 8.5 by diluting 350 μg of oxidized mAb in a total volume of 300 μl. For reduction, 10 μl of 100 mg/ml DTT were added and incubated at 50 °C for 1 h. After alkylation of free cysteines by adding 10 μl of 330 mg/ml iodoacetic acid and incubation at room temperature for 30 min, the buffer was exchanged to digestion buffer (0.1 M Tris-HCl, pH 7.0) by using a NAP5 gel filtration column. Subsequently, NAP5-eluate (500 μl) was mixed with 10 μl of a solution of 0.25 mg/ml trypsin in 10 mM HCl and incubated at 37°C for 18 h. The digestion reaction was stopped by adding 50 μl of a 10% TFA solution.

The tryptic peptide mixture was separated by reversed phase-UPLC (ACQUITY, Waters, Manchester, UK) on a C18 column (BEH C18 1,7 μm, 2,1 x 150 mm; Waters, Manchester,

UK) and the eluate online analyzed on a Q-TOF SYNAPT G2 instrument (Waters, Manchester, UK). The mobile phases of RP-HPLC consisted of 0.1 % FA in water (solvent A) and 0.1 % FA in acetonitrile (solvent B). The chromatography was performed using a linear gradient from 1 to 35 % solvent B in 45 min and finally from 35 to 80 % solvent B in 3 min using a flow rate of 300 µl/min. 3 µg digested protein was applied. UPLC-system and mass spectrometer were connected by PEEK capillary tubes. Data acquisition was controlled by MassLynxTM software (Waters, Manchester, UK).

MS/MS experiments were performed on a LTQ Orbitrap Velos electrospray mass spectrometer (Thermo Scientific, Dreieich, Germany) using the chromatographic system described above in order to identify the oxidized peptides. The fragmentation was induced by low-energy CID using helium as collision gas ("top5" mode). Data acquisition was controlled by Xcalibur software (Thermo Fisher Scientific) using a manual acquisition mode. Oxidized amino acids were identified from the MS/MS-data using the software Proteomics Discoverer (Thermo Fisher Scientific). The collision energy was adjusted according to stability and mass of the parent ion.

Peptides of interest were identified manually by searching for their theoretical m/z-values within the experimental mass spectrum. For their quantification, specific ion current (SIC) chromatograms of peptides of interest were generated on the basis of their monoisotopic mass and detected charge states using GRAMS AI software (Thermo Fisher Scientific). Relative amounts of non-oxidized and oxidized peptides were calculated by manual integration of the corresponding peaks.

Endotoxin

Endotoxin levels were measured in all samples using a Limulus Amoebocyte Lysate (LAL) assay kit according to the manufacturer's instructions.

Fourier-transform infrared microscopy (FTIR) measurements

Samples at 25mg/ml after stress were analyzed by FTIR in ATR mode. Spectra were collected from 4000 cm^{-1} to 850 cm^{-1} with a resolution of 4 cm^{-1}. 64 scans were averaged for each sample

measurement. Each spectrum was background corrected and vector normalized on the amide I band. Finally, the second derivatives of the spectra were calculated and smoothened on 25 points according to the Savitzky-Golay algorithm.

Mice and Immunization

The creation of the transgenic mouse model was published recently by our colleagues.[29] Human IgG transgenic mice on C57BL/6 background used was heterozygous for human Ig. Wild type C57BL/6 littermates were used as controls. All mice were kept in an animal facility at F. Hoffmann-La Roche, Basel. Experiments were conducted in accordance with protocols approved by the Veterinary Office of Kanton Basel. IgG1 particle samples were administered subcutaneously twice a week for a total of seven injections (10 μg per injection on the side of the abdomen).

ELISA

For determination of ADAs, ELISA plates (Nunc Immuno MaxiSorp, Rochester, NY) were coated overnight with the respective mAb (5 μg/ml) that was used for injection and ELISA was performed according to standard protocols using alkaline phosphatase-conjugated goat anti-mouse IgG (Fc gamma specific) from Jackson Immuno Research. For quantification of human IgG1 heavy chain, plates were coated with mouse anti-human IgG (heavy chain specific) and detected with biotin mouse anti-human IgG1 followed by alkaline phosphatase-conjugated streptavidin. Optical densities were read in the ELISA reader at 405 nm. Antibodies were purchased from BD Biosciences.

Results and discussion

The aim of this study was to evaluate the immunogenicity of well-characterized subvisible proteinaceous particles (presented as unfractionated material or as well-defined fractions) in a human IgG1 transgenic mouse model. The mouse model was recently described by Bessa and al.[29] In our study, a model humanized IgG1 therapeutic antibody was artificially stressed (heat stress). Unfractionated material containing protein particles with diameters ranging from hundreds of nanometers to approximately hundred micrometers were compared with well-characterized proteinaceous fractions having distinct mean sizes. The fractions were isolated from those unfractionated materials. The methods -fluorescence activated cell sorter (FACS) and differential centrifugation- to obtain the several fractions were published recently by our group.[28] Additional to the investigation of the influence of the particle size, different oxidized samples were generated (prior thermal stress) to investigate the impact of specific modifications.

Generation of specific oxidation profile for the different samples

The initial IgG1 solution was oxidized either by UV treatment or chemically using recently published methods, in order to generate samples with various and well-defined oxidation profiles.[30] More specifically, using hydrogen peroxide (H_2O_2) in combination with addition of free tryptophan allowed for selective oxidation of methionine. The use of 2,2-azobis(2-amidinopropane) dihydrochloride (AAPH) in combination with free methionine resulted in selective tryptophan oxidation whilst methionine oxidation was not significantly altered. Oxidation of methionine and tryptophan was achieved using AAPH. A mixture of various oxidation species was generated using harsh UV exposure. Those oxidized protein solutions were then exposed to heat stress followed by fractionation steps, either by centrifugation or by fluorescence activated cell sorter (FACS).

Generation and characterization of subvisible proteinaceous particle fractions

An IgG1 molecule was used as a model for this study. To obtain the unfractionated materials the initial solution was heat stressed for 3 minutes at 80°C (in addition to 1400 rpm shaking during the thermal stress). Then, the samples were homogenized by drawing in and emptying

out for 20 consecutive times the solution using a disposable syringe mounted by a needle (see material and method for details). The applied stress for this study is considered to be highly artificial and not representative of particles found in real marketed product, due to high temperature used to generate particles. This stress was used due to its reproducibility and its faculty to generate stable particle that we were able to fractionate into fractions of well-defined sizes.

Table 1: Description of the different treatments applied to the IgG1 model to generate the unfractionated materials.

Name	Treatment
Heat stressed unfractionated material	1) 3 minutes 80°C + shaking at 1400rpm + homogenization through a syringe mounted with a needle
UV treated unfractionated material	1) 30 hours at 25°C exposed to light with an irradiance energy of 765 W/m^2 (using a SunTest XLS+ device) 2) 3 minutes 80°C + shaking at 1400rpm + homogenization through a syringe mounted with a needle
H_2O_2 oxidized unfractionated material + free tryptophan	1) Treatment with 1% of H_2O_2 for 24 hours at 5°C in presence of an excess of free tryptophan 2) 3 minutes 80°C + shaking at 1400rpm + homogenization through a syringe mounted with a needle
AAPH oxidized unfractionated material	1) Treatment with 5% of AAPH for 120 hours at 40°C 2) 3 minutes 80°C + shaking at 1400rpm + homogenization through a syringe mounted with a needle
AAPH oxidized unfractionated material + free methionine	1) Treatment with 5% of AAPH for 120 hours at 40°C in presence of an excess of free methionine 2) 3 minutes 80°C + shaking at 1400rpm + homogenization through a syringe mounted with a needle

Fractionation of unfractionated material into well-defined size-fractions was executed using either fluorescence activated cell sorter (FACS) or differential centrifugation. The FACS method was used here to generate one unique size fraction per unfractionated material (reported as Fraction 1 FACS through this manuscript). The details to the isolation by FACS of this fraction were published recently by our group.[28] Briefly, the particles were sorted applying the gate limits as defined by the size standard.

Three fractions (Fraction 1-3 centrifugation) per unfractionated material were isolated by differential centrifugation using the parameters described recently in our last publication.[28]

Table 2: Summary of properties of samples used in *in vivo* tests.

Sample	Flow imaging particles/ml (1-200 µm) ± SD	Light obscuration particles/ml (1.3-100 µm) ± SD	RMM particles/ml (0.2-5 µm) ± SD	Mean diameter measured by FI (µm)	Endotoxin content EU/ml
Unfractionated material after heat stress	1.4×10^6 ± 5.7×10^3	1.6×10^4 ± 5.1×10^1	2.1×10^7 ± 3.7×10^6	10.3	< 0.5
UV exposed unfractionated material heat stress	2.8×10^6 ± 1.1×10^5	1.0×10^4 ± 4.3×10^1	3.4×10^7 ± 8.3×10^6	10.8	< 0.5
Unfractionated material H_2O_2 (1%-24h-5°C with free tryptophan) heat stress	2.9×10^6 ± 9.6×10^3	2.2×10^3 ± 2.6×10^1	1.1×10^7 ± 2.8×10^6	6.3	< 0.5
Unfractionated material AAPH heat stress	2.2×10^6 ± 1.7×10^4	1.3×10^4 ± 1.9×10^1	2.7×10^7 ± 5.7×10^6	9	< 0.5
Unfractionated material AAPH (5%-40°C-120h with free methionine) heat stress	2.8×10^6 ± 9.8×10^4	1.3×10^4 ± 1.6×10^1	1.4×10^7 ± 2.5×10^6	8	< 0.5
Fraction 1 Centrifugation	8.0×10^5 ± 3.5×10^3	9.6×10^4 ± 4.1×10^1	3.3×10^7 ± 3.4×10^6	1.4	< 0.5
Fraction 1 UV exposed Centrifugation	3.6×10^6 ± 1.0×10^5	8.4×10^4 ± 2.9×10^1	2.7×10^7 ± 1.2×10^6	1.4	< 0.5

Sample	Flow imaging particles/ml (1-200 µm) ± SD	Light obscuration particles/ml (1.3-100 µm) ± SD	RMM particles/ml (0.2-5 µm) ± SD	Mean diameter measured by FI (µm)	Endotoxin content EU/ml
Fraction 1 H_2O_2 with free tryptophan Centrifugation	1.6×10^6 $\pm 4.2 \times 10^4$	6.6×10^4 $\pm 4.2 \times 10^2$	3.5×10^7 $\pm 6.1 \times 10^6$	1.3	< 0.5
Fraction 1 AAPH Centrifugation	9.9×10^5 $\pm 2.8 \times 10^4$	4.9×10^4 $\pm 8.4 \times 10^1$	2.7×10^7 $\pm 1.1 \times 10^7$	1.3	< 0.5
Fraction 1 AAPH with free methionine Centrifugation	1.2×10^6 $\pm 1.6 \times 10^4$	7.1×10^4 $\pm 5.6 \times 10^2$	2.5×10^7 $\pm 1.8 \times 10^6$	1.3	< 0.5
Fraction 2 Centrifugation	2.9×10^5 $\pm 7.5 \times 10^3$	2.4×10^5 $\pm 9.7 \times 10^2$	9.3×10^4 $\pm 5.4 \times 10^4$	16.5	< 0.5
Fraction 2 UV exposed Centrifugation	2.5×10^5 $\pm 4.4 \times 10^3$	2.0×10^5 $\pm 6 \times 10^2$	9.7×10^3 $\pm 1.2 \times 10^4$	17.5	< 0.5
Fraction 2 H_2O_2 with free tryptophan Centrifugation	2.6×10^5 $\pm 7.5 \times 10^3$	2.0×10^5 $\pm 1.1 \times 10^3$	1.4×10^4 $\pm 1.1 \times 10^4$	15.9	< 0.5
Fraction 2 AAPH Centrifugation	3.0×10^5 $\pm 1.7 \times 10^3$	2.3×10^5 $\pm 2.8 \times 10^3$	1.7×10^5 $\pm 5.7 \times 10^4$	15.7	< 0.5
Fraction 2 AAPH with free methionine Centrifugation	2.4×10^5 $\pm 2.1 \times 10^3$	1.9×10^5 $\pm 1.4 \times 10^3$	5.1×10^4 $\pm 4.8 \times 10^4$	16.9	< 0.5
Fraction 1 FACS	7.3×10^5 $\pm 8.4 \times 10^3$	1.4×10^4 $\pm 4.3 \times 10^1$	2.7×10^5 $\pm 1.1 \times 10^5$	12.7	< 0.5
Fraction 1 UV exposed FACS	5.9×10^5 $\pm 6.5 \times 10^3$	1.7×10^4 $\pm 2.5 \times 10^2$	4.3×10^5 $\pm 4.4 \times 10^3$	12.2	2.0

Sample	Flow imaging particles/ml (1-200 µm) ± SD	Light obscuration particles/ml (1.3-100 µm) ± SD	RMM particles/ml (0.2-5 µm) ± SD	Mean diameter measured by FI (µm)	Endotoxin content EU/ml
Fraction 1 H_2O_2 with free tryptophan FACS	1.0×10^6 $\pm 1.3 \times 10^4$	6.7×10^5 $\pm 3.0 \times 10^3$	3.7×10^7 $\pm 4.2 \times 10^6$	10.1	9.9
Fraction 1 AAPH FACS	1.2×10^6 $\pm 8.7 \times 10^3$	9.4×10^5 $\pm 1.4 \times 10^3$	7.8×10^7 $\pm 3.9 \times 10^5$	9.1	128
Fraction 1 AAPH with free methionine FACS	1.2×10^6 $\pm 9.1 \times 10^3$	1.0×10^6 $\pm 1.3 \times 10^4$	8.8×10^7 $\pm 2.3 \times 10^6$	9	37.6
Fraction 3 Centrifugation	7.4×10^4 $\pm 2.7 \times 10^3$	6.7×10^4 $\pm 8.2 \times 10^2$	3.4×10^4 $\pm 3.2 \times 10^4$	36.1	< 0.5
Fraction 3 UV exposed Centrifugation	6.4×10^4 $\pm 3.9 \times 10^3$	5.0×10^4 $\pm 1.1 \times 10^3$	1.8×10^4 $\pm 1.1 \times 10^4$	36.2	< 0.5
Fraction 3 H_2O_2 with free tryptophan Centrifugation	5.3×10^4 $\pm 4.2 \times 10^3$	4.7×10^4 $\pm 3.7 \times 10^2$	1.4×10^5 $\pm 7.4 \times 10^4$	39.1	< 0.5
Fraction 3 AAPH Centrifugation	5.1×10^4 $\pm 2.7 \times 10^3$	4.4×10^4 $\pm 8.6 \times 10^2$	1.4×10^5 $\pm 4.2 \times 10^4$	38.6	< 0.5
Fraction 3 AAPH with free methionine Centrifugation	5.7×10^4 $\pm 3.9 \times 10^3$	4.5×10^4 $\pm 7.5 \times 10^2$	1.9×10^5 $\pm 1.0 \times 10^4$	38.4	< 0.5

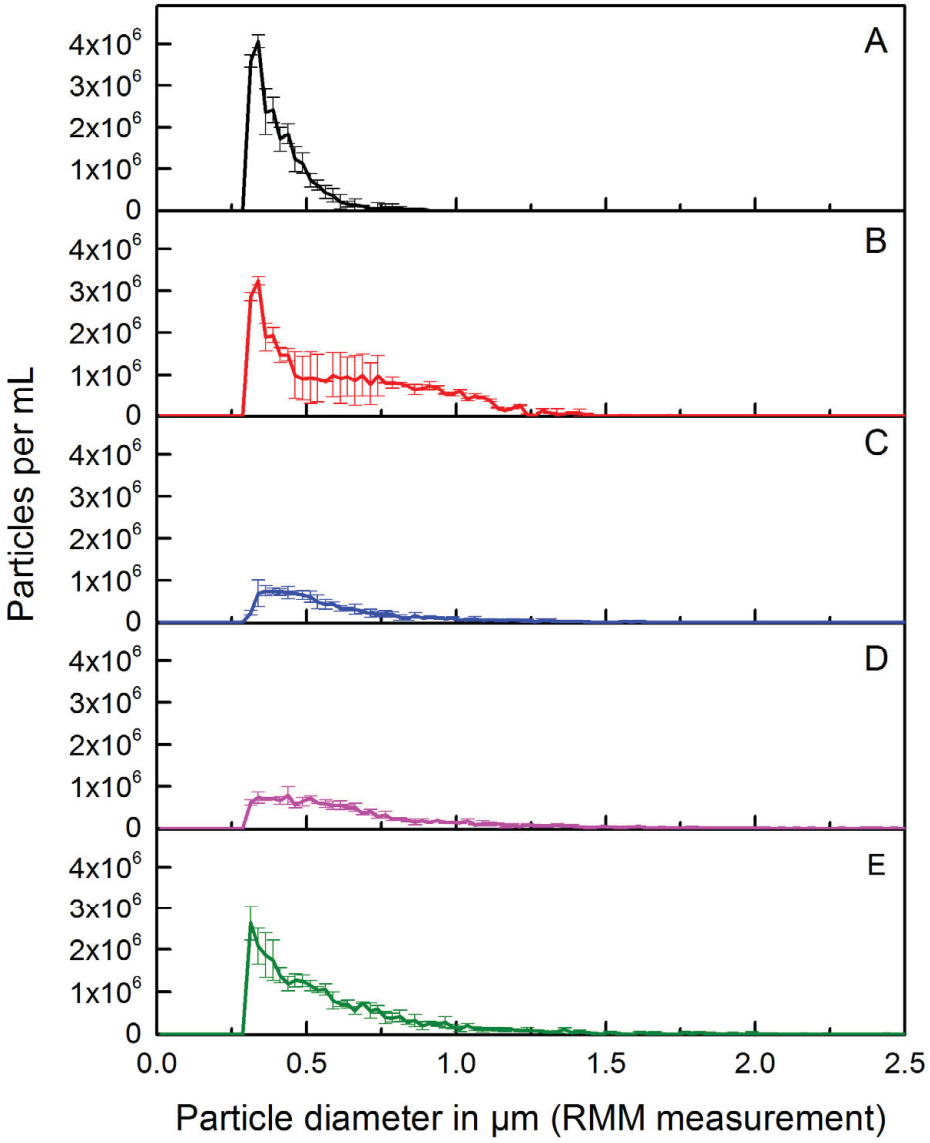

Figure 1: Size distribution of unfractionated materials measured by RMM. Heat stressed unfractionated material (black line), UV-treated unfractionated material (red line), H_2O_2 oxidized unfractionated material with addition of free tryptophan (blue line), AAPH oxidized unfractionated material (pink line) and AAPH oxidized unfractionated material with addition of free methionine (green line) are shown. Error bars represent standard deviation of three measurements.

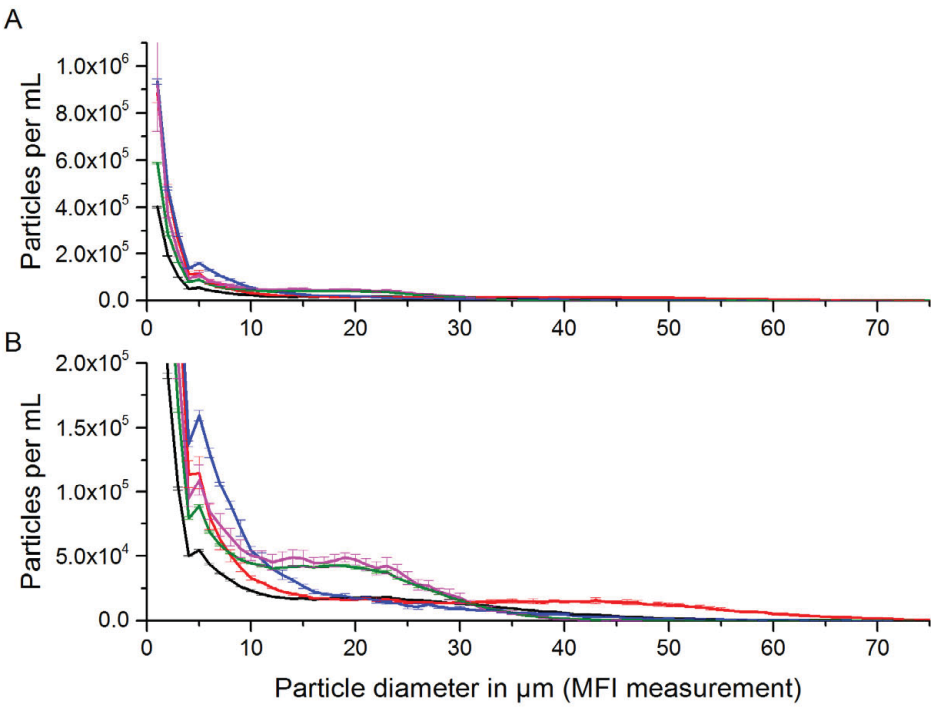

Figure 2: Size distribution of unfractionated materials measured by MFI (panel A) and corresponding zoom in (panel B). Heat stressed unfractionated material (black line), UV-treated unfractionated material (red line), H_2O_2 oxidized unfractionated material with addition of free tryptophan (blue line), AAPH oxidized unfractionated material (pink line) and AAPH oxidized unfractionated material with addition of free methionine (green line) are shown. Error bars represent standard deviation of three measurements.

The isolated fractions (4 per treatment, *i.e.* 20 in total) as well as the 5 unfractionated materials were characterized using light obscuration, micro flow imaging (MFI) and resonant mass measurements (RMM) to obtain their particle size distributions. Table 2 summarizes the characteristics of the unfractionated materials and the corresponding fractions. As expected for the unfractionated materials, the particles are broadly distributed over the full size range. However, distinct differences can be observed between the size distribution of the different unfractionated materials measured by RMM and by MFI as depicted in Figure 1 and 2. Larger particles were measured for oxidized unfractionated samples in comparison to the untreated unfractionated material obtained only after thermal stress. As a direct consequence, the resulting mean size measured by MFI was impacted and differences were noticed in the mass profile of the different unfractionated materials (data not shown here). The oxidized IgG1 was

not as stable as the unmodified IgG1 and formed therefore larger particles faster during thermal stress.

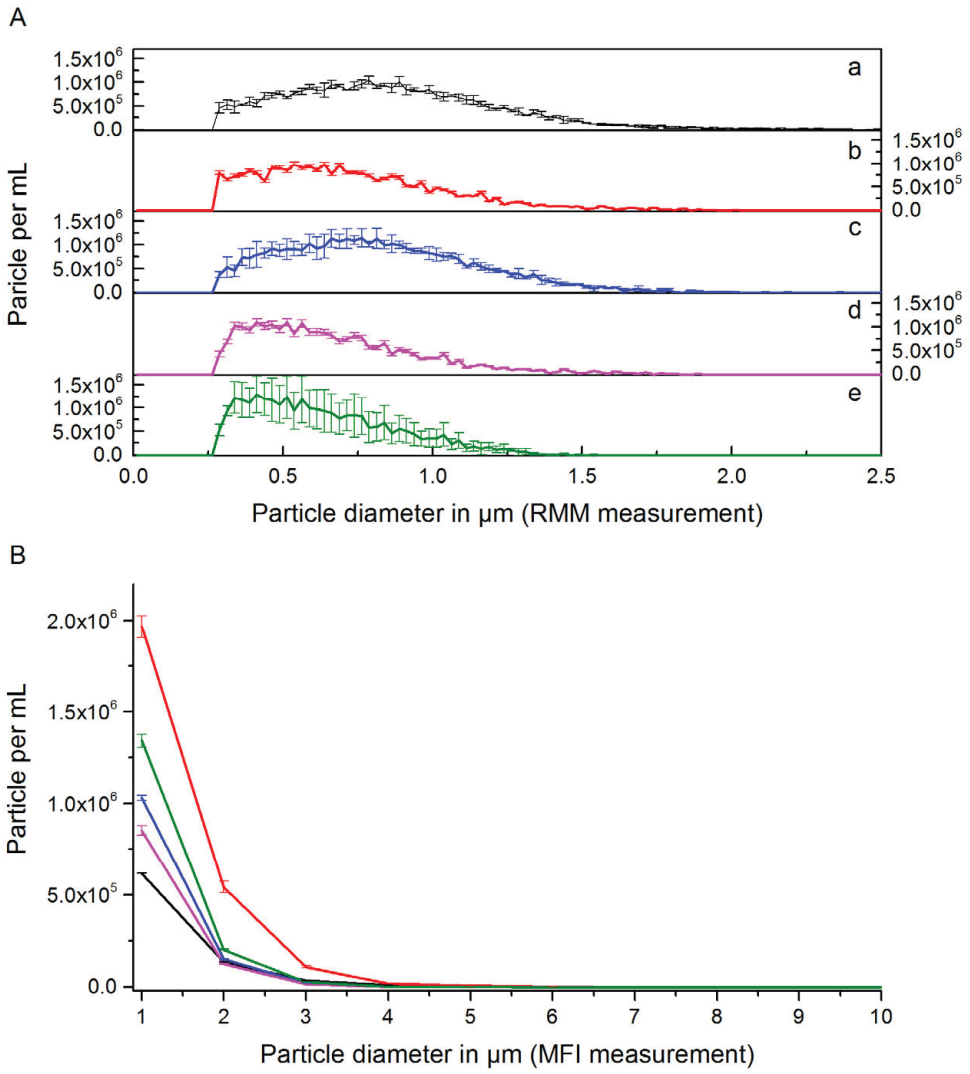

Figure 3: Size distribution of Fraction 1 (centrifugation) measured by RMM (panel A) and MFI (panel B). Heat stressed (black line), UV-treated (red line), H_2O_2 oxidized with addition of free tryptophan (blue line), AAPH oxidized (pink line) and AAPH oxidized with addition of free methionine (green line) samples are shown. Error bars represent standard deviation of three measurements.

Based on those observations, the use of unfractionated material to compare the potential immunogenicity of differently treated samples might only be partially informative due to the differences in their size profiles. This is why well-defined size fractions were prepared. Only slight differences can be seen between size distributions of fractions isolated by differential centrifugation as seen in Figure 3, Figure 4 and Figure 6 where RMM and MFI results are presented. The mean sizes obtained from MFI measurements are comparable and the size profiles are similar except with regard to the presence of nanoparticles in some of the Fraction 2 and 3 (obtained after isolation by centrifugation). The higher count of nanoparticles present in some of those fractions might be attributed to a possible manual handling mistake during the centrifugation steps where the separation of the supernatants from the pellets occurred several times to achieve the right volume and concentration. This contamination through nanoparticles remains low (10^5 particles per ml) and those differences did not impact the mass distribution of the fractions because one large particle represents much more protein than a small particle, but the differences were visible when comparing only size profiles obtained by RMM. However, the concentrations of nanoparticles in the Fractions 2-3 isolated by centrifugation are minimal in comparison to contaminations in Fractions 1 collected by FACS, where more than 10^7 particles per ml could be detected. The RMM measurements showed that those fractions contained relatively high amounts of contaminating nanoparticles (see Figure 5). Possible explanations for the presence of those nanoparticles were discussed in our last publication.[28] This can be attributed either to (1) the possible break-up or aggregation of particles upon sorting due to the mechanical forces that are applied apart, (2) coincidence of two particles in one drop or (3) partial blocking of the nozzle by large particles causing diversion of the stream.[28] A resorting by FACS of the isolated Fractions 1 would have led to higher purity but the resulting protein concentration would have been too low for the subsequent *in vivo* biological experiments. Therefore, resorting of the different fractions was not performed. The presence of nanoparticle is one major difference between similar size fractions (Fraction 1 FACS, and Fraction 2 Centrifugation). For further studies, the purification of those FACS fractions will need to be achieved, in order to obtain similar properties as obtained after isolation by centrifugation regarding levels of contaminating nanoparticles. A combination of both methods could be a good option to optimize this point.

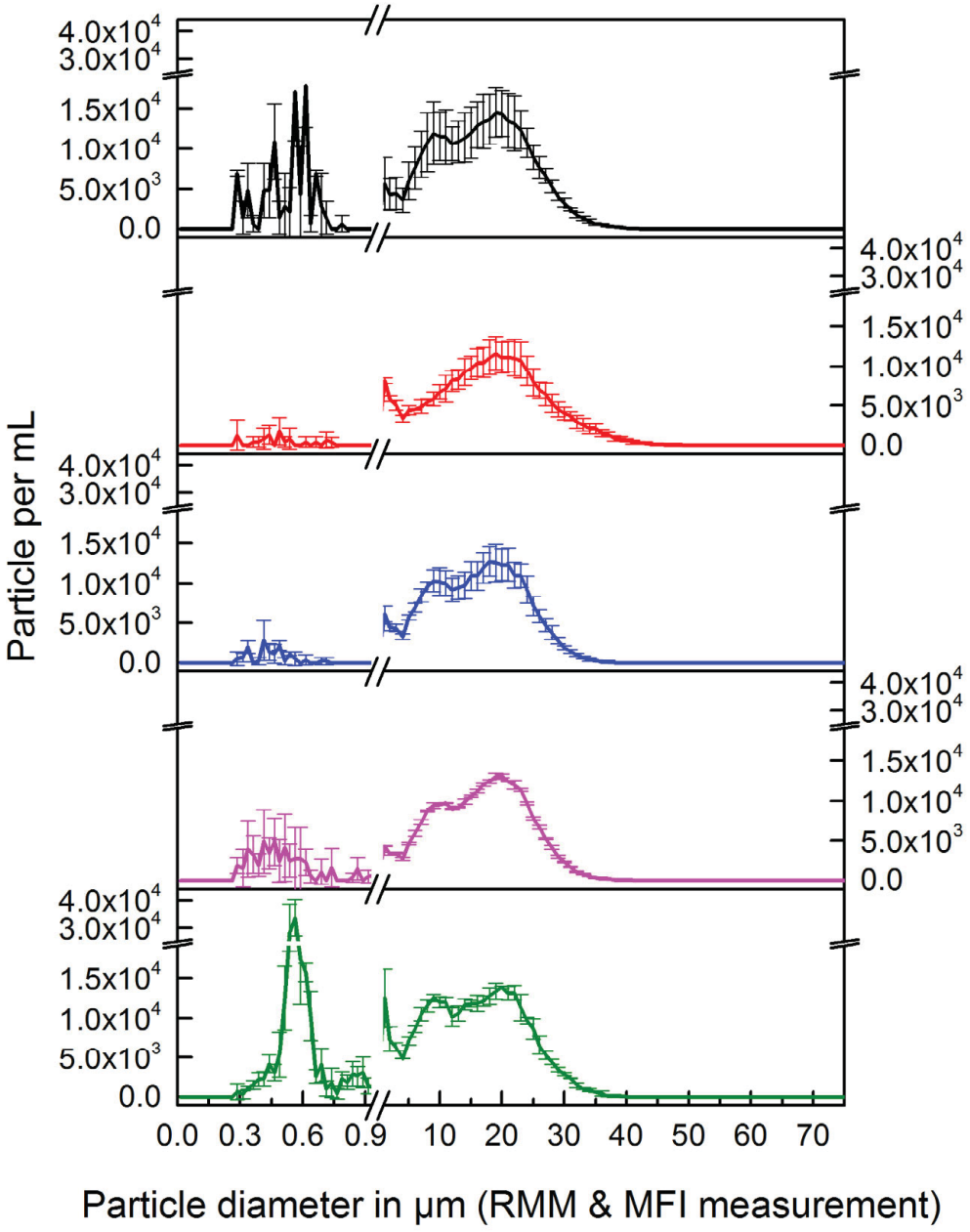

Figure 4: Size distribution of Fraction 2 (centrifugation) measured by RMM (0-1 µm) and MFI (1-100 µm). Fraction 2 heat stressed (black line), UV-treated (red line), H_2O_2 oxidized with addition of free tryptophan (blue line), AAPH oxidized (pink line) and AAPH oxidized with addition of free methionine (green line) are shown. Error bars represent standard deviation of three measurements.

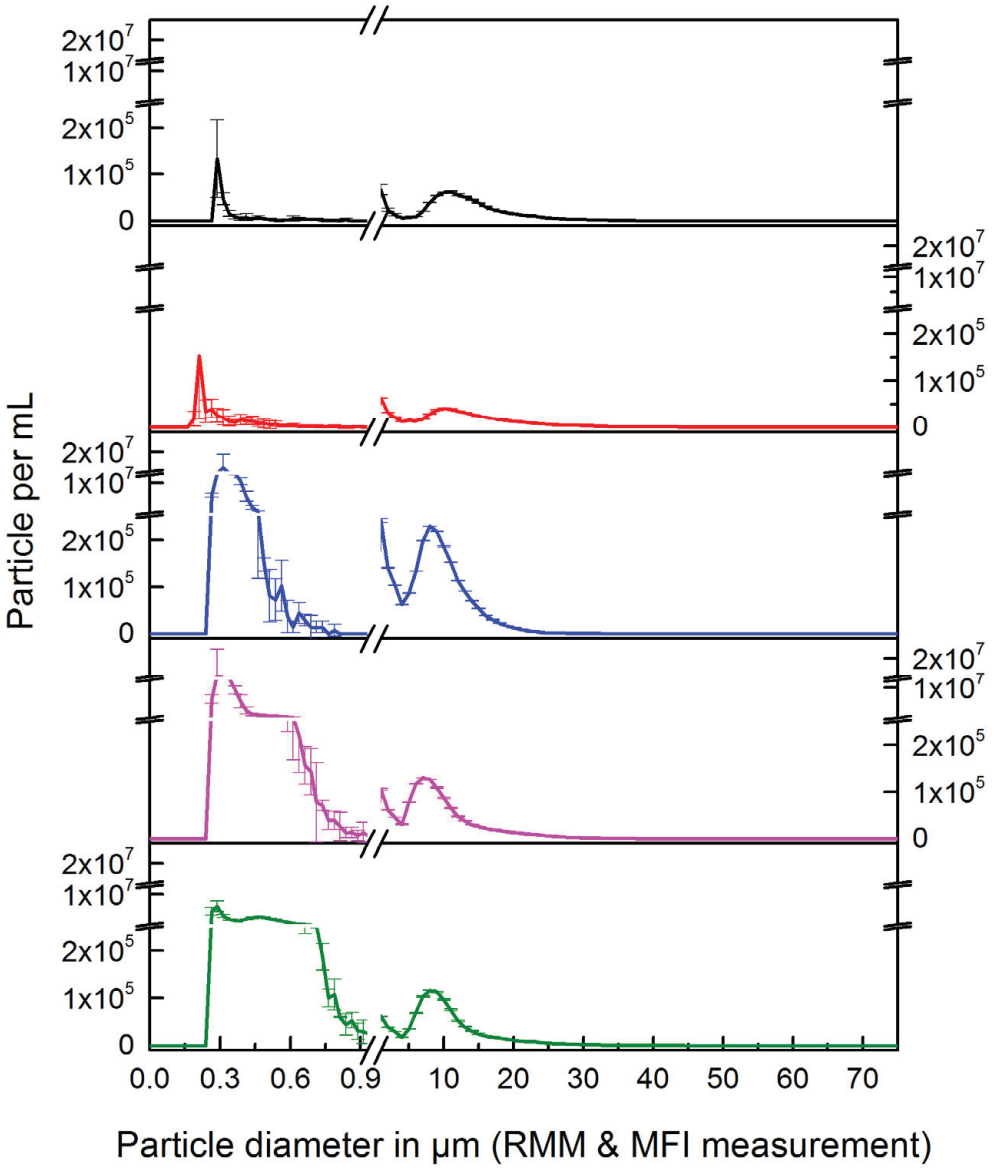

Figure 5: Size distribution of Fraction 1 (FACS) measured by RMM (0-1 µm) and MFI (1-100 µm). Fraction 1 heat stressed (black line), UV-treated (red line), H_2O_2 oxidized with addition of free tryptophan (blue line), AAPH oxidized (pink line) and AAPH oxidized with addition of free methionine (green line) are shown. Error bars represent standard deviation of three measurements.

Beside the characterization regarding the size of the particles, the secondary structure of the IgG1 was investigated using Fourier transform infrared spectroscopy (FTIR). The applied

combination of stresses (*i.e.* oxidation and/or thermal stress) did not lead to a substantial alteration of the secondary structure of the antibody as depicted in Figure 7. No differences of the secondary structure between control material in solution (*i.e.* initial sample before heat stress) and unfractionated materials (chemically modified or not) were observed. The spectra are dominated by the strong valley at 1615 cm^{-1}, associated with the typical intramolecular β-sheet structure of antibodies.

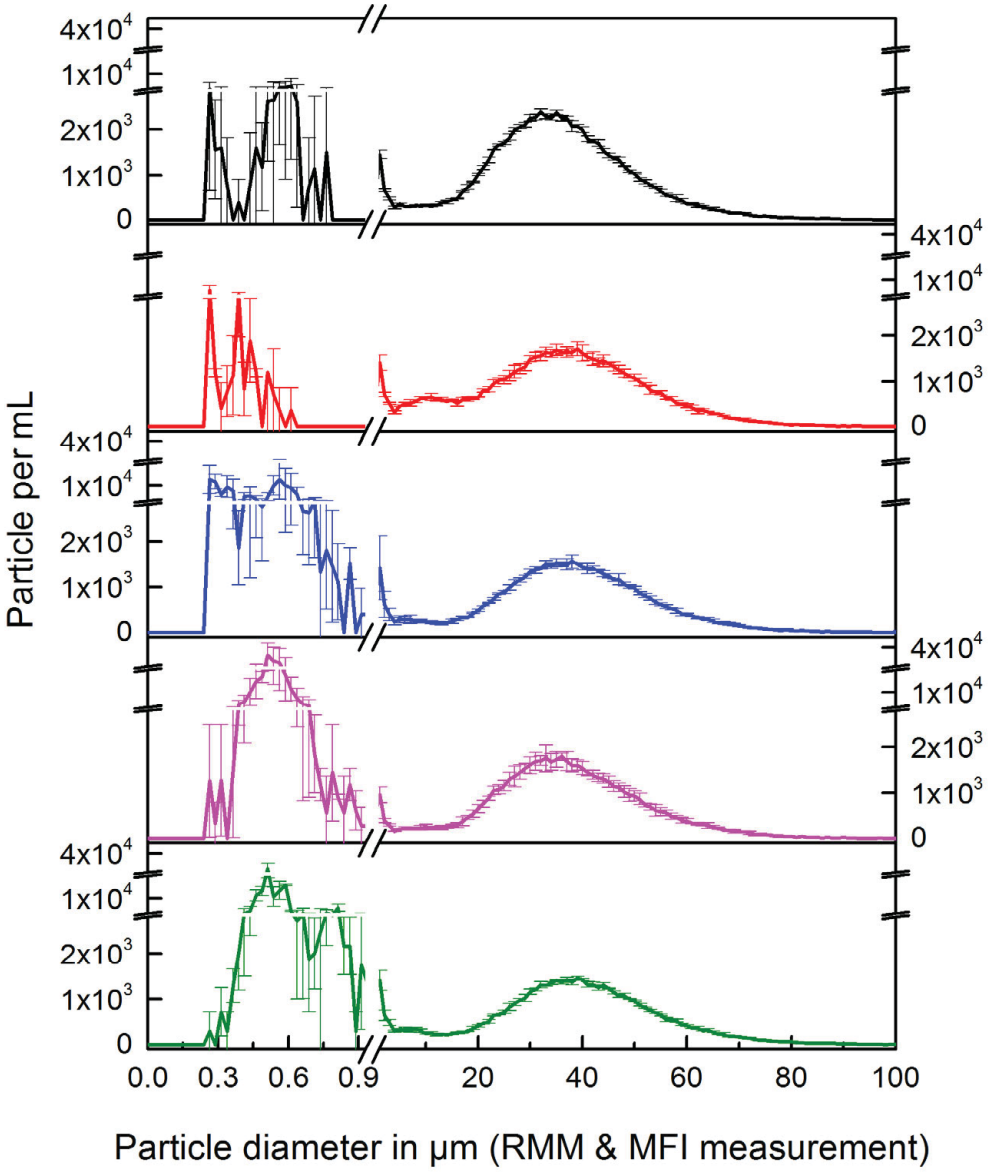

Figure 6: Size distribution of Fraction 3 (centrifugation) measured by RMM (0-1 µm) and MFI (1-100 µm). Fraction 3 heat stressed (black line), UV-treated (red line), H_2O_2 oxidized with addition of free tryptophan (blue line), AAPH oxidized (pink line) and AAPH oxidized with addition of free methionine (green line) are shown. Error bars represent standard deviation of three measurements.

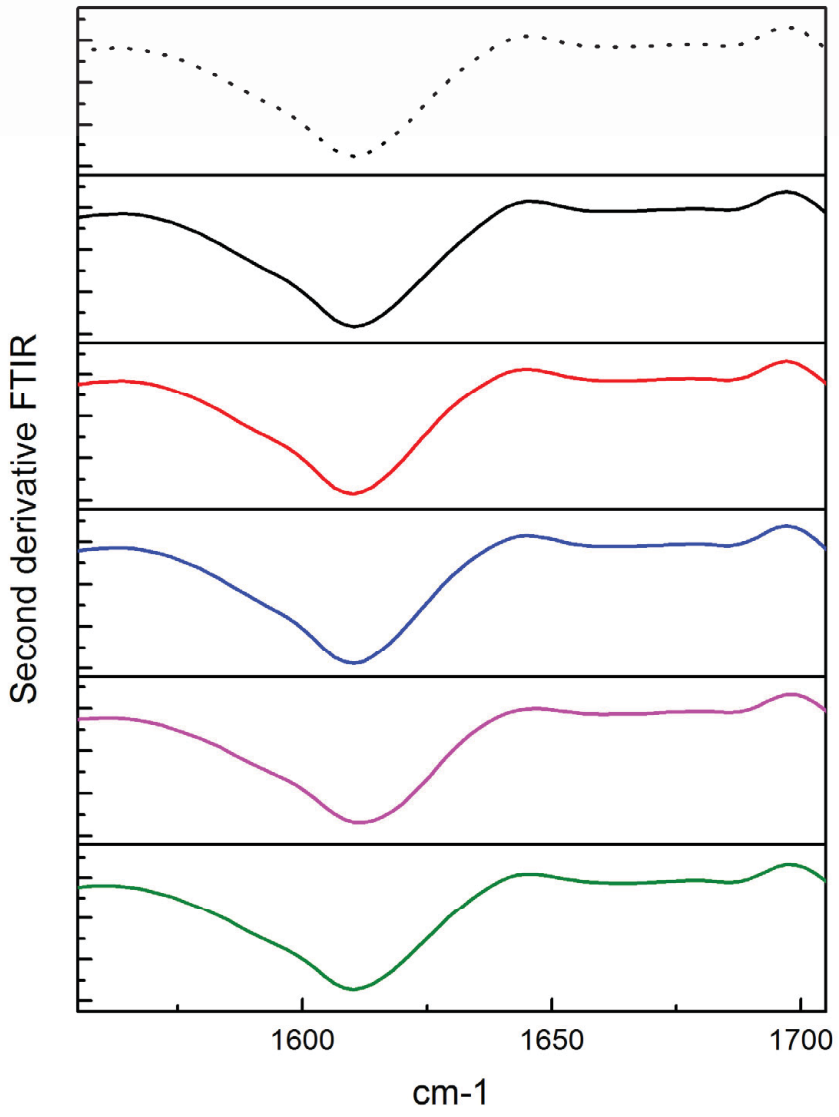

Figure 7: Second derivative - Fourier transform infrared spectroscopy (FTIR) spectra. Second derivative FTIR curves of control material (dashed black line), heat stressed unfractionated material (black line), UV-treated unfractionated material (red line), H_2O_2 oxidized with addition of free tryptophan unfractionated material (blue line), AAPH oxidized unfractionated material (pink line) and AAPH oxidized unfractionated material with addition of free methionine (green line).

LC/MS peptide mapping was used to characterize the chemical modifications present on the protein primary structure. The summary of the obtained results is depicted in Table 3. FACS-fractions present higher oxidation levels than fractions obtained by differential centrifugation. The stresses/treatments that protein particles are exposed to during the flow cytometry

fractionation process seem to induce additional modifications on the protein primary structure. This will need to be investigated in detail in a further study. During flow cytometry fractionation, the particles are exposed to several different types of stress (*i.e.* mechanical, chemical and electrical) that may induce modifications on the protein primary structure.

The first goal regarding oxidation was to generate samples presenting high levels of methionine oxidation (with low level of tryptophan oxidation). This could be achieved by using chemical treatment with H_2O_2 with addition of free tryptophan in solution as described elsewhere by Folzer *et al.*.[30] Indeed, the tryptophan oxidation was protected by the free tryptophan in solution and the corresponding oxidation remained very low after chemical oxidation (see Table 3). This remained valid after additional thermal treatment. Secondly, samples presenting high levels of tryptophan oxidation (with low level of methionine oxidation) needed to be generated. This part could be achieved by using AAPH with the addition of free methionine, as a protective agent, before performing chemical oxidation. The oxidation of methionine in these samples remained very low in comparison to tryptophan oxidation that was dominant. Last but not least, samples presenting high oxidation levels of methionine and tryptophan could be produced by using AAPH (without protection) or UV treatment. Besides methionine and tryptophan modifications, other modifications were detected in the UV-treated samples which could not be further identified yet (unknown peaks) due to the complexity of possible interaction products (identification is ongoing). Moreover, CE-SDS (reduced and non-reduced) experiments to assess the presence of covalent linkage in the various samples were performed. Clear presence of covalent bounds was visible in UV-treated samples (data not shown here).

Table 3: Summary LC/MS peptide mapping results of the different unfractionated materials and corresponding fractions for each different treatment. The mAb was denatured and the disulfide bridges were reduced using DTT. Alkylation of free cysteines was performed using iodoacetic acid. After a buffer exchange, the mAb was finally digested with trypsin. LC stands for light chain, HC stands for heavy chain. Methionine (M) and tryptophan (W) oxidation levels were quantified.

Species	unfractionated material after heat stress	Fraction 1 Centrifugation	Fraction 2 Centrifugation	Fraction 1 FACS	Fraction 3 Centrifugation
LC M4 ox	3.0	1.4	1.0	1.6	2.1
HC M34 ox	6.7	2.2	2.2	3.0	3.8
HC M83 ox	8.1	2.2	3.1	2.0	6.3
HC M258 ox	6.1	4.1	4.4	8.6	6.1
HC M364 ox	1.4	0.2	0.4	0.2	1.1
HC M434 ox	3.3	2.5	2.1	3.0	2.9
LC W96 ox	6.1	1.3	1.2	0.1	5.6
HC W50 ox	8.5	2.2	2.0	1.6	4.5
HC W108 ox	4.0	12.5	3.7	2.3	6.9
Species	UV exposed unfractionated material heat stress	Fraction 1 UV exposed Centrifugation	Fraction 2 UV exposed Centrifugation	Fraction 1 UV exposed FACS	Fraction 3 UV exposed Centrifugation
LC M4 ox	1.0	13.9	2.9	6.1	1.0
HC M34 ox	5.2	18.9	6.4	6.2	3.6
HC M83 ox	3.0	21.1	6.2	3.7	1.3
HC M258 ox	87.9	82.4	80.8	60.2	59.3
HC M364 ox	9.7	9.5	7.1	7.0	7.8
HC M434 ox	71.9	69.3	66.3	71.2	71.7
LC W96 ox	2.1	19.4	3.1	0.8	0.9
HC W50 ox	20.3	37.4	17.7	20.9	19.5
HC W108 ox	41.3	5.6	35.9	38.4	47.1
Species	unfractionated material H2O2 heat stress	Fraction 1 H2O2 Centrifugation	Fraction 2 H2O2 Centrifugation	Fraction 1 H2O2 FACS	Fraction 3 H2O2 Centrifugation
LC M4 ox	1.3	1.2	1.2	5.9	1.3
HC M34 ox	3.1	3.3	3.0	13.9	3.0
HC M83 ox	1.2	1.2	1.2	8.6	1.3
HC M258 ox	66.8	66.5	66.7	63.7	67.4
HC M364 ox	88.5	88.2	89.5	88.4	87.4
HC M434 ox	97.1	97.0	97.0	96.7	97.1
LC W96 ox	0.3	0.1	0.2	0.5	0.2
HC W50 ox	1.5	1.7	1.4	3.0	1.4
HC W108 ox	4.3	2.5	3.1	4.1	3.0
Species	unfractionated material AAPH heat stress	Fraction 1 AAPH Centrifugation	Fraction 2 AAPH Centrifugation	Fraction 1 AAPH FACS	Fraction 3 AAPH Centrifugation
LC M4 ox	4.9	4.7	4.9	5.2	4.5
HC M34 ox	4.9	4.9	4.9	6.7	4.9
HC M83 ox	5.2	4.6	5.0	4.9	4.5
HC M258 ox	62.8	63.6	64.2	64.6	65.3
HC M364 ox	6.1	5.7	5.6	6.3	5.4
HC M434 ox	72.6	73.2	72.2	73.4	72.2
LC W96 ox	0.8	0.7	0.8	0.8	0.8
HC W50 ox	17.6	17.9	17.9	17.7	17.7
HC W108 ox	71.8	74.5	77.5	71.8	77.2
Species	unfractionated material AAPH (5%-40°C-120h with free methionine) heat stress	Fraction 1 AAPH with free methionine Centrifugation	Fraction 2 AAPH with free methionine Centrifugation	Fraction 1 AAPH with free methionine FACS	Fraction 3 AAPH with free methionine Centrifugation
LC M4 ox	1.1	1.2	1.3	5.1	1.3
HC M34 ox	1.2	1.3	1.4	12.8	1.3
HC M83 ox	0.8	1.0	1.1	7.4	1.0
HC M258 ox	7.9	10.2	9.0	18.2	7.9
HC M364 ox	0.2	0.2	0.2	0.4	0.2
HC M434 ox	2.3	2.4	2.3	6.6	2.0
LC W96 ox	0.4	0.4	0.4	2.2	0.4
HC W50 ox	19.1	19.7	19.0	33.7	19.2
HC W108 ox	65.9	68.0	62.9	76.3	56.2

Since endotoxins are known to induce severe immune responses or even septic shock in patients, the samples were checked for endotoxins. Endotoxin levels were higher for FACS-fractions than for unfractionated materials and fractions isolated by centrifugation (see Table 1).[31] The presence of endotoxin in samples and corresponding effects were tested in previous study of our group and no undesirable immune responses triggered by pyrogens was shown to bias the results.[29] We assume that this remains true for the FACS fractions of this study. Moreover, investigations are performed at the moment to reduce the endotoxin levels in samples obtained after FACS.

Immune responses in human IgG1 transgenic mice and wild type mice

The transgenic mouse model developed by Bessa et *al.* was used for our investigation.[29] The same immunization protocol was applied for our experiment as the one used by our colleagues in their previous study.[29] An immunization protocol using repeated subcutaneous applications of 10 μg protein per injection (twice a week; for a total of 7 injections) was used. A total of 5 wild type mice and 5 transgenic mice were immunized with each sample (unfractionated or fractions; total of 25 samples). After 28 days, humoral responses under the form of anti-drug antibodies (ADAs) were characterized by ELISA for both the wild type and the transgenic mice. In order to assess the ADAs production for each individual mouse, the optical densities at 405 nm in the serum were measured (after dilution) and compared to the buffer control. Injected samples presented level of particles tested that were considerably higher than one would measure in marketed product. Indeed, hundred percent of the protein amount contained in the sample was present under the form of particles. Such a sample would definitely not go through analytical testing performed before delivery to the market.

In contrast to the antibody response observed in wild type non-transgenic littermate C57BL/6 control mice, human IgG1 transgenic mice were clearly unresponsive to thermal stressed unfractionated material (generated only by artificial heat stress). Immunization with unmodified corresponding fractions revealed that whereas all five samples were highly immunogenic in wild type animals, no response was observed in the transgenic mouse model (only one transgenic mouse elicited a low immune response in the case of Fraction 3 centrifugation – large particles).

No significant differences between immune responses for the different stresses obtained after injection into wild type animals were observed. All five samples (unfractionated materials and fractions) per type of treatment were highly immunogenic and broke tolerance in wild type animals as depicted in Figure 8 for all oxidized samples obtained after the different treatments (UV, H_2O_2, AAPH and AAPH with addition of free methionine). However, the immune responses are clearly lower for oxidized samples injected into the transgenic animals than responses obtained after injection into wild type animals (see Figure 8).

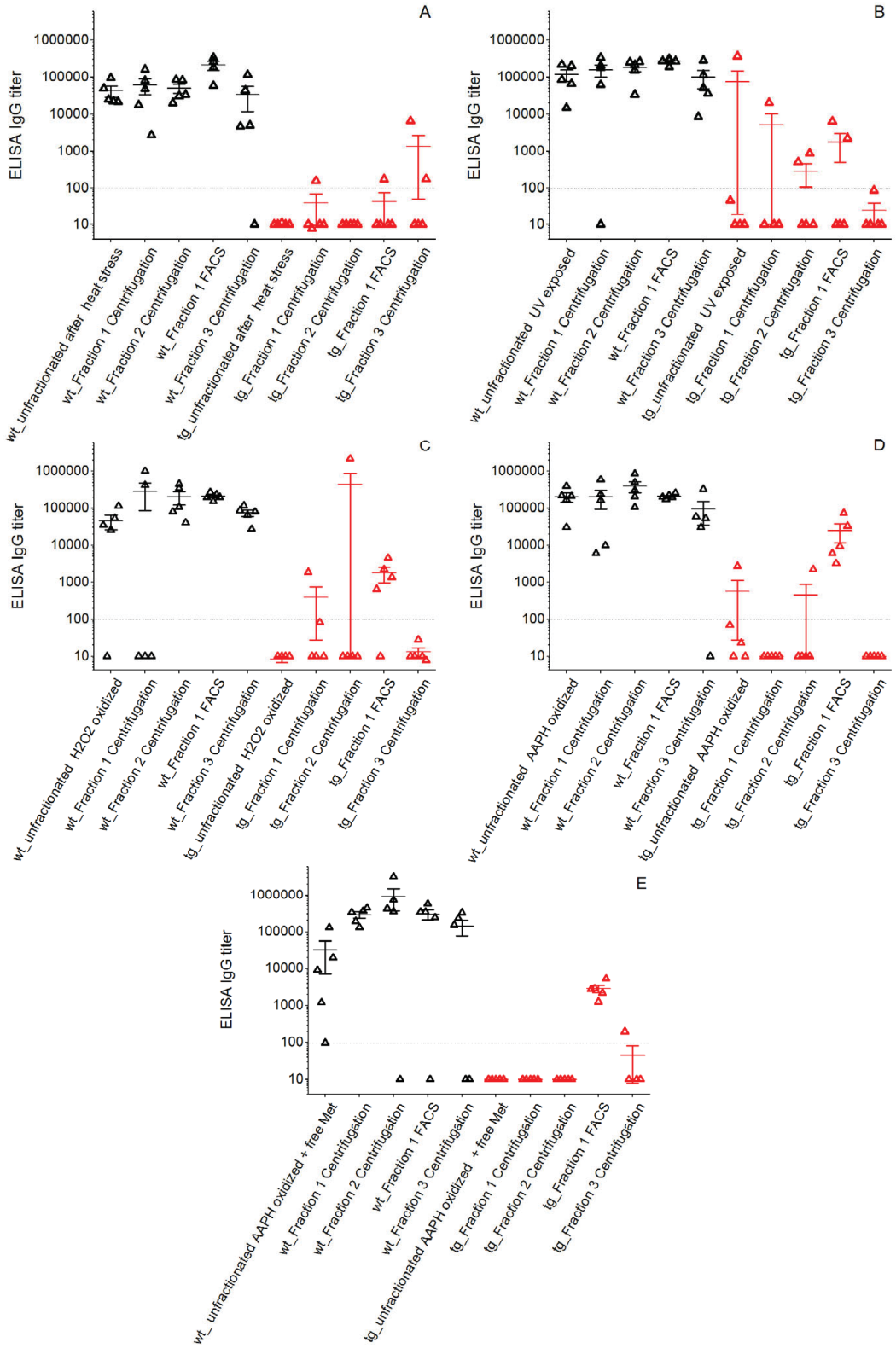
A
ELISA IgG titer
1000000
100000
10000
1000
100
10
wt_unfractionated after heat stress
wt_Fraction 1 Centrifugation
wt_Fraction 2 Centrifugation
wt_Fraction 1 FACS
wt_Fraction 3 Centrifugation
tg_unfractionated after heat stress
tg_Fraction 1 Centrifugation
tg_Fraction 2 Centrifugation
tg_Fraction 1 FACS
tg_Fraction 3 Centrifugation
B
ELISA IgG titer
wt_unfractionated UV exposed
wt_Fraction 1 Centrifugation
wt_Fraction 2 Centrifugation
wt_Fraction 1 FACS
wt_Fraction 3 Centrifugation
tg_unfractionated UV exposed
tg_Fraction 1 Centrifugation
tg_Fraction 2 Centrifugation
tg_Fraction 1 FACS
tg_Fraction 3 Centrifugation
C
ELISA IgG titer
wt_unfractionated H2O2 oxidized
wt_Fraction 1 Centrifugation
wt_Fraction 2 Centrifugation
wt_Fraction 1 FACS
wt_Fraction 3 Centrifugation
tg_unfractionated H2O2 oxidized
tg_Fraction 1 Centrifugation
tg_Fraction 2 Centrifugation
tg_Fraction 1 FACS
tg_Fraction 3 Centrifugation
D
ELISA IgG titer
wt_unfractionated AAPH oxidized
wt_Fraction 1 Centrifugation
wt_Fraction 2 Centrifugation
wt_Fraction 1 FACS
wt_Fraction 3 Centrifugation
tg_unfractionated AAPH oxidized
tg_Fraction 1 Centrifugation
tg_Fraction 2 Centrifugation
tg_Fraction 1 FACS
tg_Fraction 3 Centrifugation
E
ELISA IgG titer
wt_ unfractionated AAPH oxidized + free Met
wt_Fraction 1 Centrifugation
wt_Fraction 2 Centrifugation
wt_Fraction 1 FACS
wt_Fraction 3 Centrifugation
tg_unfractionated AAPH oxidized + free Met
tg_Fraction 1 Centrifugation
tg_Fraction 2 Centrifugation
tg_Fraction 1 FACS
tg_Fraction 3 Centrifugation

Figure 8: Immune responses induced by heat stressed samples (panel A), UV-treated samples (panel B), H_2O_2 oxidized with addition of free tryptophan samples (panel C) AAPH oxidized samples (panel D) and AAPH oxidized with addition of free methionine samples (panel E). Specific IgG responses were determined by ELISA 28 days post the first immunization in wild type animals (black triangles, wt) and transgenic animal (red triangles, tg). Data shown represent mean IgG ELISA titers ± SEM of 5 mice per group.

A maximum of two transgenic animals responded to oxidized samples in the case of unfractionated materials or fractions isolated by centrifugation whereas the level of responses is higher for FACS fractions, where up to five transgenic animals (out of 5) showed a breakage of tolerance, for example in the case of AAPH oxidations (panel D and E, Figure 8). FACS fractions always showed higher immune responses than almost similar size-fractions separated by differential centrifugation (Fraction 3 centrifugation) as presented in Figure 8. High level of contaminating nanoparticles in the FACS fractions and not in the centrifugation fractions is the only difference beside higher level of oxidation observed in FACS fractions. This has to be kept in mind for the interpretation of the immune responses because small particles might potentially be taken up easily and faster than large particles.

As a general remark when looking at the *in vivo* results (Figure 8), the explanation offered by Bessa et *al.* that the immunogenic potential of soluble aggregates of human IgG1 strongly depends on the presence of neoepitopes resulting from harsh stress conditions, *i.e.* extensive exposure to artificial light or in our case harsh chemical treatment seem to remain valid for subvisible particles as well.[29] It is likely that the chemical amino acid modifications were rendering oxidized samples more immunogenic than their unmodified counterpart. Indeed, samples carrying a high degree of chemical modifications (neoepitopes) within the primary structure were more immunogenic than unmodified samples in the transgenic mice. Oxidized subvisible particles may mimic immune complexes and may bind to FcγR on antigen-presenting cells (APCs) allowing presentation of chemically modified epitopes. Moreover, B cells specific for both modified and native structures of IgG1 particles are present in transgenic mice. By challenging transgenic mice with native IgG1, they will not be activated due to the absence of auto reactive T-cells specific for native IgG1 epitopes. However, CD4+ T-cells specific for neoepitopes can be activated in transgenic mice. Once activated they will provide help to B cells recognizing IgG1 that will lead to plasma cell differentiation and ADAs production.[29]

Nevertheless, it has to be mentioned that the immunogenic response using UV-treated subvisible particles (panel B, Figure 8) was drastically lower than in the case of UV-treated oligomers observed by Bessa et *al.* using the same IgG1 model and the same transgenic mouse model.[29] This is again a hint, to say that specific aggregate and particle sizes may potentially enhance the immune response triggered by the neoepitopes as already observed between monomers, dimers and oligomers. The uptake seems to be different according to sizes but this needs surely to be verified in future studies.

In our study the immunization was done subcutaneously. In the case of micrometer-sized particles, it might not be the most favorable injection method because large particles will have difficulties for being taken up in the blood steam and lymphatic system. A protein depot might change or alter the pharmacokinetic profile. In literature, higher immunogenicity in comparison to subcutaneous injection was observed for recombinant murine growth hormone subvisible particles injected intravenously.[32] Injection of labelled size fractions (with and without chemical modifications in their primary structure), would be very useful in order to identify the uptake mechanism and assess if there is a size-dependency or not. The method of injection as well as a detailed pharmacokinetic profile should also be investigated in the future, especially in the case of large subvisible particles.

As already mentioned in literature, other factors beside the extent of chemical modifications, like the hydrophobicity, the solubility and the conformation of aggregates or protein particles may also play an important role in influencing the pharmacokinetic and their related immunogenicity.[33] To understand all those attributes, further investigations are clearly needed.

Conclusions

This study showed that unmodified subvisible particles (unfractionated or well-defined size fractions) obtained after highly artificial heat stress were not immunogenic in transgenic mice expressing a mini-repertoire of human IgG1 antibodies, whereas corresponding artificially generated subvisible particles presenting high levels of chemical modifications in their primary structure resulting of UV-treatment or chemical oxidation with H_2O_2 or AAPH prior to heat stress were immunogenic and a break of tolerance was visible. The immune response of modified samples is however quite low in comparison to the response induced in a previous study using light exposed oligomers (see Bessa et *al.*).[29] For the moment, with the available results, it is not possible to understand whether the immune response is size-dependent or not. Nevertheless, one plausible hypothesis, would lead us to say that the observed immune response seem to depend on the extent of chemical modifications present in the protein primary structure. This point remains hypothetical due to the fact that no specific modification could be identified as enhancer of the immune response and because of the presence of modifications which were not quantifiable (*i.e.* stayed as unknown peaks in the LC/MS peptide mapping analysis). Further investigation will be needed to understand why FACS fractions have always shown higher immune responses than similar size-fractions separated by differential centrifugation.

The use of this transgenic mouse model will hopefully be a very useful tool in the future, allowing the identification of potentially immunogenic modifications in subvisible particles. Last but not least, it would be very interesting to identify how much particulated material of a defined size is really needed to break tolerance.

As different antibodies react differently upon stress conditions, the use of a single IgG1 as a model mAb for our experiments is limiting the general nature of our findings.[15] Experiments using a second IgG1 molecule and different stresses are currently ongoing in our lab.

Acknowledgements

The authors would like to thank the following people for interesting discussions and for their help during the experimental work: Laetitia Petersen and Jürg Marty (mouse immunization), Stefanie Kueng (FACS), Fabian Stump (FTIR), Andrea Heyne (CE-SDS), Katrin Bomans and Katharina Diepold (LC/MS peptide mapping).

References

(1) Mahler, H. C.; Friess, W.; Grauschopf, U.; Kiese, S. *J Pharm Sci* **2009**, *98*, 2909.

(2) Bhatnagar, B. S.; Bogner, R. H.; Pikal, M. J. *Pharm Dev Technol* **2007**, *12*, 505.

(3) Chi, E. Y.; Krishnan, S.; Randolph, T. W.; Carpenter, J. F. *Pharm Res* **2003**, *20*, 1325.

(4) den Engelsman, J.; Garidel, P.; Smulders, R.; Koll, H.; Smith, B.; Bassarab, S.; Seidl, A.; Hainzl, O.; Jiskoot, W. *Pharm Res* **2011**, *28*, 920.

(5) Hawe, A.; Kasper, J. C.; Friess, W.; Jiskoot, W. *Eur J Pharm Sci* **2009**, *38*, 79.

(6) Tyagi, A. K.; Randolph, T. W.; Dong, A.; Maloney, K. M.; Hitscherich, C., Jr.; Carpenter, J. F. *J Pharm Sci* **2009**, *98*, 94.

(7) Carpenter, J. F.; Randolph, T. W.; Jiskoot, W.; Crommelin, D. J.; Middaugh, C. R.; Winter, G.; Fan, Y. X.; Kirshner, S.; Verthelyi, D.; Kozlowski, S.; Clouse, K. A.; Swann, P. G.; Rosenberg, A.; Cherney, B. *J Pharm Sci* **2009**, *98*, 1201.

(8) Barnard, J. G.; Singh, S.; Randolph, T. W.; Carpenter, J. F. *J Pharm Sci* **2011**, *100*, 492.

(9) Ratanji, K. D.; Derrick, J. P.; Dearman, R. J.; Kimber, I. *J Immunotoxicol* **2014**, *11*, 99.

(10) Hermeling, S.; Aranha, L.; Damen, J. M.; Slijper, M.; Schellekens, H.; Crommelin, D. J.; Jiskoot, W. *Pharm Res* **2005**, *22*, 1997.

(11) Rosenberg, A. S. *Aaps J* **2006**, *8*, E501.

(12) Spohn, G.; Bachmann, M. F. *Expert Rev Vaccines* **2008**, *7*, 43.

(13) Vugmeyster, Y.; Xu, X.; Theil, F. P.; Khawli, L. A.; Leach, M. W. *World J Biol Chem* **2012**, *3*, 73.

(14) Filipe, V.; Jiskoot, W.; Basmeleh, A. H.; Halim, A.; Schellekens, H.; Brinks, V. *MAbs* **2012**, *4*, 740.

(15) Joubert, M. K.; Hokom, M.; Eakin, C.; Zhou, L.; Deshpande, M.; Baker, M. P.; Goletz, T. J.; Kerwin, B. A.; Chirmule, N.; Narhi, L. O.; Jawa, V. *J Biol Chem* **2012**, *287*, 25266.

(16) Bi, V.; Jawa, V.; Joubert, M. K.; Kaliyaperumal, A.; Eakin, C.; Richmond, K.; Pan, O.; Sun, J.; Hokom, M.; Goletz, T. J.; Wypych, J.; Zhou, L.; Kerwin, B. A.; Narhi, L. O.; Arora, T. *J Pharm Sci* **2013**, *102*, 3545.

(17) Human, P.; Ilsley, H.; Roberson, C.; Grovender, E.; Van Antwerp, B.; Fogt, E.; Zilla, P. *J Pharm Sci* **2015**, *104*, 722.

(18) Van Beers, M. M.; Gilli, F.; Schellekens, H.; Randolph, T. W.; Jiskoot, W. *J Pharm Sci* **2012**, *101*, 187.

(19) Van Beers, M. M.; Sauerborn, M.; Gilli, F.; Brinks, V.; Schellekens, H.; Jiskoot, W. *Pharm Res* **2011**, *28*, 2393.

(20) van Beers, M. M.; Jiskoot, W.; Schellekens, H. *J Interferon Cytokine Res* **2010**, *30*, 767.

(21) Sauerborn, M. *Bioanalysis* **2013**, *5*, 743.

(22) Sauerborn, M.; Schellekens, H. *Curr Opin Biotechnol* **2009**, *20*, 715.

(23) Fradkin, A. H.; Carpenter, J. F.; Randolph, T. W. *J Pharm Sci* **2009**, *98*, 3247.

(24) Telikepalli, S. N.; Kumru, O. S.; Kalonia, C.; Esfandiary, R.; Joshi, S. B.; Middaugh, C. R.; Volkin, D. B. *J Pharm Sci* **2014**, *103*, 796.

(25) Rombach-Riegraf, V.; Allard, C.; Angevaare, E.; Matter, A.; Ossuli, B.; Strehl, R.; Raulf, F.; Bluemel, M.; Egodage, K.; Jeschke, M.; Koulov, A. V. *J Pharm Sci* **2013**, *102*, 2128.

(26) Paul, R.; Graff-Meyer, A.; Stahlberg, H.; Lauer, M. E.; Rufer, A. C.; Beck, H.; Briguet, A.; Schnaible, V.; Buckel, T.; Boeckle, S. *Pharm Res* **2012**, *29*, 2047.

(27) Hawe, A.; Romeijn, S.; Filipe, V.; Jiskoot, W. *J Pharm Sci* **2012**, *101*, 4129.

(28) Boll, B.; Folzer, E.; Finkler, C.; Huwyler, J.; Mahler, H. C.; Schmidt, R.; Koulov, A. V. *Pharm Res* **2015**.

(29) Bessa, J.; Boeckle, S.; Beck, H.; Buckel, T.; Schlicht, S.; Ebeling, M.; Kiialainen, A.; Koulov, A.; Boll, B.; Weiser, T.; Singer, T.; Rolink, A. G.; Iglesias, A. *Pharm Res* **2015**, *32*, 2344.

(30) Folzer, E.; Diepold, K.; Bomans, K.; Finkler, C.; Schmidt, R.; Bulau, P.; Huwyler, J.; Mahler, H. C.; Koulov, A. V. *J Pharm Sci* **2015**, *104*, 2824.

(31) Morrison, D. C.; Ryan, J. L. *Adv Immunol* **1979**, *28*, 293.

(32) Christie, M.; Torres, R. M.; Kedl, R. M.; Randolph, T. W.; Carpenter, J. F. *J Pharm Sci* **2014**, *103*, 128.

(33) Freitag, A. J.; Shomali, M.; Michalakis, S.; Biel, M.; Siedler, M.; Kaymakcalan, Z.; Carpenter, J. F.; Randolph, T. W.; Winter, G.; Engert, J. *Pharm Res* **2014**.

FINAL CONCLUSIONS

With respect to quality of protein biotherapeutics, protein aggregation and particle formation have recently received increased interest from industry, academia, and regulators because some aggregates and/or particles may have biological consequences such as unexpected immunogenicity, altered bioactivity and/or altered pharmacokinetics. Besides many other factors, unexpected immunogenicity is particularly supposed to be related to aggregates and particles which are suspected to activate the immune system and to initiate the elicitation of antibodies by B cells.[8-10] However, it is still unknown, if aggregates/particles in general or only some particular structures are responsible for the activation of the immune system.

The overall aim of this thesis was to investigate the potential immunogenicity of well-characterized protein subvisible particles using an in-house previously established *in vivo* mouse model.[15] In order to achieve this goal; some tools had first to be developed.

Chapter 1: Determination of the density of protein particles using a suspended microchannel resonator

Chapter 1 describes the method development for determination of the density of proteinaceous particles without extrapolation using RMM as known as Archimedes. Unfortunately up to now, the density of proteinaceous particles, as a crucial particle parameter for weight-based techniques like RMM, have not been determined experimentally. All prior published studies reporting characterization of proteinaceous submicron/subvisible particles using RMM utilize therefore estimates of the density of these particles, thus introducing unknown error into these measurements. In our work, particles created by stressing three different proteins (2 different IgG1 monoclonal antibodies and BSA) using four different types of stress conditions (heat, solvent-induced precipitation, stirring and shaking) were measured after an optimization of the method with commercially available standard beads (latex, polymethacrylate and melamine) of defined sizes and densities. Media with increasing densities from 1.00 to 1.65 g/cm^3 (water, PBS, D_2O, CsCl 20%, CsCl 30%, CsCl 40%, CsCl 50%, CsCl 55% w/w) were used to measure in triplicate the buoyant mass of the various samples over selected size ranges. The determinations of particle densities were

performed by evaluating the change in the mean buoyant mass of the measured particles relative to changes in solution density. The intercept of the linear regression with the Y-axis (where the buoyant mass is equal to zero, neutral density) gave the density of the measured particles. Interestingly, the measured densities for proteinaceous particles (1.28-1.33 g/cm^3) originating from three different proteins and various stress conditions (heat, solvent-induced precipitation, stirring and shaking) were slightly lower than previous estimates and relatively small differences were observed between different proteins and different stress conditions. We could observe that using the newly determined density value of 1.28 g/cm^3 for mAb-derived particles instead of previously suggested 1.32 or 1.35 g/cm^3 has a slight impact on the particle size distribution measured by RMM. This impact increases as a consequence of increasing particle sizes.

Chapter 2: Comparative evaluation of two methods for preparative fractionation of proteinaceous subvisible particles - differential centrifugation and FACS

Species larger than hundreds of nanometer in diameter are currently difficult to fractionate to study their individual physical and biological properties. Recently, fractionation of particles using a cell sorter (FACS) was presented to physically separate discrete micrometer size fractions of subvisible proteinaceous particles out of a mixture of aggregates encompassing a continuous size distribution.[11,12] In other studies, rather crude centrifugation was applied to obtain mostly two fractions: one pellet (insoluble protein, *i.e.* particles) and soluble protein (including aggregates) present in the supernatant.[13] In chapter 2, we describe the method development of a differential centrifugation separation strategy for fractionation of proteinaceous subvisible particles. Four different fractions were isolated using a first set of exploratory experiments in order to identify the critical experimental parameters that might have an impact on the process performances. The fractionation strategy was further optimized using a DoE-approach, which allowed refinement of all parameters leading to higher purity of the selected fractions. The differential centrifugation separation strategy was then compared to the fractionation of particles using a cell sorter (FACS). Similar size-fractions of proteinaceous subvisible particles were isolated using both methodologies. It was noticed that both techniques present advantages and disadvantages regarding the unwanted presence of

nanoparticles, the purity [peak sharpness], the final particle concentration, the size range applicability, the preparation time and the need of additives to achieve fractionation. Both methods will likely find complementary use in the research practice. The new differential centrifugation strategy is a valuable addition to the toolbox of methods for researching subvisible proteinaceous particles in relevant models.

Chapter 3: Selective oxidation of methionine and tryptophan residues in a therapeutic IgG1 molecule

In literature, beside the type of stress to generate aggregate and/or particles, it was reported that the related oxidation profile also plays an important role for potential induced immunogenicity of those species.[14] Cysteine, histidine, methionine, phenylalanine, tryptophan and tyrosine residues were identified as major oxidation sites in proteins due to the high reactivity of sulfur atoms and aromatic rings towards various reactive oxygen species. Most of the time after stress or forced oxidation studies, several residues (*i.e.* amino acids) are concurrently oxidized, making the definition of the individual contribution of these individual residues to the overall effects difficult to delineate. We could observe that samples that were first irradiated with UV light (Atlas Suntest instrument) and were then heat stressed to generate large amount of subvisible particles were able to break immune tolerance (whereas only heat stressed samples were not able). Those samples presented not only a broad oxidation of methionine and tryptophan residues but also non-identified species. It was therefore difficult to draw conclusions and to link our observation to individual contribution of specific chemical modifications. Thus, we developed a method to selectively oxidize methionine and tryptophan in a model mAb in order to improve the understanding of the relationship between structure and functional consequences. Using hydrogen peroxide (H_2O_2) or tert-butyl hydroperoxide (t-BHP) in combination with addition of free L-tryptophan (as a protective agent) allowed for selective oxidation of methionine. The use of 2,2-azobis(2-amidinopropane) dihydrochloride (AAPH) in combination with free L-methionine resulted in selective tryptophan oxidation. Different reaction conditions such as incubation temperature, reaction time and oxidant concentration were evaluated and selected to achieve our goal.

Chapter 4: Evaluation of the biological effect of proteinaceous particles by using a transgenic mouse model

We assessed the immunogenicity of well-defined size fractions prepared either by differential centrifugation or by fluorescence activated cell sorter (FACS) using an in-house transgenic mouse model expressing a mini-repertoire of human IgG1 antibodies. The size (mean diameter) of these fractions ranged from 1 to 40 μm including chemically unmodified material as well as oxidized material obtained following different treatments (UV exposure or chemical oxidations using methods reported in chapter 3). This study showed that native subvisible particles (unfractionated material or well defined fractions, without chemical modification) were not immunogenic in our transgenic mouse model whereas corresponding highly oxidized samples presenting high levels of chemical modifications in their primary structure were immunogenic and showed breakage of tolerance. This response seems to be size-dependent and also is most probably dependent on the extent of chemical modifications. Those last two points remained as hypothetical for the moment.

In this last chapter we could show that the use of this transgenic mouse model is appropriate and is a very useful tool allowing the identification of potential immunogenicity for subvisible particles. However, research needs to be done in order to identify which specific modification plays a role in the observed breakage of tolerance. In the future, injections of labeled size fractions (with or without chemical modifications in their primary structure) will be performed, it will be very useful in order to identify the uptake pathway of subvisible particles and assess if the uptake of subvisible particles is size dependent or not. Last but not least, the planned experiment for the future will also help to assess if the method of injection and the dose have an impact on the level of observed immune responses (especially in the case of large subvisible particles).

References

(1) Bee, J. S.; Randolph, T. W.; Carpenter, J. F.; Bishop, S. M.; Dimitrova, M. N. *J Pharm Sci* 2011, *100*, 4158.

(2) Chang, B. S.; Hershenson, S. *Pharm Biotechnol* 2002, *13*, 1.

(3) Mahler, H. C.; Friess, W.; Grauschopf, U.; Kiese, S. *J Pharm Sci* 2009, *98*, 2909.

(4) Manning, M. C.; Chou, D. K.; Murphy, B. M.; Payne, R. W.; Katayama, D. S. *Pharm Res* 2010, *27*, 544.

(5) Manning, M. C.; Patel, K.; Borchardt, R. T. *Pharm Res* 1989, *6*, 903.

(6) Randolph, T. W.; Carpenter, J. F. *AIChE Journal* 2007, *53*, 1902.

(7) Wang, W. *Int J Pharm* 1999, *185*, 129.

(8) Braun, A.; Kwee, L.; Labow, M. A.; Alsenz, J. *Pharm Res* 1997, *14*, 1472.

(9) Carpenter, J. F.; Randolph, T. W.; Jiskoot, W.; Crommelin, D. J.; Middaugh, C. R.; Winter, G.; Fan, Y. X.; Kirshner, S.; Verthelyi, D.; Kozlowski, S.; Clouse, K. A.; Swann, P. G.; Rosenberg, A.; Cherney, B. *J Pharm Sci* 2009, *98*, 1201.

(10) Hermeling, S.; Schellekens, H.; Maas, C.; Gebbink, M. F.; Crommelin, D. J.; Jiskoot, W. *J Pharm Sci* 2006, *95*, 1084.

(11) Rombach-Riegraf, V.; Allard, C.; Angevaare, E.; Matter, A.; Ossuli, B.; Strehl, R.; Raulf, F.; Bluemel, M.; Egodage, K.; Jeschke, M.; Koulov, A. V. *J Pharm Sci* 2013, *102*, 2128.

(12) Telikepalli, S.; Shinogle, H. E.; Thapa, P. S.; Kim, J. H.; Deshpande, M.; Jawa, V.; Middaugh, C. R.; Narhi, L. O.; Joubert, M. K.; Volkin, D. B. *J Pharm Sci* 2015, *104*, 1575.

(13) Freitag, A. J.; Shomali, M.; Michalakis, S.; Biel, M.; Siedler, M.; Kaymakcalan, Z.; Carpenter, J. F.; Randolph, T. W.; Winter, G.; Engert, J. *Pharm Res* 2015, *32*, 430.

(14) Filipe, V.; Jiskoot, W.; Basmeleh, A. H.; Halim, A.; Schellekens, H.; Brinks, V. *MAbs* 2012, *4*, 740.

(15) Bessa, J.; Boeckle, S.; Beck, H.; Buckel, T.; Schlicht, S.; Ebeling, M.; Kiialainen, A.; Koulov, A.; Boll, B.; Weiser, T.; Singer, T.; Rolink, A. G.; Iglesias, A. *Pharm Res* 2015, *32*, 2344.